



# Kent Academic Repository

Yang, Yankun (2022) *Sliding Mode Control Design for Two-wheeled Mobile Robots*. Doctor of Philosophy (PhD) thesis, University of Kent,.

## Downloaded from

<https://kar.kent.ac.uk/93951/> The University of Kent's Academic Repository KAR

## The version of record is available from

<https://doi.org/10.22024/UniKent/01.02.93951>

## This document version

UNSPECIFIED

## DOI for this version

## Licence for this version

UNSPECIFIED

## Additional information

## Versions of research works

### Versions of Record

If this version is the version of record, it is the same as the published version available on the publisher's web site. Cite as the published version.

### Author Accepted Manuscripts

If this document is identified as the Author Accepted Manuscript it is the version after peer review but before type setting, copy editing or publisher branding. Cite as Surname, Initial. (Year) 'Title of article'. To be published in *Title of Journal*, Volume and issue numbers [peer-reviewed accepted version]. Available at: DOI or URL (Accessed: date).

## Enquiries

If you have questions about this document contact [ResearchSupport@kent.ac.uk](mailto:ResearchSupport@kent.ac.uk). Please include the URL of the record in KAR. If you believe that your, or a third party's rights have been compromised through this document please see our [Take Down policy](https://www.kent.ac.uk/guides/kar-the-kent-academic-repository#policies) (available from <https://www.kent.ac.uk/guides/kar-the-kent-academic-repository#policies>).

UNIVERSITY OF KENT

**Sliding Mode Control Design  
for  
Two-wheeled Mobile Robots**

A Thesis Submitted to the  
University of Kent  
For the Degree of Doctor of Philosophy in  
Electronic Engineering

*By*

**Yankun Yang**

July 2021

Supervisors: Dr Konstantinos Sirlantzis  
Dr Xinggang Yan  
Professor Gareth Howells

# ABSTRACT

This thesis not only concerns the development of sliding mode control (SMC) design for two-wheeled mobile robot (TWMR) systems in a rigorous mathematical manner but also focuses on the application of the developed theoretical SMC algorithms in the practical TWMR systems. The significant contents involve trajectory tracking control on a TWMR with caster wheels and setpoint regulation controls for a two-wheeled inverted pendulum (TWIP). For trajectory tracking SMC of the TWMR system, it is assumed that all the system states are accessible for design. In contrast, both full states and partial states are allowed to be accessible for the controls of a TWIP system. The main achievements in this thesis are summarised as follows.

- The kinematic system is considered with matched and unmatched uncertainty in the trajectory tracking control of a TWMR system. A new structure of the sliding functions is proposed to help derive the reduced-order sliding mode dynamic, which reduces conservatism in the stability analysis. In the presence of both matched and unmatched uncertainty, the proposed SMC can track the predefined trajectories effectively and robustly.
  - A conventional SMC, based on a regular-form approach, is developed for the TWIP system under assumption that all system state variables are accessible. The bounds on both matched and unmatched uncertainties are assumed as known functions used in the SMC design to reject uncertainties and improve robustness. Compared with previous work that used constant or linear bounds on the uncertainties, the developed results allow more general nonlinear forms for the bounds on the uncertainties. As a result, the obtained results can tolerate a broader range of uncertainties.
  - A static output feedback SMC scheme is proposed to regulate the TWIP system when only partial state information is available. Both the stabilisation and setpoint regulation control problems of the TWIP system are addressed. A novel method is introduced to select the feedback gains for regulating the TWIP system intuitively.
  - A self-developed real-time operating system (RTOS) based software architecture is implemented for the practical TWIP platform to improve the system performance.
-

Moreover, the proposed SMC laws are demonstrated in simulation and on a practical TWMR with passive wheels for trajectory tracking control and a TWIP platform for setpoint regulation control subject to the matched and unmatched uncertainties. The results show the effectiveness and robustness of the designed control schemes when implemented in practical TWIP systems.

The simulations of the SMC approaches mentioned above are conducted using Matlab and Simulink tools. Moreover, the associated experimental verifications of the trajectory tracking and setpoint regulation controls are demonstrated on two different TWMR platforms assembled based on the ARM Cortex-M series microcontroller boards as the primary central processing unit.

---

---

## NOTATION AND SYMBOLS

$\forall$	For all
$\in$	Belongs to
$\Rightarrow$	Implies
$\mathbb{R}$	The set of real numbers
$\mathbb{R}^{n \times m}$	The set of $n \times m$ matrices with $n$ rows and $m$ columns in $R$
$ a $	The absolute value of a scalar $a$
$\ \cdot\ $	The Euclidean norm or its induced norm
$I_n$	The identity matrix with dimension $n$
$Im(A)$	The range space of matrix $A$
$A^T$	The transpose of matrix $A$
$A > 0$	$A$ is a symmetric positive definite matrix
$A < 0$	$A$ is a symmetric negative definite matrix
$\lambda_{min}(A)$	The minimum eigenvalue of the square matrix $A$
$\lambda_{max}(A)$	The maximum eigenvalue of the square matrix $A$
$min\{a, b\}$	The minimum value of $a$ and $b$
$\mathcal{L}_f$	The Lipschitz constant of the function $f(\cdot)$
$\frac{\partial f(x)}{\partial x}$	The partial derivative of the function $f(x)$
$\dot{y}$	The first derivative of $y$ with respect to time
$A := B$	$A$ is defined by $B$
$A \Rightarrow B$	$A$ implies $B$
$A \Leftrightarrow B$	$A$ is equivalent to $B$
$A \mapsto B$	$A$ is mapped to $B$
$sgn(\cdot)$	The signum function
$SO(n)$	Special Orthogonal Group $n$ , where $n = 1, 2, 3$ , etc.

---

---

# LIST OF ABBREVIATIONS

<i>WMR</i>	Wheeled Mobile Robot
<i>LMR</i>	Legged Mobile Robot
<i>TWMR</i>	Two-wheeled Mobile Robot
<i>TWIP</i>	Two-wheeled Inverted Pendulum
<i>UAV</i>	Unmanned Aerial Vehicle
<i>AUV</i>	Autonomous Underwater Vehicle
<i>RISC</i>	Reduced Instruction Set Computer
<i>ARM</i>	Advanced RISC Machines
<i>DSP</i>	Digital Signal Processor
<i>FPGA</i>	Field Programmable Gate Array
<i>PWM</i>	Pulse Width Modulation
<i>RTOS</i>	Real Time Operating System
<i>GPIO</i>	General Purpose Input Output
<i>I<sup>2</sup>C</i>	Inter-Integrated Circuit
<i>SPI</i>	Serial Peripheral Interface
<i>USART</i>	Universal Synchronous Asynchronous Receiver and Transmitter
<i>CCD</i>	Charge-Coupled Device
<i>API</i>	Application Programming Interface
<i>IDE</i>	Integrated Development Environment
<i>VSC</i>	Variable Structure Control
<i>SMC</i>	Sliding Mode Control
<i>TSMC</i>	Terminal Sliding Mode Control
<i>MPC</i>	Model Predictive Control
<i>NN</i>	Neural Network
<i>WNN</i>	Wavelet Neural Network
<i>RBFNN</i>	Radial Basis Function Neural Network
<i>DFL</i>	Dynamic Feedback Linearisation
<i>LMI</i>	Linear Matrix Inequality
<i>SOFC</i>	Static Output Feedback Control

---

# ACKNOWLEDGMENTS

Under the influence of the Covid-19 pandemic, this thesis is the result of a three years' prolonged research activity that I have carried out at the School of Engineering and Digital Arts-the University of Kent. I would like to thank some people who have helped me to complete this thesis.

First of all, I would like to thank my supervisors Dr Konstantinos Sirlantzis and Professor Gareth Howells for allowing me to participate in the European Interreg project named "Empowerment of Disabled people through the User Co-production of Assistive Technology (EDUCAT)" with funding to support my research.

Second, I would like to thank my supervisor Dr. Xinggang Yan for his continuous support, professional suggestions and kind guidance during the stages of my research. His patience, enthusiasm, motivation, and immense knowledge in control discipline made my learning process and research experience much more enjoyable and memorable.

Third, I would like to thank my mom and dad so much for their support for me and encourage me while I was in the anxiety, depression moods during my PhD studies.

My thoughts will always be with my colleagues at the School of Engineering and Digital Arts. Namely, I would like to thank my colleagues Michael Gillham, Paul Oprea, Elhassan Mohamed, and Sotirios Chatzidimitriadis for the productive and valuable discussion on research problems. In addition, I would like to thank all the academic staff in the school for providing a collaborative working environment.

Last, but certainly not least, I would like to dedicate this thesis to my parents. I could not have done this without their support. I would also like to thank all my friends for incredibly loving and supportive for all times.

---

---

# CONTENTS

---

<b>Abstract</b>	<b>i</b>
<b>Notation and Symbols</b>	<b>iii</b>
<b>List of Abbreviations</b>	<b>iv</b>
<b>Acknowledgments</b>	<b>v</b>
<b>List of Figures</b>	<b>xv</b>
<b>List of Tables</b>	<b>xvi</b>
<b>1 Introduction</b>	<b>1</b>
1.1 Background and Motivation . . . . .	2
1.1.1 Trajectory Tracking Control of TWMR Systems . . . . .	4
1.1.2 Regulation Control of TWIP Systems . . . . .	7
1.1.3 Motivations . . . . .	10
1.2 Contributions . . . . .	12

---

1.3	Thesis Outline . . . . .	13
<b>2</b>	<b>Mathematical Preliminaries</b>	<b>15</b>
2.1	Basic Mathematics . . . . .	15
2.2	Lyapunov Stability . . . . .	17
2.3	Others . . . . .	20
<b>3</b>	<b>Review of Control Theories and Basic Concept</b>	<b>22</b>
3.1	Fundamental Control Concepts . . . . .	23
3.1.1	State Space Representation . . . . .	23
3.1.2	Types of Feedback Control . . . . .	24
3.2	Sliding Mode Control . . . . .	29
3.2.1	Existence of the Sliding Motion . . . . .	32
3.2.2	Existence of Solution for Discontinuous Systems . . . . .	34
3.2.3	Equivalent Control and Regular Form Approaches of the Sliding Phase . . . . .	35
3.2.4	Conditions of the Reaching Phase . . . . .	38
3.2.5	Characteristics of the Conventional SMC . . . . .	42
3.3	Nonholonomic Systems . . . . .	43
3.3.1	Nonholonomic and Pfaffian Constraints . . . . .	43
3.3.2	Practical example . . . . .	45
3.4	Summary . . . . .	47
<b>4</b>	<b>Trajectory Tracking Control for a Two-wheeled Mobile Robot</b>	<b>48</b>
4.1	System Description . . . . .	49
4.2	Stability Analysis of the Sliding Motion . . . . .	55

---

4.3	Reachability Analysis . . . . .	56
4.4	Description of Control Architecture . . . . .	59
4.5	Simulation and Experimental Results . . . . .	64
4.5.1	Simulation Results . . . . .	65
4.5.2	Experimental Results . . . . .	67
4.6	Conclusion . . . . .	71
<b>5</b>	<b>State Feedback Control of a Two-wheeled Inverted Pendulum</b>	<b>72</b>
5.1	System Description and Preliminaries . . . . .	73
5.2	Sliding Mode Analysis and Control Design . . . . .	76
5.2.1	Stability Analysis of Sliding Motion . . . . .	78
5.2.2	Sliding Mode Control Design . . . . .	80
5.3	Description of Control Architecture . . . . .	82
5.4	Real-time Operating System Based Embedded Architecture Design for Control of the Two-wheeled Inverted Pendulum . . . . .	86
5.5	Simulation and Experiment Research . . . . .	89
5.5.1	Numerical Simulation . . . . .	89
5.5.2	Experimental Results . . . . .	92
5.6	Conclusion . . . . .	95
<b>6</b>	<b>Static Output Feedback Control of a Two-wheeled Inverted Pendulum</b>	<b>96</b>
6.1	Problem Formulation and Preliminaries . . . . .	97
6.1.1	System Descriptions . . . . .	97
6.1.2	Analysis of the Attitude Equilibrium . . . . .	100
6.1.3	Basic Assumptions . . . . .	101
6.1.4	Control Objective . . . . .	103

---

6.2	Sliding Mode Analysis and Control Design . . . . .	104
6.2.1	Stability Analysis of the Sliding Mode . . . . .	105
6.2.2	Reachability Analysis . . . . .	106
6.3	Simulation Study . . . . .	109
6.4	Conclusion . . . . .	115
<b>7</b>	<b>Conclusions and Future Work</b>	<b>116</b>
7.1	Summary and Conclusions . . . . .	116
7.2	Ideas for Future Research . . . . .	117
	<b>Appendices</b>	<b>119</b>
<b>A</b>	<b>Dynamic Modelling of A Two-wheeled Inverted Pendulum</b>	<b>120</b>
<b>B</b>	<b>Hardware Descriptions for Two-wheeled Mobile Robots</b>	<b>125</b>
B.1	Choice of Microcontroller Boards . . . . .	125
B.2	Option of Actuators and Motor Drivers . . . . .	126
B.3	Selection of Sensors . . . . .	127
<b>C</b>	<b>Software Descriptions for Two-wheeled Mobile Robots</b>	<b>131</b>
C.1	MATLAB Simulation . . . . .	131
C.1.1	Graphical User Interface For Trajectory Tracking Control of a Two-wheeled Mobile Robot . . . . .	131
C.2	Practical Experimentation . . . . .	133
C.2.1	Orientation Filter Fusion Using Mahony Algorithm For Inertial Measurement Unit . . . . .	133
C.2.2	Parameter Identification of DC Brushed Motors . . . . .	135

---

**D List of Publication**

**141**

**Bibliography**

**143**

---

## LIST OF FIGURES

---

3.1	Diagram of system in state-space representation . . . . .	23
3.2	Block diagram of the time-invariant linear system . . . . .	25
3.3	Block diagram of the state feedback control for system (3.5) . . . . .	26
3.4	Block diagram of the static output feedback control for systems (3.5) and (3.6) . . . . .	27
3.5	Stick balancing example referenced from [1] . . . . .	30
3.6	State responses of the stick balancing example . . . . .	31
3.7	Phase portrait of the stick balancing example . . . . .	31
3.8	Domain of the sliding motion modified from [2] . . . . .	33
3.9	Ideas of the Filippov approach for solving discontinuous right-hand side dynamical equations . . . . .	34
3.10	The example of chattering phenomenon . . . . .	40
3.11	The control signal of the stick balancing example with chattering . . . . .	41
3.12	The chattering-free control signal of the stick balancing example using smoothing constant $\eta = 0.05$ in (3.56) . . . . .	41
3.13	The geometry of a bicycle . . . . .	46

4.1	Nonholonomic system of a two-wheeled mobile robot . . . . .	49
4.2	Tracking motion of a two-wheeled mobile robot . . . . .	52
4.3	Prototype of the two-wheeled mobile robot for sliding mode trajectory tracking control . . . . .	60
4.4	Hardware architecture of the two-wheeled mobile robot . . . . .	60
4.5	Trajectory Tracking Sliding Mode Control Architecture of a Two-wheeled Mobile Robot . . . . .	62
4.6	Simulation results of trajectory motion under line tracking in $x_G$ - $y_G$ plane	68
4.7	Experiment results of trajectory motion under line tracking in $x_G$ - $y_G$ plane	68
4.8	Simulation results of error signals $(x_{G_d} - x_G, y_{G_d} - y_G, \theta_d - \theta)$ under line tracking . . . . .	68
4.9	Experiment results of error signals $(x_{G_d} - x_G, y_{G_d} - y_G, \theta_d - \theta)$ under line tracking . . . . .	68
4.10	Simulation results of control signals $(v, \omega)$ under line tracking . . . . .	68
4.11	Experiment results of control signals $(v, \omega)$ under line tracking . . . . .	68
4.12	Simulation results of trajectory motion under circular tracking in $x_G$ - $y_G$ plane . . . . .	69
4.13	Experiment results of trajectory motion under circular tracking in $x_G$ - $y_G$ plane . . . . .	69
4.14	Simulation results of error signals $(x_{G_d} - x_G, y_{G_d} - y_G, \theta_d - \theta)$ under circular tracking . . . . .	69
4.15	Experiment results of error signals $(x_{G_d} - x_G, y_{G_d} - y_G, \theta_d - \theta)$ under circular tracking . . . . .	69
4.16	Simulation results of control signals $(v, \omega)$ under circular tracking . . . . .	69
4.17	Experiment results of control signals $(v, \omega)$ under circular tracking . . . . .	69

4.18	Simulation results of trajectory motion under lemniscate tracking in $x_G$ - $y_G$ plane . . . . .	70
4.19	Experiment results of trajectory motion under lemniscate tracking in $x_G$ - $y_G$ plane . . . . .	70
4.20	Simulation results of error signals $(x_{G_d} - x_G, y_{G_d} - y_G, \theta_d - \theta)$ under lemniscate tracking . . . . .	70
4.21	Experiment results of error signals $(x_{G_d} - x_G, y_{G_d} - y_G, \theta_d - \theta)$ under lemniscate tracking . . . . .	70
4.22	Simulation results of control signals $(v, \omega)$ under lemniscate tracking . . .	70
4.23	Experiment results of control signals $(v, \omega)$ under lemniscate tracking . .	70
5.1	Model of a two-wheeled inverted pendulum . . . . .	73
5.2	State Feedback Sliding Mode Control Architecture of a Two-wheeled In- verted Pendulum . . . . .	82
5.3	The prototype of the TWIP platform . . . . .	83
5.4	Hardware architecture of the Two-wheeled Inverted Pendulum . . . . .	83
5.5	Real-time Operating System Based Software Architecture of the TWIP System . . . . .	86
5.6	The responses of the system states under simulation . . . . .	92
5.7	The responses of the error system under simulation . . . . .	93
5.8	The response of the control under simulation . . . . .	93
5.9	The responses of the system states on a practical TWI platform . . . . .	94
5.10	The responses of the error system on a practical TWIP platform . . . . .	94
5.11	The response of the control on a practical TWIP platform . . . . .	95
6.1	Description of a two-wheeled inverted pendulum . . . . .	97
6.2	The admissible region of gains $K_1$ and $K_2$ to satisfy Assumption 6.2 . . .	111

6.3	Time responses of the system outputs $y(t)$ under matched and unmatched uncertainties of the TWIP system driven on an inclined surface $\alpha = 5^\circ$ . . .	113
6.4	Time responses of the error outputs $e_y(t)$ under matched and unmatched uncertainties of the TWIP system driven on an inclined surface $\alpha = 5^\circ$ . . .	113
6.5	Time responses of the control signal of the TWIP system driven on an inclined surface $\alpha = 5^\circ$ . . . . .	114
A.1	Modelling of a two-wheeled inverted pendulum . . . . .	121
B.1	Microcontroller boards. (a) Arduino Due. (b) STM32F407 . . . . .	125
B.2	(a) IMU. (b) DC brushed motor with encoder. (c) High power dual motor driver . . . . .	128
B.3	Outputs of encoder channel A and B when the motor runs at 12V . . . . .	129
C.1	Graphical user interface for the trajectory tracking control of a TWMR system under Matlab simulation . . . . .	132
C.2	Details information of the trajectory tracking control on a TWMR system under Matlab simulation . . . . .	132
C.3	Results of calibration and filtration of three-axis accelerometer data . . . . .	133
C.4	Calibration results of three-axis gyroscope data . . . . .	133
C.5	Filtration results of three-axis gyroscope data . . . . .	134
C.6	Drift-free results of three-axis gyroscope data . . . . .	134
C.7	Roll, pitch, and yaw Euler angles computed by Mahony algorithm . . . . .	134
C.8	The motor testing rig for obtaining the friction constant $B_M$ and the moment of inertia $J_M$ . . . . .	137
C.9	The results of obtaining the friction constant $B_M$ of the motor using linear and parabolic fitting methods . . . . .	138

---

C.10 The results of the total torque $T_{\text{Total}}$ and the velocity difference $(\omega_2 - \omega_1)$ during the acceleration stage . . . . .	139
C.11 The results of the moment of inertia $J_M$ under 45 repetitive experiment .	140

---

## LIST OF TABLES

---

4.1	Parameters of the TWMR, sliding surfaces and control law . . . . .	61
5.1	Model parameters for the TWIP . . . . .	84
6.1	Model parameters for the TWIP . . . . .	110
B.1	Specifications of DC Brushed Motor . . . . .	127
B.2	Specifications of gyroscope and accelerometer . . . . .	129

# CHAPTER. 1

---

## INTRODUCTION

---

Mobile robots are autonomous robots that can move from one location to another without the assistance of external human operators. Unlike most industrial robots, which can only move within a specific workspace, mobile robots have the unique ability to move freely within a predefined workspace to accomplish their objectives. This mobility enables them to be used in a wide variety of applications in both structured and unstructured environments. Wheeled mobile robots (WMRs), legged mobile robots (LMRs), unmanned aerial vehicles (UAVs), and autonomous underwater vehicles (AUVs) are the primary types of mobile robots [3]. Among these types, WMRs are widely used in reality, such as planetary exploration, emergency rescue operations, industrial automation, medical care, and personal service, etc due to relatively low mechanical complexity and energy consumption.

WMR control is concerned with determining the forces and torques that must be applied to the wheels in order for the robot to track a reference trajectory, regulate to a reference point with the desired performance requirements. Due to nonlinearity, uncertainties, modelling errors, and coupling reaction forces, the solution of control problems in robotics is more complicated than usual with the performance requirements of both the transient and

steady-state periods. In this thesis, studies on the robust tracking and regulation control problems for the WMRs, particularly on the TWMR and TWIP systems, will be carried out with detailed system analysis and control design.

## 1.1. BACKGROUND AND MOTIVATION

The differential drive mobile robot is a typical TWMR composed of two fixed powered independently driven wheels mounted on the left and right sides of the robot platform with one or two caster wheels for balance and stability. The differential drive is the simplest mechanical drive as it does not require the rotation of a driven axis. The TWMR is driven solely based on the directions and velocities of the two wheels. For example, the robot usually moves forward or backward in a straight line if both wheels rotate at the same speeds in same directions. If one wheel spins faster than the other, the robot follows a curved path along the arc of an instantaneous circle. If both wheels rotate at the same speeds in opposite directions, the robot turns about the midpoint of the two driving wheels.

The control of TWMR systems is a challenging topic in terms of both its theoretical and practical matters. As a typical nonholonomic system, TWMR is a complex nonlinear, coupled underactuated system, and the number of states is greater than the number of inputs. In the past few decades, various control approaches have been developed for TWMR systems. The Lyapunov-based method [4, 5, 6, 7] can be applied to both linear and nonlinear systems. Such a method shows that a system is stable in the sense of Lyapunov, including the selection of a positive definite Lyapunov energy-based function satisfying the Lyapunov properties, whose derivative decreases along the system trajectories. The feedback linearisation method [8, 9, 10, 11] converts TWMR's nonlinear kinematics or dynamics into linear systems via static (time-invariant) state feedback or dynamic (time-varying) state-feedback approaches. Then the controller is designed based on the linearised systems. In practice, the TWMR systems often have slowly varying unknown parameters, uncertainties and disturbances due to load variation, fuel consumption, complex changeable environment, and other effects. Therefore, some advanced con-

control methods are further investigated, such as fuzzy logic, neural network, adaptive, and SMC [12]. Fuzzy logic [13, 14, 15, 16] shows an effective method to naturally capture the approximation, which has high intelligence. By defining a set of linguistic control rules and its fuzzy implication and compositional rule of inference, the fuzzy logic control provides an algorithm based on expert knowledge of the dynamics rather than the mathematical models, making it more attractive for the analysis of complex systems with unknown uncertainties and disturbances. However, one of the disadvantages of the fuzzy logic method is the lack of systematic procedures to establish the fuzzy rules. The neural network is another approximation approach [17, 18, 19, 20], that is, it can approximate any nonlinear function with desired accuracy by employing either unsupervised learning or supervised learning or reinforcement learning with the evaluation of the system performance [21]. Nevertheless, the neural network's learning process is time-consuming and requires enormous space for executing the control algorithm recurrently. An adaptive control is a well-known method used in system control, which is mainly used to estimate parameters and thus it is powerful to deal with parametric uncertainties. However, if the considered systems have unstructured uncertainties or disturbances, the adaptive laws can not be readily employed. In addition, model predictive control (MPC) is yet another popular control methodology for the WMR systems which is used to control a process while satisfying a set of constraints [22]. The main advantage of MPC is the fact that it allows the current timeslot to be optimised, while keeping future timeslots in account. This is achieved by optimising a finite time-horizon, but only implementing the current timeslot and then optimising repeatedly. Nevertheless, the drawback of MPC is that it requires powerful microcontrollers with large memory space due to the fact that the optimisation process occurs at each time step.

Among all the control approaches mentioned above, SMC has become one of the most powerful control strategies because of its reduced-order characteristics and strong robustness against parameter variations and insensitivity to matched uncertainty [23]. SMC is a nonlinear control paradigm that varies the dynamics of a nonlinear system purposely by applying discontinuous control signals that force the system to "slide", as the name suggests, on a predefined hyperplane, which is called sliding surface. This control method is a particular variable structure control (VSC) first evolved by Russian

researchers named Emel'yanov and Barbashin in the early 1960s. The theory did not draw attention to the control community until the mid-1970s when Itkis and Utkin published a book [24] and a survey paper [2], respectively. Since then, the SMC approach has been extensively explored by many researchers in electrical and mechanical systems [25], and several different significant methods have emerged in the past few decades, such as the conventional SMC, the integral SMC, and the terminal SMC, etc [23, 26, 27]. Due to its high robustness against uncertainties and disturbances, SMC has been widely combined with other approaches to provide better results in both theoretical research and practical applications. In connection with this numerous interesting results have been proposed, such as adaptive SMC [28, 29, 30], backstepping based SMC [31, 32], fuzzy SMC [33, 34], observer-based SMC [35, 36, 37], and decentralised SMC [38, 39] with applications in broad areas such as WMR systems, UAV control, power systems, communication networks, and biology. It can also be applied to systems with the consideration of output information only [40], time-delay [41] and large-scale interconnected systems [38].

The popular control problems of the TWMR can be divided into three categories: path following, trajectory tracking, and setpoint regulation. This thesis is mainly concerned with trajectory tracking control of a TWMR system as well as regulation control of a TWIP system.

### **1.1.1. TRAJECTORY TRACKING CONTROL OF TWMR SYSTEMS**

Trajectory tracking control refers to design feedback control laws to drive the TWMR system to follow a pre-defined time-varying trajectory from given initial conditions. Path following control is similar to trajectory tracking control to follow a pre-defined path but does not involve time constraints.

Conventionally, the linear control approaches might not achieve the desired performance due to the intrinsically nonlinear nature of the nonholonomic TWMR systems. Hence, many researchers focus on investigating the nonlinear control techniques. As mentioned by Brockett's theorem [42], it is infeasible to design continuous differentiable time-invariant state-feedback control laws for stabilising nonholonomic systems. Therefore, great effort has been expended to discover continuous time-varying control laws

[43, 44, 45, 46, 47, 6, 48, 49] and discontinuous ones [50, 51, 52, 53, 54, 55]. A few surveys on motion control of nonholonomic WMR are also available in [56, 57]. Although time-invariant smooth trajectory tracking state feedback control is unattainable [42], the stabilisation of posture of actual TWMR to its desired virtual robot turns out to be viable if the desired mobile robot does not have the motionless configuration [58]. Since the nonholonomic constraints are closely related to the kinematic modelling of the TWMR, most of the earlier papers about trajectory tracking control were based upon kinematics [59, 60, 61, 62, 63]. In [59] and [60], Samson *et al* and Kanayama *et al* proposed two trajectory tracking controls based on the Lyapunov approach. However, these methodologies are not readily apparent for practical implementation. Kim *et al* [61] derived an input-output linearisation control scheme applied to a linearised robot system. However, the system performance was affected by the modelling errors due to the linearisation process on the nonlinear robot model and the utilisation of charge-coupled device (CCD) camera also restricted the robot testing area. To improve the system performance, Fierro *et al* [62] presented a backstepping control method with the combination of two feedback control laws for controlling both kinematics and dynamics of the robot to reduce the tracking errors. Nevertheless, the proposed control only works for square systems, which is not applicable for TWMR systems. In [63], Fierro *et al* proposed a neural network (NN) based control law on the TWMR dynamics to deal with the unmodeled bounded disturbances, and a backstepping control approach to posture of the robot. However, the dynamic controller employs multilayer feedforward NN which is computationally complex and expensive.

In general, the control inputs are chosen as linear and angular velocities in the control design of the TWMR kinematics. However, in practice, the actual control signals, fed into the actuators, are the pulse width modulation (PWM) signals applied to both motors [8, 64]. It is necessary to design the actuator dynamics to convert linear and angular velocities of the TWMR to the corresponding angular velocities of the actuators [64, 65, 66]. As most of the trajectory tracking controls deal with driftless TWMR systems [58], the majorities of the uncertainty issue from input channels of the actuators, which can be categorised as matched uncertainty. As mentioned previously, SMC is one of the most superior control methodologies owing to the completely invariant to matched uncertainties

[67]. Therefore, SMC methodologies can provide an attractive solution to the problem of trajectory tracking control in practical systems. Yang *et al* [68] proposed a SMC law to stabilise a practical TWMR with consideration of both kinematics and dynamics. However, linear sliding surfaces were employed, and the localisation data are obtained only by the vision system, which results in slow sampling rate, sluggish responses and poor tracking accuracy. A dynamic feedback linearisation (DFL) based SMC method was applied to a WMR system by Belhocine *et al* [69]. Some decent simulated results were presented to show the performance in both trajectory tracking and stabilisation task. Nevertheless, this approach requires the control input to be designed as linear and angular accelerations so that the non-singularity condition of the decoupling matrix can be satisfied by the feedback linearisation process, which is infeasible from the practical implementation point of view. Park *et al* [70] proposed an adaptive neural network sliding mode trajectory tracking controller. The learning process is trained by self recurrent wavelet neural networks (WNN) to attenuate the disturbances. However, WNN requires a considerable amount of wavelet memory spaces to execute recurrently, which causes this approach time-consuming and computationally expensive. Both Azzabi *et al* [71] and Koubaa *et al* [72] designed SMC with adaptive capability to unknown disturbances for trajectory tracking of WMRs. Although both the simulation results present some good robustness against the uncertainties, the SMC law was only applied to the dynamic model, which only guarantees the tracking performance of the desired linear and angular velocities. Moreover, the proposed adaptive laws only work for unknown uncertainties with constant upper bounds.

Although SMC owns the strong robustness against matched uncertainties during sliding motion, the system may still be affected by unmatched uncertainties in reaching phase. Hence, numerous techniques have been employed to reduce the time required to reach the sliding manifold [73], such as time-varying sliding surfaces [74], gain adaptation [75], artificial neural networks [76], and fuzzy moving sliding surfaces [77]. However, applying the time-dependent functions and online learning process to the system using time-varying sliding surfaces and radial basis function neural network (RBFNN) methods inevitably needs extra computation time [73]. The fuzzy logic method requires sophisticated pre-defined fuzzy rules for designing the fuzzy moving sliding surfaces, which may not be

readily available. Moreover, the linear sliding surface dynamics can not satisfy the global properties of the controlled system. Therefore, nonlinear sliding surfaces can be alternative approaches to minimise the reaching time and achieve better system performance [78].

### 1.1.2. REGULATION CONTROL OF TWIP SYSTEMS

With the development of modern technologies, the evolution of the TWMRs tends to compact size, flexible manoeuvrability, versatility in congested urban areas, and energy-saving. Therefore, the TWMR platform without the passive wheels, usually called the TWIP-type vehicles, has received great attention to the researchers in recent decades [79, 80, 81, 82, 83, 84, 85]. Conventionally, a TWIP is composed of a body of inverted pendulum and two independently driven wheels attached on the same axle in parallel. The control objective is to maintain the motion of the TWIP whilst regulating the attitude of the pendulum to its equilibrium point at all times.

It is well-known that a reliable dynamic model is a prerequisite requirement for the model-based regulation control designs of the TWIP systems [80, 82, 15, 86, 87, 88, 89, 20]. The characteristics of the TWIP systems can be studied by dynamic analysis [90], model identification [91], and controllability analysis [92]. The dynamic modelling of the TWIP consists of three possible methods, the Newtonian approach, the Lagrangian approach, and Kane's approach [93]. The Newtonian method focuses on the interactive forces between the body and the wheels. It provides an intuitive understanding of the robot's motion by using vector relationships between forces and accelerations [94, 95, 96]. The Lagrangian approach is the most frequently used method for modelling the TWIP system, which considers the kinetic and potential energies defined as functions of generalised coordinates rather than utilising the constraint forces [97, 98, 92, 9, 99]. Lastly, Kane's method is based on vector operations similar to the Newtonian approach in this regard. However, rather than deriving energy functions via the Lagrangian approach or examining interactive forces through the Newtonian mechanics, it is based on determining the generalised active and inertia forces as functions of generalised coordinates [90, 100]. In this thesis, the TWIP system is modelled based on the popular Lagrangian approach.

A variety of controllers have been proposed for TWIP systems in the past (see [101] and the reference therein). Several researchers have applied linear control methods to TWIP systems in earlier stage, including LQR [102], PID [103] and  $H_\infty$  [104], linear state feedback control [94]. However, the systems were modelled without considerations of uncertainties, leading to unsatisfactory results in the presence of disturbances. In [103], Lin *et al* presented traditional PID controllers to a human transportation vehicle for teaching purposes. In [105], Huang *et al* proposed four linear full-state feedback controllers with linear matrix inequalities (LMI) to balance the wheeled mobile vehicles even under the changes of traction environment. However, only the unmatched uncertainties are considered in the system. Some authors have designed nonlinear control algorithms to improve system performance, such as partial feedback linearisation [9], fuzzy control [15, 96], adaptive control [106, 107] and neural network control [108, 89]. Pathak *et al* [9] derived partial feedback linearisation equations for designing double two-level velocity balancing and position controllers of a TWIP. Nevertheless, the system dynamics do not involve matched and unmatched uncertainties, which might affect the system performance due to the lack of handling uncertainties in controller design. In [15], Huang *et al* presented three integrating interval type-2 fuzzy logic controllers to balance and regulate the position and direction of the TWIP. However, the method can not deal with uncertainties either because of the absence of uncertainty considerations in their system dynamics. In [96], Huang *et al* proposed three fuzzy controllers on a TWIP system, that is fuzzy balanced standing control, fuzzy travelling & position control and fuzzy yaw steering control, respectively. It should be noted that all these control laws rely heavily on sophisticated fuzzy logic rules, which are not readily obtained, and the fuzzy rules table increases the complexity of implementation. In [106], Li *et al* developed an adaptive robust dynamic balance control on the TWIP, the results show some good regulation performance compared to the robust non-adaptive and model-based controls. However, the adaptation technique only deals with parametric and linear uncertainties. Lin *et al* [107] designed adaptive regulators to control the attitude and yaw motion of the robot. Although the proposed method has some advantages over the traditional state feedback control, the controllers were applied to the Newtonian model with linear bounds on the uncertainties, which resulted in large modelling errors and limited disturbance handling

capability. In [89], RBFNN controllers were developed on a self-balancing two-wheeled scooter for controlling the attitude angle and yaw motion. However, as the neural network structure has to be established in advance, it requires extra spaces to store the information and the computation of RBFNN is time-consuming.

Practical systems often inevitably suffer from uncertainties and disturbances which will affect the system performance tremendously. As mentioned earlier, the SMC technique has been widely recognised as one of the most popular nonlinear control strategies because of its strong robustness against uncertainty and insensitivity to parameter variations during the sliding motion. Although matched uncertainties are completely nullified when sliding mode occurs, the reaching phase can still be affected by the matched and unmatched uncertainties that can not be reduced or rejected by the control. Such uncertainties could affect system performance or even devastate system stability. Numerous SMC techniques have been developed to make classes of linear and nonlinear systems robust against disturbances and uncertainties [87, 88, 109]. In [87], Yue *et al* presented a zero dynamics based adaptive SMC to stabilise the wheeled inverted pendulum. However, the control law is proposed based on the reference acceleration of the robot, which is difficult for controller design. Huang *et al* [88] proposed two terminal SMC (TSMC) laws to regulate the velocity and braking of the TWIP whilst maintaining the body upright. Although TSMC has a better convergence rate than the traditional SMC, TSMC suffers from an unacceptable singularity issue. In [109], Xu *et al* proposed an integral SMC control scheme to regulate the TWMR in the presence of both matched and unmatched uncertainties. However, the dimension of the sliding mode dynamics using integral SMC is the same order of the original system rather than a reduced-order system [110], which results in conservatism issue in the stability analysis. For the applications of the TWIP systems, some of the researchers tend to lump all the disturbances and/or uncertainties together and use disturbance observers to handle them. In [37], Huang *et al* proposed a high-order disturbance-observer-based SMC for a practical TWIP. Nevertheless, it is required that the bounds on the lumped uncertainties are linear due to the limitation of the utilisation of the LMI technique. In [111], a nonlinear disturbance observer-based SMC was developed with linear bounds on disturbances as well. It should be mentioned that augmenting a disturbance observer through the controller design will increase the dimension of the

system, which leads to complex implementations in practice.

The majorities of the existing literature employ full-state information to regulate TWIP systems. However, system state variables are not always measurable, or the measured data is insufficient to meet system performance requirements. Although observers can estimate the unavailable states [80], the system complexity will inevitably be increased due to the expanded system dimensions if an extra observer is designed. As a result, static output feedback control (SOFC) is an alternative way to control such systems. From the literature, SOFC has been applied to many different mechanical and electrical systems, such as autonomous underwater vehicles [112], narrow tilting vehicles [113], rotorcraft [114], stochastic hybrid systems [115], etc. In [116], Edwards *et al* developed a static output feedback SMC to balance an inverted pendulum cart. However, the system model does not consider the uncertainties, which is not ideal in practice. A few discrete output feedback controls are investigated in [117, 118]. Nevertheless, the system stability might be degraded by converting continuous data to digital ones, and the associated conversion causes latency. Besides, the uncertainties are not taken into account in the inverted pendulum models. Therefore, it is necessary to consider the output feedback control for TWIP system in the presence of uncertainties.

### 1.1.3. MOTIVATIONS

- **From the theoretical perspective:**

- It should be noted that in most of the existing work related to the trajectory tracking control of a TWMR system, the majority of the uncertainties are considered in the dynamic models. Moreover, the associated robust control methods are designed in the dynamic layer to reject the uncertainties/disturbances, which only guarantee the performance of the velocities tracking, not the postures tracking. For posture tracking in the kinematic layer, most of the literature employs the auxiliary control laws based on the Lyapunov backstepping method without tackling the uncertainties [60, 62], leading to poor posture tracking performance and raise conservatism issue of the stability analysis. Therefore, the robust SMC design in the kinematic layer with uncertainties

and the utilisation of reduced-order sliding mode dynamics to weaken the conservatism are interesting subjects to investigate.

- It can be noted from the numerous existing researches that the uncertainties are bounded by positive scalars or linear functions, which are not ideal in practice. Moreover, the vast majority of the literature employs full-state variables in their proposed control laws to regulate the TWIP systems. However, it might not be able to measure all the system states in real applications. Therefore, the SOFC design using only partial state information is significant and full of challenges. Since many of the previous SOFC work concern the stabilisation problems, the setpoint regulation of SOFC is also an interesting topic to study. Besides, another challenge mentioned from the SOFC survey paper [119] is that it is not straightforward to find the gain of SOFC to stabilise the system such that the poles can be placed arbitrarily. Hence, it is significant to determine the parameters of SOFC gains in an intuitive way for the TWIP system.
- **From the practical perspective:** It is challenging to bridge the gap between the theoretical control algorithms and the associated practical implementation to satisfy the desired control performance requirement on physical TWMR platforms. It requires not only high-level understanding of advanced control theory to develop novel rigorous results but also integrated knowledge of mechanical layout, hardware and software designs to achieve the control objectives of the TWMR systems. Moreover, the majority of the available open-source software architectures and integrated development environment (IDE), such as the FreeRTOS and  $\mu$ C/OS, Arduino and STM32CubeMX IDEs, are designed for general-purpose application projects. Such software architectures inevitably contain redundant programs even after tailoring the unnecessary functionalities. One of the challenges is to develop a software architecture that is efficient, reusable, easily expandable for our application-specific projects. For example, the WMR systems in this thesis. Moreover, the significance of practical implementation and verification is not only to demonstrate the feasibility of employing modern robust control techniques on the prototype WMR plat-

forms in the laboratory but also to gain some practical testing and parameters tuning experience and push one step further for the future realisation in real engineering applications in order to adapt complex environment and improve people's quality of life, for example, robust tracking control of TWIP-type wheelchairs for assisting people to pass through a narrow doorway accurately and safely, etc.

## 1.2. CONTRIBUTIONS

This thesis contributes to the knowledge and research not only for the development of SMC designs for the TWMR systems in a rigorous mathematical manner but also for reducing the gap between the theoretical SMC and the practical application. The approaches developed in this thesis have been applied to trajectory tracking control on a TWMR system with passive wheels and setpoint regulation controls for a TWIP system. The contributions of this thesis can be summarised as follows.

- In trajectory tracking control of a TWMR system, the kinematic system is considered with matched and unmatched uncertainties. A new structure of the sliding functions is proposed to help to derive the reduced-order sliding mode dynamic to facilitate the stability analysis, which reduces conservatism. The proposed SMC law can guarantee that the controlled system track the pre-defined trajectories effectively and robustly in the presence of both matched and unmatched uncertainties.
- A regular-form based conventional SMC is developed for the TWIP system using state feedback. The bounds on both the matched and unmatched uncertainties are considered to be known functions, which are employed in the SMC design to reject the uncertainties and enhance the robustness. The developed results allow the bounds on the uncertainties to have more general nonlinear form when compared with other existing work which assume bounds on uncertainties are constant or linear. Thus the obtained results are able to tolerate a broader class of uncertainties.
- Considering that some states of the TWIP system may not be accessible, static output feedback SMC scheme is proposed to regulate the TWIP system. The utili-

sation of the regular form SMC approach and reduced-order sliding mode dynamics reduce the conservatism in stability analysis based on the designed sliding surface which uses output information only. A novel method has been introduced to select the matrix gains intuitively for regulating the TWIP system whilst satisfying the assumption of output feedback stabilisation.

- The developed rigorous theoretical results are successfully implemented on real TWMR platforms. This not only contributes to the area of TWMR but also brings excellent perspectives of the methodology proposed in this thesis. Moreover, a self-developed RTOS-based software architecture is implemented for the practical TWIP platform to improve the system performance from the software perspective. The proposed SMC laws are demonstrated in simulation and on a practical TWMR with caster wheels for trajectory tracking control and a TWIP platform for setpoint regulation control subject to matched and unmatched uncertainties. The results show the effectiveness and robustness of the designed control schemes.

## 1.3. THESIS OUTLINE

This thesis is organised as seven chapters:

**Chapter 1** introduces the literature reviews of the trajectory tracking and setpoint regulation controls for TWMR and TWIP systems respectively. Moreover, the motivation and contributions are described based on the theoretical and practical perspectives separately.

**Chapter 2** outlines some essential mathematical preliminaries necessary for the control analysis and design for the subsequent chapters, including the definitions and foundational conclusions of Lyapunov stability theory and Brockett's necessary condition.

**Chapter 3** reviews fundamental concepts to help readers better understanding this thesis. Basic knowledge of the state-space representation and the state/output feedback controls are presented, followed by the theories and characteristics of the SMC methodology. Finally, the nonholonomic constraints, Pfaffian constraints, and nonholonomic system are discussed with a bicycle example.

**Chapter 4** proposes a nonlinear SMC design for tracking the predefined time-based trajectories on a differential-drive TWMR with passive wheels using tracking error kinematics. The proposed sliding manifold shows that the regular form-based SMC design can apply to systems that do not even have a regular form. The simulation and experiment results demonstrate that the designed SMC law is able to control the TWMR to track given trajectories effectively with better performance than a classical PID controller.

**Chapter 5** is focused on designing a full-state feedback SMC law to regulate a TWIP dynamic system in the presence of matched and unmatched uncertainties. A set of sufficient conditions is developed to guarantee that the controlled system is uniformly ultimately bounded. The nonlinear bounds of matched and unmatched uncertainties are assumed to be known, which are utilised in the SMC design to reduce the conservatism and enhance robustness. The simulation and experiment results show the validity and effectiveness of the proposed SMC law.

**Chapter 6** presents a static output feedback SMC algorithm to regulate the TWIP system when only partial system states are available compared with the one using full-state in Chapter 5. An output-dependent sliding surface is designed, and the stability is analysed based on the reduced-order sliding mode dynamics. The proposed output feedback SMC law is applied to the TWIP system. Simulation related to the setpoint regulation control on the TWIP system confirms the obtained theoretical results as expected.

**Chapter 7** summarises the thesis with conclusions and includes some discussions of potential future work.

Finally, **Appendix** shows the detailed mathematical derivations of the dynamic modelling of the TWIP system used in the chapters 5 and 6. Moreover, the primary hardware components and software descriptions are also elucidated for the trajectory tracking control of a TWMR system and regulation control on a TWIP system, including the choices of the microcontroller boards, sensors, actuators and the graphical user interface (GUI) for simulating the trajectory tracking control of a TWMR system, orientation filter fusion algorithm of the inertial measurement unit (IMU), parameter identification of the motors.

## CHAPTER. 2

---

# MATHEMATICAL PRELIMINARIES

---

This chapter provides some fundamental mathematical definitions and lemmas to help clarify the mathematical terms used repeatedly in the subsequent chapters.

### 2.1. BASIC MATHEMATICS

The set of all  $n$ -dimensional vectors  $x = \text{col}(x_1, \dots, x_n)$ , where  $x_1, \dots, x_n$  are real numbers. Define the  $n$ -dimensional Euclidean space denoted by  $\mathbb{R}^n$ . The one-dimensional Euclidean space consists of all real numbers and is denoted by  $\mathbb{R}$ . Vectors in  $\mathbb{R}^n$  can be augmented by adding their corresponding components. They can be multiplied by a scalar by multiplying each component by the scalar. The inner product of two vectors  $x$  and  $y$  is  $x^T y = \sum_{i=1}^n x_i y_i$ .

**Definition 2.1.1 [120]:** The norm  $\|x\|$  of a vector  $x$  is a real valued function with the following properties

- $\|x\| \geq 0, \forall x \in \mathbb{R}^n$ , with  $\|x\| = 0$  if and only if  $x = 0$ .
- $\|\beta x\| = |\beta| \|x\|, \forall \beta \in \mathbb{R}$  and  $x \in \mathbb{R}^n$ .

- $\|x + y\| \leq \|x\| + \|y\|, \forall x, y \in \mathbb{R}^n$ .

For a vector  $x = \text{col}(x_1, \dots, x_n)$ , its  $p$ -norm can be defined as

$$\|x\|_p = \left( |x_1|^p + \dots + |x_n|^p \right)^{\frac{1}{p}}, \quad 1 \leq p < \infty \quad (2.1)$$

and

$$\|x\|_\infty = \max_i |x_i| \quad (2.2)$$

Throughout the thesis, the Euclidean norm ( $p = 2$ ) is used frequently, which is defined by

$$\|x\|_2 = \left( |x_1|^2 + \dots + |x_n|^2 \right)^{\frac{1}{2}} = \sqrt{x^T x} \quad (2.3)$$

**Definition 2.1.2 [116]:** A quadratic form is a function  $Q$  of  $n$  real variables  $x_1, x_2, \dots, x_n$  such that

$$Q(x_1, x_2, \dots, x_n) = \sum_{i,j=1}^n q_{ij} x_i x_j \quad q_{ij} = q_{ji} \quad (2.4)$$

where the  $q_{ij}$  can be treated as the entries of a particular matrix  $Q$  and the  $x_i$  can be considered as the components of the vector  $x$ . Hence, the quadratic form (2.4) can be alternatively described by

$$Q(x_1, x_2, \dots, x_n) = x^T Q x \quad (2.5)$$

Quadratic forms always satisfy the Rayleigh principle as follows

$$\lambda_{\min}(Q) \|x\|^2 \leq x^T Q x \leq \lambda_{\max}(Q) \|x\|^2 \quad (2.6)$$

**Definition 2.1.3 [116]:** The quadratic form  $x^T Q x$  where  $Q$  is a real symmetric matrix is said to be positive definite if

$$x^T Q x > 0 \quad \forall x$$

and positive semidefinite if

$$x^T Q x \geq 0 \quad x \neq 0$$

and the matrix  $Q$  is said to be positive definite and positive semidefinite matrix, respectively.

The following proposition describes some useful properties related to partitioned symmetric positive definite matrices.

**Proposition 2.1.1 [116]:** Let  $P$  be a real symmetric matrix partitioned as

$$P = \begin{bmatrix} P_{11} & P_{12} \\ P_{12}^T & P_{22} \end{bmatrix} \quad (2.7)$$

where the matrix sub-blocks  $P_{11}$  and  $P_{22}$  are square.

If the above symmetric matrix  $P$  is greater than zero, i.e.,  $P > 0$ , then the following are also satisfied

$$\begin{aligned} P_{11} > 0 \quad \text{and} \quad P_{22} > P_{12}^T P_{11}^{-1} P_{12} \\ P_{22} > 0 \quad \text{and} \quad P_{11} > P_{12} P_{22}^{-1} P_{12}^T \end{aligned} \quad (2.8)$$

**Definition 2.1.4 [67]:** A function  $f(x) : \mathbb{R}^n \mapsto \mathbb{R}^m$  is said to satisfy the *local Lipschitz condition* in the domain  $\Omega \subset \mathbb{R}^n$  if there exists a non-negative constant  $L$  such that the inequality

$$\|f(x) - f(\hat{x})\| \leq L\|x - \hat{x}\| \quad (2.9)$$

holds for any  $x \in \Omega$  and  $\hat{x} \in \Omega$ . Then  $L$  is called the *Lipschitz constant* and  $f(x)$  is called a *Lipschitz function* in  $\Omega$ . Then  $f(x)$  is said to satisfy *global Lipschitz condition* if  $\Omega = \mathbb{R}^n$ .

## 2.2. LYAPUNOV STABILITY

Stability theory is of immense significance during the entire development of the control system analysis and design. The stability of equilibrium points, which is frequently discussed in this thesis, is typically defined in terms of Lyapunov, named after a Russian mathematician and engineer who laid the groundwork for the entire theory [121]. As a result, this section discusses some of the most important results regarding the stability of equilibrium points.

The following Lyapunov stability criterion is defined for autonomous and non-autonomous systems.

Consider the following autonomous system

$$\dot{x} = f(x) \quad (2.10)$$

where  $f : D \mapsto \mathbb{R}^n$  is a locally *Lipschitz* mapping in domain  $D$  and  $x \in D \subset \mathbb{R}^n$ .

**Definition 2.2.1 (Stability and Asymptotically Stability) [121] :** An equilibrium point  $x = 0$  of system (2.10) is said to be

- stable if, for each  $\epsilon > 0$ , there exists  $\delta = \delta(\epsilon) > 0$  such that

$$\|x(0)\| < \delta \Rightarrow \|x(t)\| < \epsilon, \quad \forall t \geq 0 \quad (2.11)$$

- unstable if it is not stable.
- asymptotically stable if it is stable and  $\delta$  can be chosen such that

$$\|x(0)\| < \delta \Rightarrow \lim_{x \rightarrow \infty} x(t) = 0 \quad (2.12)$$

Further, consider the non-autonomous system with the *Lipschitz condition* defined in Definition 2.1.4

$$\dot{x} = f(t, x) \quad (2.13)$$

where  $f : [0, \infty) \times D \mapsto \mathbb{R}^n$  is piecewise continuous in  $t$  and locally Lipschitz in  $x$  on  $f : [0, \infty) \times D \subset \mathbb{R}^n$  is a domain that contains the origin  $x = 0$  is an equilibrium point for (2.13) at  $t = 0$  if

$$f(t, 0) = 0, \quad \forall t \geq 0 \quad (2.14)$$

**Definition 2.2.2 (Stability and Asymptotically Stability) [121] :** An equilibrium point  $x = 0$  of system (2.13) is said to be

- stable if, for each  $\epsilon > 0$ , there exists  $\delta = \delta(\epsilon) > 0$  such that

$$\|x(t_0)\| < \delta \Rightarrow \|x(t)\| < \epsilon, \quad \forall t \geq t_0 \geq 0 \quad (2.15)$$

- uniformly stable if, for each  $\epsilon > 0$ , there exists  $\delta = \delta(\epsilon) > 0$ , independent of  $t_0$  such that (2.15) is satisfied.
- unstable if it is not stable.
- asymptotically stable if it is stable and there is a positive constant  $c = c(t_0)$  such that  $x(t) \rightarrow 0$  as  $t \rightarrow \infty$ , for all  $\|x(t_0)\| < c$ .
- uniformly asymptotically stable if it is uniformly stable and there is a positive constant  $c$  independent of  $t_0$  such that for all  $\|x(t_0)\| < c$ ,  $x(t) \rightarrow 0$  as  $t \rightarrow \infty$ , uniformly in  $t_0$ ; that is, for each  $\eta > 0$ , there is  $T = T(\eta)$  such that

$$\|x(t)\| < \eta, \quad \forall t \geq t_0 + T(\eta), \quad \|x(t)\| < c \quad (2.16)$$

- globally uniformly asymptotically stable if it is uniformly stable,  $\delta(\epsilon)$  can be chosen to satisfy  $\lim_{\epsilon \rightarrow \infty} \delta(\epsilon) = \infty$ , and for each pair of positive numbers  $\eta$  and  $c$ , there is  $T = T(\eta, c) > 0$  such that

$$\|x(t)\| < \eta, \quad \forall t \geq t_0 + T(\eta, c), \quad \|x(t)\| < c \quad (2.17)$$

Further, without loss of generality, consider a linear autonomous system

$$\dot{x} = Ax \quad (2.18)$$

where  $x \in \mathbb{R}^n$ .

**Lemma 2.2.1 (Stability of Linear System) [121] :** An equilibrium point  $x_0$  of system (2.18) is said to be stable if and only if all eigenvalues  $\lambda_i$  of  $A$  satisfy  $Re\lambda_i \leq 0$  and for every eigenvalue with  $Re\lambda_i = 0$  and algebraic multiplicity  $q_i \geq 0$ ,  $rank(A - \lambda_i I) = n - q_i$ , where  $n$  is the dimension of  $x$ . The equilibrium point is said to be asymptotically stable if and only if all eigenvalues of  $A$  satisfy  $Re\lambda_i < 0$ .

**Definition 2.2.3 (Hurwitz Matrix and Lyapunov Equation) [121] :** A matrix  $A \in \mathbb{R}^{n \times n}$  of system (2.18) is said to be *Hurwitz* if and only if for any given positive definite symmetric matrix  $Q$ , there exists a positive definite symmetric matrix  $P$  satisfying

$$PA + A^T P = -Q \quad (2.19)$$

Moreover, equation (2.19) is called the *Lyapunov function*. And if  $A$  is Hurwitz, then  $P$  is the unique solution of (2.19).

**Definition 2.2.4 (Boundedness and Ultimate Boundedness) [121]** : Consider the non-autonomous system (2.13). The solutions of (2.13) are

- uniformly bounded if there exists a positive constant  $c$ , independent of  $t_0 \geq 0$ , and for every  $a \in (0, c)$ , there is  $\beta = \beta(a) > 0$ , independent of  $t_0$ , such that

$$\|x(t_0)\| \leq a \Rightarrow \|x(t)\| \leq \beta, \quad \forall t \geq t_0 \quad (2.20)$$

- globally uniformly bounded if (2.20) holds for arbitrarily large  $a$ .
- uniformly ultimately bounded (UUB) with ultimate bound  $b$  if there exist positive constants  $b$  and  $c$ , independent of  $t_0 \geq 0$ , and for every  $a \in (0, c)$ , there is  $T = T(a, b) \geq 0$ , independent of  $t_0$ , such that

$$\|x(t_0)\| \leq a \Rightarrow \|x(t)\| \leq b, \quad \forall t \geq t_0 + T \quad (2.21)$$

- globally uniformly ultimately bounded if (2.21) holds for arbitrarily large  $a$ .

For the case of autonomous systems, Definition 2.2.4 can be redefined without the word "uniformly" as the solution depends only on  $t - t_0$ .

## 2.3. OTHERS

The following definition and lemma provide some necessary background for analysis and design of trajectory tracking control of the TWMR system in Chapter 4.

**Definition 2.3.1 (Class  $\mathcal{C}^k$  function) [122]** : Let  $\mathcal{D} \subset \mathbb{R}^d$  be open, and let  $f : \mathcal{D} \mapsto \mathbb{R}$ . For  $k$  a non-negative integer, if the partial derivatives  $\frac{\partial^\alpha f}{\partial r^\alpha}$  exist and are continuous on  $\mathcal{D}$  for  $|\alpha| \leq k$ .  $f$  is said to be *differentiable of class  $\mathcal{C}^k$*  on  $\mathcal{D}$  (or simply that  $f$  is  $\mathcal{C}^k$ ). In particular,  $f$  is  $\mathcal{C}^0$  if  $f$  is continuous. If  $f : \mathcal{D} \mapsto \mathbb{R}^n$ , then  $f$  is said to be *differentiable of class  $\mathcal{C}^k$*  if each of the component function  $f_i = r_i \circ f$  is  $\mathcal{C}^k$ . Moreover,  $f$  is said to be  $\mathcal{C}^\infty$  if it is  $\mathcal{C}^k$  for all  $k \geq 0$ .

Consider a system

$$\dot{x} = f(x, u) \quad (2.22)$$

where  $x \in \mathbb{R}^n$  is the system states,  $u \in \mathbb{R}^m$  is the control input. The vector field  $f : \mathbb{R}^n \mapsto \mathbb{R}^n$  is  $\mathcal{C}^1$ .

Given a point  $x_0 \in \mathbb{R}^n$ , and a  $\mathcal{C}^1$  feedback control law

$$u = u(x) \quad (2.23)$$

such that the system is locally asymptotically stable at the equilibrium point  $x_0$  and without loss of generality, assume  $x_0 = 0$ .

**Lemma 2.3.1 (Brockett's necessary condition) [42]** : A necessary condition for the existence of a class  $\mathcal{C}^1$  feedback control scheme (2.23) rendering  $x_0 \in \mathbb{R}^n$  locally asymptotically stability for the closed-loop system (2.22) is that for all  $\|y\|$  is sufficiently small, the vector field  $\tilde{f} : \mathbb{R}^n \mapsto \mathbb{R}^n$  defined by

$$\tilde{f}(x) = f(x, u) - y \quad (2.24)$$

where  $f$  is defined in (2.22), which has an equilibrium point.

## CHAPTER. 3

---

# REVIEW OF CONTROL THEORIES AND BASIC CONCEPT

---

The previous chapter has introduced some mathematical background for controlling TWMR systems. Before diving into the main contents, it is necessary to review some basic concepts related to this thesis. Section 3.1 presents the fundamental control concepts, involving state-space representation and the state and output feedback controls. The background knowledge of the SMC will be introduced in Section 3.2. Specifically, the existence of sliding motion and solution of discontinuous systems is going to be discussed in Section 3.2.1 and 3.2.2, respectively. Section 3.2.3 will deliver two approaches for the derivation of the reduced-order sliding mode dynamics to facilitate the stability analysis during the sliding phase. The condition of the reaching phase will be studied in Section 3.2.4 to guarantee the reachability of the system trajectory. Then, Section 3.2.5 summarises the characteristics of the conventional SMC methodology. Before concluding this chapter, the nonholonomic and Pfaffian constraints with a nonholonomic bicycle example will be reviewed in Section 3.3.

## 3.1. FUNDAMENTAL CONTROL CONCEPTS

### 3.1.1. STATE SPACE REPRESENTATION

The term "state-space" refers to a collection of coupled first-order differential equations with a set of internal variables, which is the fundamental concept of modern control theory. State variables represent a minimal set of variables that can fully describe the system with its response to any given set of inputs. Moreover, the outputs describe a collection of algebraic equations with the relationship between the state variables and the physical output variables. Figure 3.1 illustrates the  $n$ -th order system in state-space representation with  $m$  input and  $p$  outputs.

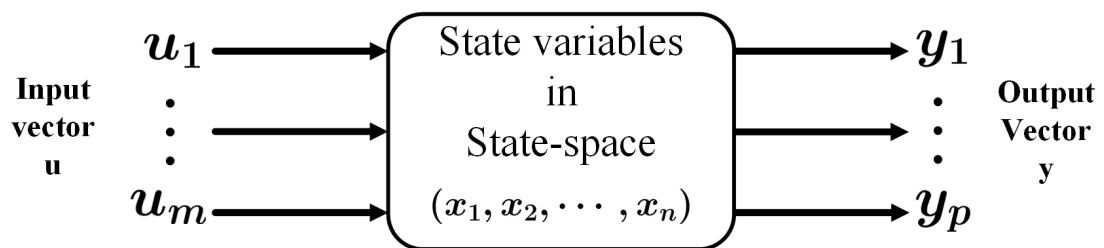


Figure 3.1: Diagram of system in state-space representation

As mentioned previously, the system dynamics in Figure 3.1 can be described as a series of first-order differential equations by

$$\begin{aligned}
 \dot{x}_1(t) &= f_1(t, x, u) \\
 \dot{x}_2(t) &= f_2(t, x, u) \\
 &\dots \\
 \dot{x}_n(t) &= f_n(t, x, u)
 \end{aligned} \tag{3.1}$$

where  $\dot{x}_i = dx/dt$  for  $i = 1, 2, \dots, n$ .  $t \in \mathbb{R}^+$  is the time variable.  $x(t) = [x_1(t), x_2(t), \dots, x_n(t)]^T \in \mathbb{R}^n$  represents the system states.  $u(t) = [u_1(t), u_2(t), \dots, u_m(t)]^T \in \mathbb{R}^m$  denotes the system input vector. Moreover,  $f(t, x, u) = [f_1(t, x, u), f_2(t, x, u), \dots, f_n(t, x, u)]^T$  corresponds to the system dynamics in terms of the time  $t$ , state variables  $x$ , and input vector

$u$ .

Further, the associated output vector can be described as

$$\begin{aligned} y_1(t) &= h_1(t, x) \\ y_2(t) &= h_2(t, x) \\ &\dots \\ y_p(t) &= h_p(t, x) \end{aligned} \tag{3.2}$$

where  $y(t) = [y_1(t), y_2(t), \dots, y_p(t)]^T \in \mathbb{R}^p$  represents the system outputs.  $h_i(t, x)$  is the output dynamics for  $i = 1, 2, \dots, p$ .

Based on (3.1) and (3.2), the corresponding system dynamics can be rewritten by

$$\dot{x}(t) = f(t, x, u) \tag{3.3}$$

$$y(t) = h(t, x) \tag{3.4}$$

Now, a system is called *single-input single-output* (SISO) if the input and output dimensions are configured to one, i.e.,  $m = 1, p = 1$  of (3.1)-(3.2) and the system is called *multi-input multi-output* (MIMO) if  $m$  and  $p$  are greater than one.

To further elucidate the concepts of feedback control, consider the time-invariant linear system as follows [1].

$$\dot{x}(t) = Ax(t) + Bu(t) \tag{3.5}$$

$$y(t) = Cx(t) \tag{3.6}$$

where  $A \in \mathbb{R}^{n \times n}$ ,  $B \in \mathbb{R}^{n \times m}$ , and  $C \in \mathbb{R}^{p \times n}$  represent the constant matrices. Moreover, assume the pairs  $(A, B)$  and  $(A, C)$  are controllable and observable, respectively. The block diagram of the system (3.5) and (3.6) can be illustrated in Figure 3.2.

### 3.1.2. TYPES OF FEEDBACK CONTROL

Feedback control has been one of the most rigorously research topics in recent decades, and it has evolved into the fundamental mechanism for regulating equilibrium or homeostasis for mechanical, electrical, biological systems, etc. According to the mathematical and control theories, the appropriate feedback control law is designed to determine control signals based on the difference between the actual system states variables

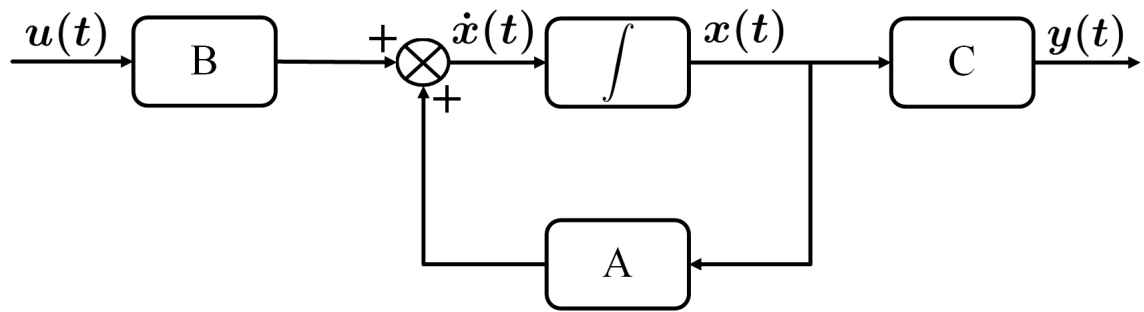


Figure 3.2: Block diagram of the time-invariant linear system

and their desired states. Thus, the closed-loop control schemes ensure that the system will always make adjustments towards the desired equilibrium. Furthermore, it is consensus that the controlled system may fail to satisfy the desired performance or even result in instability for practical systems due to modelling errors and external disturbances. As a result, the effect of these uncertainties on the control design process should be carefully considered to ensure that the system can still be adequately controlled in the worst-case scenarios.

From the control theory perspective, the types of feedback controls can be categorised as *state feedback control* and *output feedback control* [67]. For output feedback controls, there are two primary interesting research fields, the former is the *static output feedback control*, and the latter is the *dynamic output feedback control* [116].

The *state feedback control* is relevant to the control design that employs the entire system state for utilisation of controller  $u(t)$ . The system output matrix  $C$  is configured to be the identity matrix for state feedback control. Because the state at time  $t$  contains all of the information necessary to predict the system's future behaviour, the most general time-invariant control law is a function of the state, i.e.,  $u(t) = u(x(t))$ . If a linear state feedback is applied to the system (3.5)-(3.6), the control law  $u(t)$  can be written as

$$u(t) = -K_s x(t) \quad (3.7)$$

where  $K_s \in \mathbb{R}^{m \times n}$  is a designed constant matrix, the negative sign indicates that the negative feedback is considered in this case.

The associated closed-loop system obtained when the feedback control (3.7) is ap-

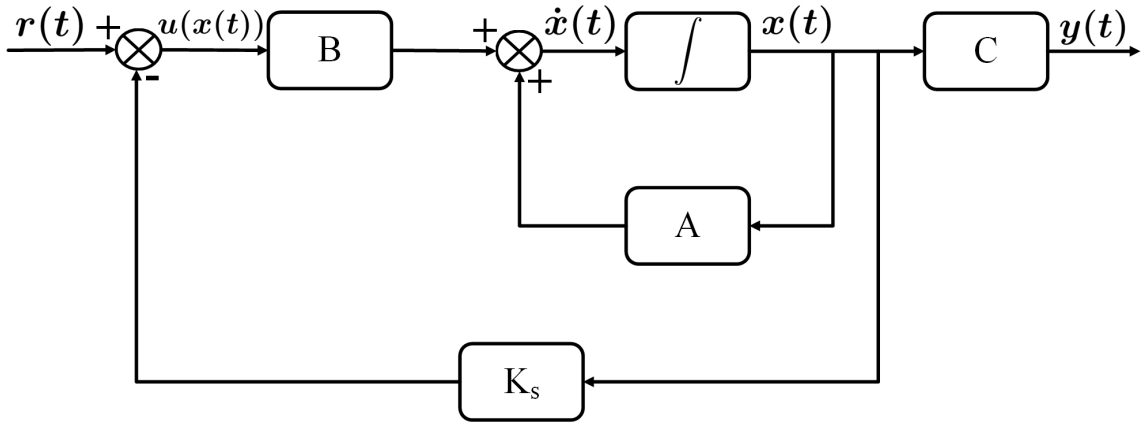


Figure 3.3: Block diagram of the state feedback control for system (3.5)

plied to the system (3.5)-(3.6) can be described by

$$\dot{x}(t) = (A - BK_s)x(t) \quad (3.8)$$

Then, the state feedback control design problem is to determine an appropriate feedback gain matrix  $K_s$  such that the  $(A - BK_s)$  matrix of the closed-loop system is Hurwitz stable. This control problem is called the *eigenvalue assignment problem* or the *pole placement problem*. Moreover, it is well-known from the linear control theory that the poles of a linear time-invariant controllable and observable system can be assigned arbitrarily by state feedback. The corresponding block diagram of a state feedback control is depicted in Figure 3.3 and  $r(t)$  is the reference signal of the system.

From the practical perspective, however, it may not be feasible to access all the state information for system (3.5) and (3.6). If only a subset of state variables is available, the dimension of the output matrix  $C$  of (3.6) would be less than the dimension of the system states, i.e.,  $p < n$  and  $p$  denotes the dimension for the numbers of accessible states. The control law, in this case, utilises only the output information  $y(t)$  represented as  $u(t) = u(y(t))$  and  $u(y(t))$  is known as *static output feedback control scheme* and the corresponding output control law can be described as

$$u(t) = -K_o C x(t) = -K_o y(t) \quad (3.9)$$

where  $K_o \in \mathbb{R}^{m \times p}$  is the designed gain matrix. It should be mentioned that the dimension of matrix  $K_o$  is different from the dimension of matrix  $K_s$  in which  $K_s$  is dependent on the full-state variables, whereas  $K_o$  is subjected to the output information.

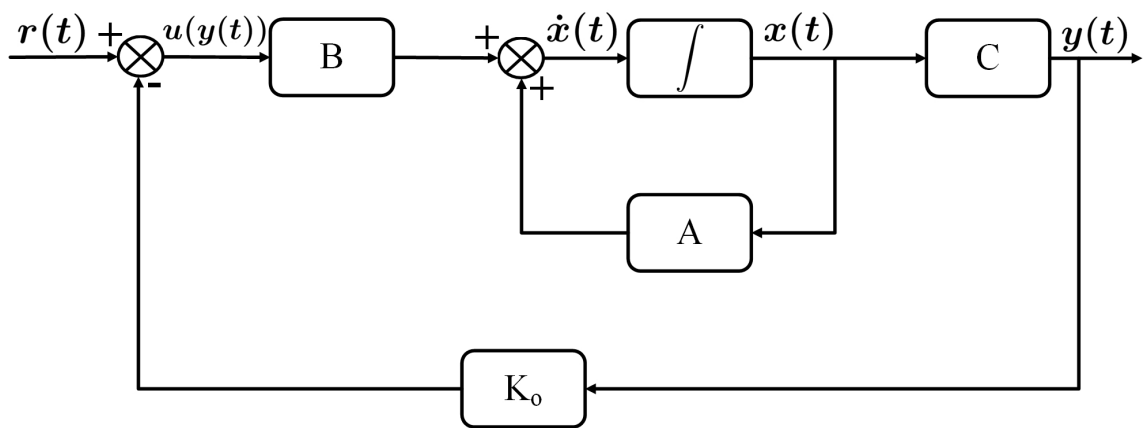


Figure 3.4: Block diagram of the static output feedback control for systems (3.5) and (3.6)

Applying the static output feedback control law (3.9) to system (3.5) and (3.6), the associated closed-loop dynamics can be described by

$$\dot{x}(t) = (A - BK_oC)x(t) \quad (3.10)$$

Further, the static output feedback control problem aims to find a suitable gain matrix  $K_o$  such that  $(A - BK_oC)$  is Hurwitz stable. Figure 3.4 illustrates the block diagram of the static output feedback control.

In contrast to the process of finding the gain matrix  $K_s$  of the state feedback control, it is not straightforward to obtain the gain  $K_o$  of the static output feedback control such that the poles can be placed arbitrarily as mentioned in [119]. Although several methodologies have been introduced in [119] to acquire a gain  $K_o$  for stabilisation of SISO systems, such as Youla parameterization method, inverse linear-quadratic approach, covariance assignability by output feedback, output structural constraint approach, coupled linear matrix inequality formulation, nonlinear programming methods, and decision methods. The detailed descriptions of these methods can be discovered in [119]. Nevertheless, all the proposed methods mentioned above cannot be readily applied to the MIMO systems. For the pole placement problem, it has been shown that if the system is minimal (i.e., controllable and observable) and the matrices  $B$  and  $C$  have full ranks, then for almost all the pairs  $(B, C)$ , an output feedback gain can be found so that  $A - BK_oC$  has  $\min(n, m + p - 1)$  poles can be assigned arbitrarily using output feedback [123, 124, 125, 126]. Moreover, it is also shown from [126, 127, 128] that the "Kimura-

Davison" sufficient condition for the existence of gain  $K_o$  is provided as follow.

$$m + p - 1 \geq n \quad (3.11)$$

Although there exists above-mentioned approaches to determine the gain  $K_o$ , the static output feedback problems are still an open unsolved problem due to the computational complexity issue [129, 130, 131].

For the situations where the condition (3.11) fail to satisfy or the solution set of obtaining gain matrices  $K_o$  is restricted. In this case, the *dynamic output feedback control* is necessary. In essence, the dynamic output feedback control is a state feedback control in conjunction with a dynamical system whose objective is to estimate the system state and the resulting estimated state is denoted as  $\hat{x}(t)$ . Such the dynamical system is called a *compensator* or an *observer*, which can be defined by

$$\dot{\hat{x}}(t) = (A + LC)\hat{x}(t) + Bu(t) - Ly(t) \quad (3.12)$$

where  $L$  is a designed constant matrix to guarantee the matrix  $A + LC$  has negative real parts. Further, if the error between the real state and the estimated state is defined as

$$e(t) = x(t) - \hat{x}(t) \quad (3.13)$$

Then the associated error dynamics can be described by

$$\dot{e}(t) = (A + LC)e(t) \quad (3.14)$$

It is noticeable from (3.14) that the matrix  $(A + LC)$  is stable from chosen  $L$  in (3.12). The error  $e(t)$  will converge to zero as  $t$  goes to infinity. Hence, the estimated state  $\hat{x}(t)$  will converge to the real state  $x(t)$  [1].

From a real engineering perspective, it is impractical to neglect the uncertainties in the nominal systems (3.5) and (3.6). Without loss of generality, systems (3.5)-(3.6) with considerations of uncertainties can be described as

$$\dot{x}(t) = Ax + B(u(t) + \Phi(t, x)) + \Psi(t, x) \quad (3.15)$$

$$y(t) = Cx(t) \quad (3.16)$$

where  $\Phi(t, x) \in \mathbb{R}^m$  represents the uncertainty acting in the input channels, which refers to the *matched uncertainty*.  $\Psi(t, x) \in \mathbb{R}^n$  denotes the *unmatched uncertainty*, which does not act in the input channels.

Applying the state feedback control (3.7) and static output feedback control (3.9) to the systems (3.15)-(3.16), the corresponding closed-loop dynamics can be written as

$$\dot{x}(t) = (A - BK_s)x(t) + B\Phi(t, x) + \Psi(t, x) \quad (3.17)$$

$$\dot{x}(t) = (A - BK_oC)x(t) + B\Phi(t, x) + \Psi(t, x) \quad (3.18)$$

It can be seen from (3.17) and (3.18) that both systems are affected by the matched and unmatched uncertainties. Therefore, it is paramount to design robust state/output feedback control schemes to attenuate such uncertainties. Furthermore, this thesis considers the design of both state and static output feedback control laws.

## 3.2. SLIDING MODE CONTROL

By utilising a discontinuous control signal, sliding mode control modifies the system dynamics. This approach has been extensively developed and applied with other control approaches in theoretical research and engineering design to solve a variety of control problems [30, 31, 33, 35]. The following example will be provided to gain an intuitive understanding of the subsequent SMC concepts.

Consider a simple stick balancing example [1] illustrated in Figure 3.5. Assuming the stick is nearly at the equilibrium point in the vertical position with small  $\theta$ . Define the state as  $x(t) = [x_1(t), x_2(t)]^T = [x_s(t), \dot{x}_s(t)]^T$  where  $x_s(t)$  and  $\dot{x}_s(t)$  denote the displacement and velocity of the stick, respectively. The associated linear system can be represented in state-space as

$$\begin{bmatrix} \dot{x}_1(t) \\ \dot{x}_2(t) \end{bmatrix} = \begin{bmatrix} 0 & 1 \\ \frac{g}{L} & 0 \end{bmatrix} \begin{bmatrix} x_1(t) \\ x_2(t) \end{bmatrix} + \begin{bmatrix} 0 \\ -\frac{g}{L} \end{bmatrix} u(t) \quad (3.19)$$

where  $L$  is the length of the stick,  $g$  is the gravitational acceleration.

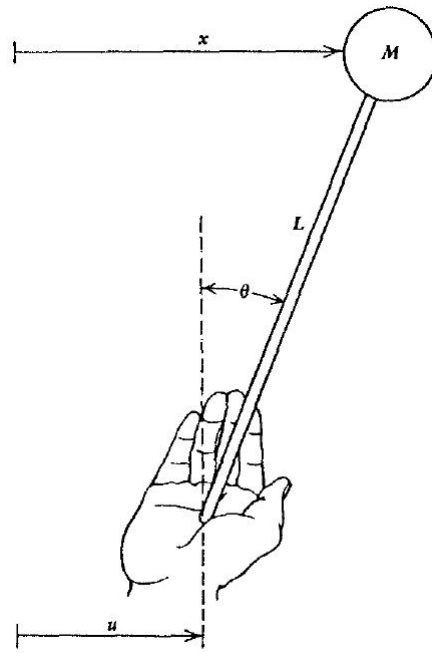


Figure 3.5: Stick balancing example referenced from [1]

Further, employ a traditional linear *switching function* as

$$\sigma(x(t)) = \varpi x_1(t) + x_2(t) \quad (3.20)$$

where  $\varpi$  denotes a designed parameter. And the state feedback discontinuous SMC law can be presented by

$$u(t) = \begin{cases} \frac{L}{g} (\varpi x_2 + \frac{g}{L} x_1 - \delta), & \text{if } \sigma(x(t)) < 0. \\ \frac{L}{g} (\varpi x_2 + \frac{g}{L} x_1 + \delta), & \text{if } \sigma(x(t)) > 0. \end{cases} \quad (3.21)$$

where  $\delta$  is a positive constant.

By configuring  $L = 1$ ,  $g = 9.81$  and choosing  $\varpi = 2$ ,  $\delta = 4$  with the initial condition  $x_0 = [x_{10}, x_{20}]^T = [1, 0]^T$ , the corresponding time responses of the system states and the phase portrait are illustrated in Figures 3.6 and 3.7, respectively.

In Figure 3.7, the sliding surface is presented by the red dotted-dashed line and the system trajectory is illustrated in blue color. It is obvious to see from Figure 3.7 that the system motion of the SMC methodology can be divided into two phases: the *sliding phase* and *reaching phase* [116].

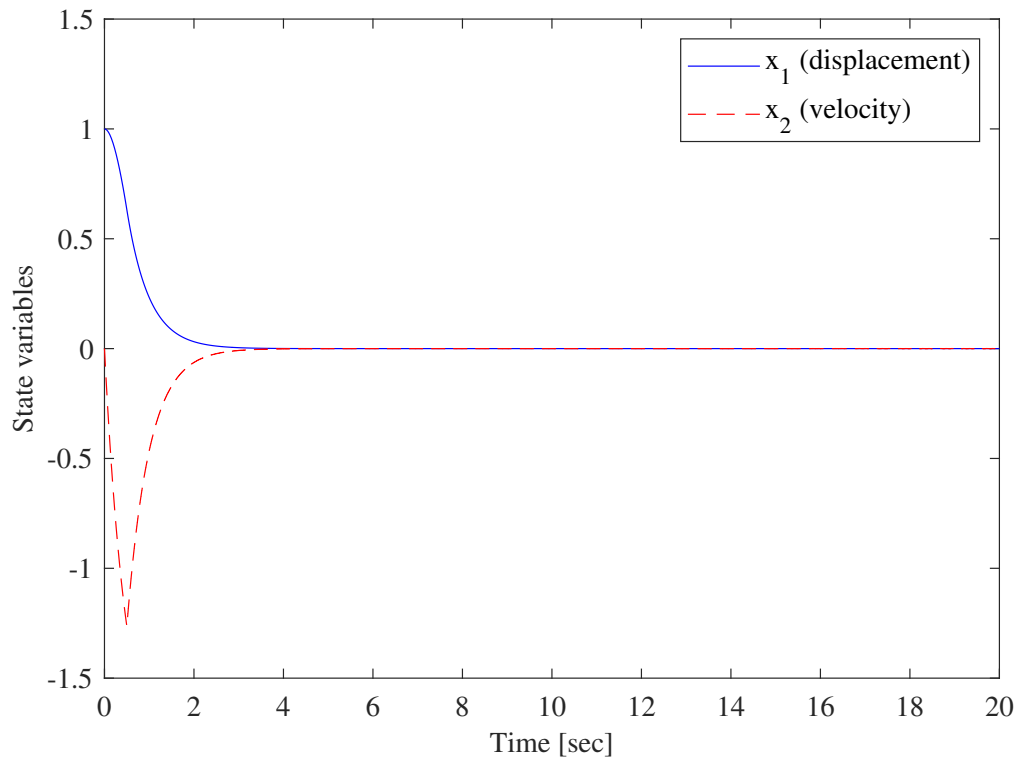


Figure 3.6: State responses of the stick balancing example

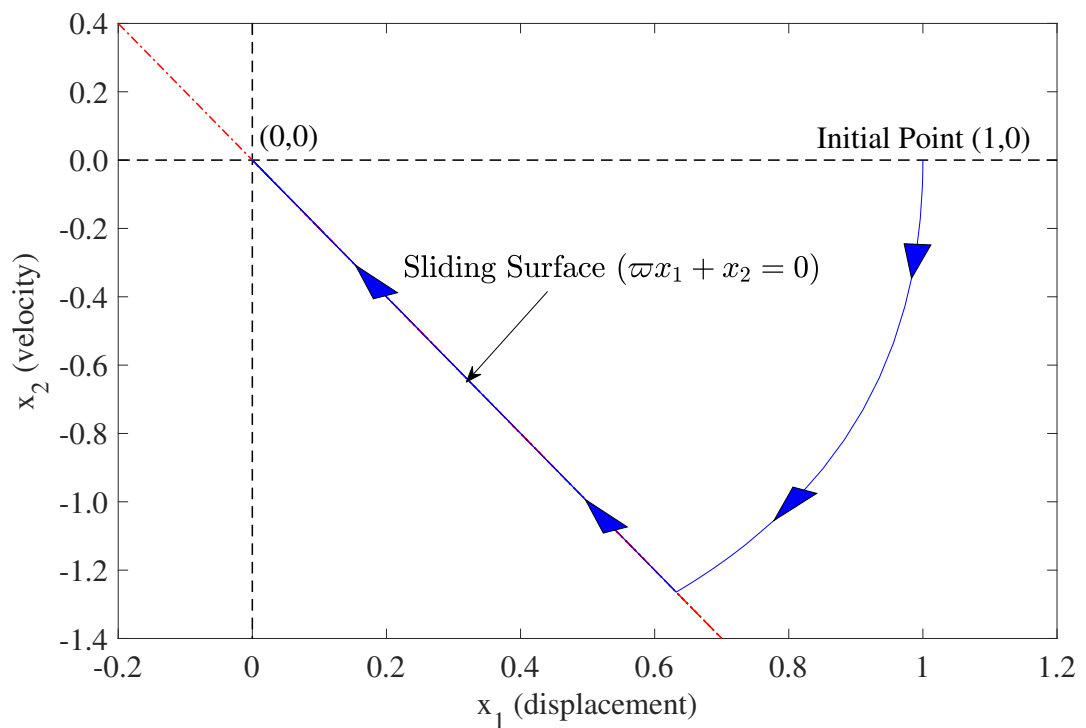


Figure 3.7: Phase portrait of the stick balancing example

- **Sliding Phase** refers to the motion when the system trajectory moves along the sliding surface which is designed by a predefined switching function, such as (3.20) in the stick balancing example.
- **Reaching Phase** denotes the motion when the system trajectory drives from the initial point towards the sliding surface.

Therefore, the design process of SMC can now be described in the following two steps.

**Step 1:** The design of a sliding surface such that the system achieves the desired performance when it is limited to the sliding hyperplane.

**Step 2:** The design of a sliding mode control law that drives the system to the sliding surface in finite time and maintains a sliding motion on it thereafter.

### 3.2.1. EXISTENCE OF THE SLIDING MOTION

The conditions for the existence of the sliding motion can be treated as a generic stability problem which requires the convergence of system states to the vicinity of the predefined sliding surface [2].

Consider the system as follows.

$$\dot{x}(t) = F(t, x) + G(t, x)u(t) \quad (3.22)$$

where  $x(t) \in \mathbb{R}^n$ ,  $F(t, x) \in \mathbb{R}^n$ ,  $G(t, x) \in \mathbb{R}^{n \times m}$  and  $u(t)$  is the discontinuous control law defined by

$$u(t) = \begin{cases} u^+(t, x), & \text{if } \sigma(x(t)) > 0. \\ u^-(t, x), & \text{if } \sigma(x(t)) < 0. \end{cases} \quad (3.23)$$

and the sliding surface with  $(n - m)$ -dimension is defined by

$$\sigma(x(t)) = [\sigma_1(x(t)), \sigma_2(x(t)), \dots, \sigma_m(x(t))] = 0 \quad (3.24)$$

**Definition 3.1 (Domain of the Sliding Motion) [2]:** A domain  $S$  in the manifold  $\sigma(x(t)) = 0$  is said to be a sliding mode domain if for each  $\epsilon > 0$ , a  $\delta > 0$  exists such that any motion

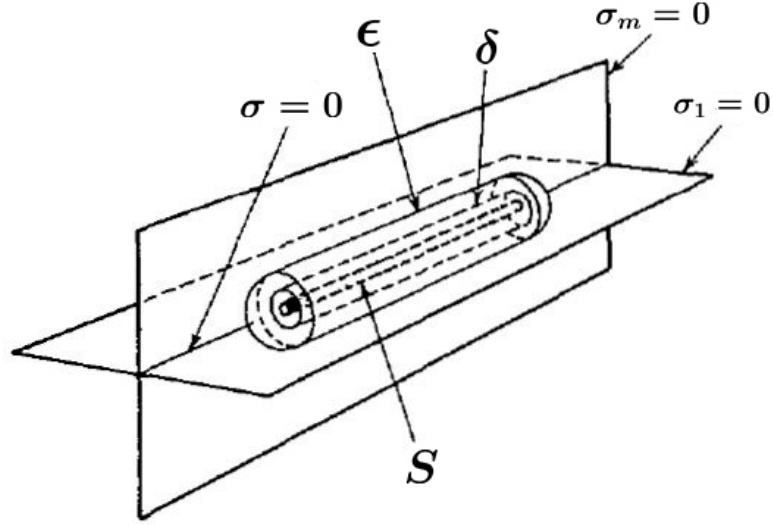


Figure 3.8: Domain of the sliding motion modified from [2]

starting in the  $n$ -dimensional  $\delta$ -vicinity of  $S$  may leave the  $n$ -dimensional  $\epsilon$ -vicinity of  $S$  only through the  $n$ -dimensional  $\epsilon$ -vicinity of the boundaries of  $S$  (See Figure 3.8).

Having defined the definition of the sliding mode domain, the existence of the sliding motion can be presented in the following Theorem.

**Theorem 3.1 (Existence of the Sliding Motion) [2]:** For the  $(n - m)$ -dimensional domain  $S$  to be the domain of sliding mode, it is sufficient that in some  $n$ -dimensional domain  $\Omega$ ,  $S \subset \Omega$ , there exists a  $C^1$  (Definition 2.3.1 in Section 2.3) function  $V(t, x, \sigma)$ , satisfying the following conditions.

- $V$  is positive definite with respect to  $\sigma(x(t))$  and for any  $x \in S$  and  $t$

$$\inf_{\|\sigma\|=\beta} V = h_\beta, \quad \sup_{\|\sigma\|=\beta} V = H_\beta \quad (3.25)$$

where  $\beta$  is a positive constant,  $h_\beta \neq 0$ ,  $h_\beta$  and  $H_\beta$  depend only on  $\beta$ .

- Time derivative of  $V$  for system (3.22) has negative supremum on small enough sphere  $\|\sigma\| = \beta$  with removed points on the discontinuity surfaces where this derivative does not exist.

The dynamics of the sliding motion (3.24) can be written as

$$\dot{\sigma}(x(t)) = \frac{\partial \sigma}{\partial x} F(t, x) + \frac{\partial \sigma}{\partial x} G(t, x) u(t) \quad (3.26)$$

where  $\sigma$  is defined in (3.24),  $F(t, x)$ ,  $G(t, x)$  and  $u(t)$  are specified in (3.22), respectively.

Moreover, the domain  $S$ , illustrated in Figure 3.8, is a set of  $x$  for which the origin in subspace  $[\sigma_1, \sigma_2, \dots, \sigma_m]$  is an asymptotically stable equilibrium point for the dynamics (3.26). For the positive definite function  $V$  mentioned in (3.25), there is no systematic approach to generate such Lyapunov function  $V$  for system (3.26).

### 3.2.2. EXISTENCE OF SOLUTION FOR DISCONTINUOUS SYSTEMS

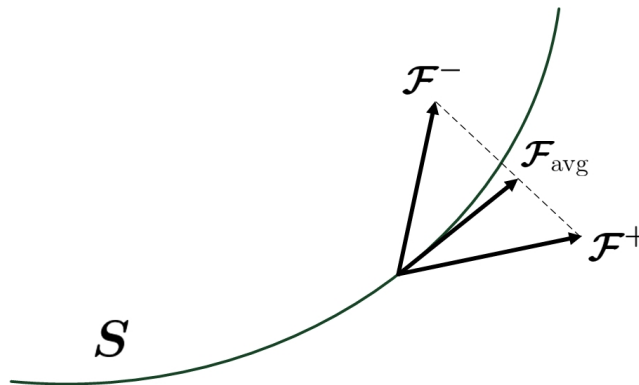


Figure 3.9: Ideas of the Filippov approach for solving discontinuous right-hand side dynamical equations

From (3.23), it is obvious to see that the controller is discontinuous. When (3.23) is applied to the system (3.22), the closed-loop system will contain a set of ordinary differential equations with discontinuous right hand side, which can be described as follows.

$$\dot{x}(t) = \mathcal{F}(t, x) \quad (3.27)$$

where  $\mathcal{F} : \mathbb{R} \times \mathbb{R}^n \mapsto \mathbb{R}^n$  is discontinuous with respect to the state vector.

For system (3.27), it may not be feasible to obtain the solutions using the classical method of differential equations as Lipschitz conditions (Definition 2.1.4 of Section 2.1) are usually involved to ensure the existence of a unique solution and any function satisfying Lipschitz conditions is necessarily continuous. Therefore, as mentioned in [116, 67, 132], an alternative approach has been proposed by Filippov [133, 134] for system (3.27) by producing the 'average' of the solutions obtained from approaching the

point of discontinuity with two different solution vectors. Define  $x_0$  is a point of discontinuity on the surface  $S$  and  $\mathcal{F}^-(t, x_0)$  and  $\mathcal{F}^+(t, x_0)$  denote the limits of  $\mathcal{F}(t, x)$  as the point  $x_0$  is approached from opposite sides of the tangent plane to  $S$  at  $x_0$ , then the solution of (3.27) can be retrieved from the following equation [116, 133]

$$\dot{x}(t) = \mathcal{F}_{\text{avg}}(t, x) = (1 - \gamma)\mathcal{F}^-(t, x) + \gamma\mathcal{F}^+(t, x) \quad (3.28)$$

where  $\gamma$  is a constant satisfying  $0 < \gamma < 1$ ,  $\mathcal{F}_{\text{avg}}$  is tangent to the surface  $S$  as illustrated in Figure 3.9.

### 3.2.3. EQUIVALENT CONTROL AND REGULAR FORM APPROACHES OF THE SLIDING PHASE

The advantage of the conventional SMC methodology is to employ the *reduced-order sliding mode dynamics* to facilitate the stability analysis.

Reconsider the system (3.22) with the following sliding surface

$$\sigma(t) = \sigma(x(t)) \quad (3.29)$$

such that the resulting sliding motion satisfies the desired system performance.

In SMC theory, there are two approaches commonly used to obtain the sliding mode dynamics, namely the *equivalent control* and the *regular form*, which transform the stability of the sliding motion to the problem of guaranteeing the stability of an unforced system.

- **Equivalent Control:** When the system (3.22) is restricted to the sliding surface, it follows that

$$\sigma(x(t)) = 0, \quad \text{and} \quad \dot{\sigma}(x(t)) = 0 \quad (3.30)$$

The time derivative of  $\sigma(x(t))$  along the system (3.22) is described by

$$\dot{\sigma}(x(t)) = \frac{\partial \sigma}{\partial x} \dot{x}(t) = \frac{\partial \sigma}{\partial x} (F(t, x) + G(t, x)u(t)) \quad (3.31)$$

During the sliding motion and from (3.30), it follows that

$$\frac{\partial \sigma}{\partial x} (F(t, x) + G(t, x)u(t)) = 0 \quad (3.32)$$

Further, assume a solution  $u(t)$  in (3.32) can be defined as

$$u(t) = u_{eq}(t, x) \quad (3.33)$$

where  $u_{eq}$  represents the *equivalent control* [132].

Then the reduced-order sliding mode dynamics governed by the sliding motion can be described by

$$\dot{x}(t) = F(t, x) + G(t, x)u_{eq}(t, x) \quad \text{when} \quad \sigma(x(t)) = 0 \quad (3.34)$$

According to (3.30), the associated equivalent control is derived as

$$u_{eq}(t) = - [\sigma(x(t))G(t, x)]^{-1} \sigma(x(t))F(t, x) \quad (3.35)$$

where  $\sigma(x(t))G(t, x)$  must be non-singular for the chosen switching function  $\sigma(x(t))$ .

Applying the equivalent control (3.35) to the system (3.22), the corresponding reduced-order sliding mode dynamics can be described by

$$\dot{x}(t) = F(t, x) - G(t, x) [\sigma(x(t))G(t, x)]^{-1} \sigma(x(t))F(t, x) \quad (3.36)$$

It is worth noting that the equivalent control (3.35) is used solely to analyse the stability of the sliding motion. Although this is not the actual control law applied to the system (3.22), it can be thought of as the control signal that must be applied "on average" to maintain the sliding motion [132, 2].

- **Regular Form:** Another technique to obtain the sliding mode dynamics associated with the sliding surface (3.30) is the well-known *regular form* approach. To elucidate this method, reconsider the time-invariant linear system of (3.5) in Section 3.1.1.

Assume the matrix  $B$  is full rank, i.e.,  $\text{rank}(B) = m$ . There exists a coordinate transformation with an invertible matrix  $T_r \in \mathbb{R}^{n \times n}$  such that the matrix  $\bar{B}$  in the

new coordinate can be decomposed as follows.

$$\bar{B} = T_r B = \begin{bmatrix} 0 \\ \bar{B}_2 \end{bmatrix} \quad (3.37)$$

where  $\bar{B}_2 \in \mathbb{R}^{m \times m}$ .

By using the transformation  $\omega(t) = T_r x(t)$ , the system (3.5) can be derived as

$$\dot{\omega}_1(t) = \bar{A}_1 \omega_1(t) + \bar{A}_2 \omega_2(t) \quad (3.38)$$

$$\dot{\omega}_2(t) = \bar{A}_3 \omega_1(t) + \bar{A}_4 \omega_2(t) + \bar{B}_2 u(t) \quad (3.39)$$

where  $\omega(t) = [\omega_1(t), \omega_2(t)]^T \in \mathbb{R}^n$ ,  $\omega_1(t) \in \mathbb{R}^{n-m}$ ,  $\omega_2(t) \in \mathbb{R}^m$ , and

$$\bar{A} = T_r A T_r^{-1} = \begin{bmatrix} \bar{A}_1 & \bar{A}_2 \\ \bar{A}_3 & \bar{A}_4 \end{bmatrix} \quad (3.40)$$

**Lemma 3.1 [116]:** The matrix pair  $(\bar{A}_1, \bar{A}_2)$  of system (3.38) is controllable if and only if the pair  $(A, B)$  of system (3.5) is controllable.

The systems (3.38) and (3.39) are referred to as *regular form* or *canonical form*. It is noticeable that dynamics (3.38) is an unforced system which can be described as the *null space dynamics* whereas the system (3.39) is related to the control law  $u(t)$ , which is described as the *range space dynamics* [116].

Further, define a linear switching manifold

$$\sigma(\omega(t)) = S\omega(t) = S_1 \omega_1(t) + S_2 \omega_2(t) \quad (3.41)$$

where  $S = [S_1 \ S_2] \in \mathbb{R}^{m \times n}$  denotes a constant matrix with  $S_1 \in \mathbb{R}^{m \times (n-m)}$  and  $S_2 \in \mathbb{R}^{m \times m}$ .

And the associated sliding surface is defined by

$$\sigma(\omega(t)) = S_1 \omega_1(t) + S_2 \omega_2(t) = 0 \quad (3.42)$$

When the systems (3.38) and (3.39) are limited to the sliding surface (3.42), it follows that

$$\omega_2(t) = -\frac{S_1}{S_2} \omega_1(t) \quad (3.43)$$

Hence, the sliding mode dynamics can be derived from (3.38) and (3.43)

$$\dot{\omega}_1(t) = \left( \bar{A}_1 - \bar{A}_2 \frac{S_1}{S_2} \right) \omega_1(t) \quad (3.44)$$

It can be seen that (3.44) is a reduced-order dynamics compared to the system (3.5). Moreover, based on Lemma 3.1, since the pair  $(\bar{A}_1, \bar{A}_2)$  is controllable, the reduced-order sliding mode dynamics are asymptotically stable if the matrix  $\left( \bar{A}_1 - \bar{A}_2 \frac{S_1}{S_2} \right)$  is Hurwitz with suitable selections of the parameters  $S_1$  and  $S_2$ .

Now, reconsider the system (3.15) with matched and unmatched uncertainties in Section 3.1.2. By applying the same coordinate transformation using the matrix  $T_r$ , the system (3.15) can be transformed into the following regular form

$$\dot{\omega}_1(t) = \bar{A}_1 \omega_1(t) + \bar{A}_2 \omega_2(t) + \Psi_1(t, T_r^{-1} \omega) \quad (3.45)$$

$$\dot{\omega}_2(t) = \bar{A}_3 \omega_1(t) + \bar{A}_4 \omega_2(t) + \bar{B}_2 (u(t) + \Phi(t, T_r^{-1} \omega)) + \Psi_2(t, T_r^{-1} \omega) \quad (3.46)$$

where  $\Psi_1(\cdot) \in \mathbb{R}^{n-m}$  and  $\Psi_2(\cdot) \in \mathbb{R}^m$  are the subset of the unmatched uncertainty  $\Psi(\cdot)$ .

The associated reduced-order sliding mode dynamics is described by

$$\dot{\omega}_1(t) = \left( \bar{A}_1 - \bar{A}_2 \frac{S_1}{S_2} \right) \omega_1(t) + \Psi_1 \left( t, \omega_1, -\frac{S_1}{S_2} \omega_1 \right) \quad (3.47)$$

By comparing the reduced-order sliding mode dynamics (3.47) with the closed-loop systems (3.17) and (3.18), it can be seen that the sliding mode dynamics are completely insensitive to matched uncertainty  $\Phi(\cdot)$  and are only partially affected by the unmatched one  $\Psi_1(\cdot)$ . However, the systems (3.17)-(3.18) contain both the matched and unmatched uncertainties with the utilisation of the full-state variable after applying the state and static output feedback controls. Therefore, The particular structure of the sliding mode dynamics reduces the conservatism of the stability analysis, which is an excellent advantage of employing the sliding mode dynamics of the SMC paradigm [116, 67].

### 3.2.4. CONDITIONS OF THE REACHING PHASE

Having described the approaches of the sliding phase for deriving the reduced-order sliding mode dynamics to underpin the stability analysis. This section will introduce the

control design and the conditions to guarantee the system trajectories to reach the sliding surface (3.42) in finite time and maintain on it afterwards.

For the nominal system (3.22), the discontinuous control signal  $u(t)$  can be defined by [116]

$$u(t) = u_{eq}(t) + u_{sw}(t) \quad (3.48)$$

where  $u_{eq}(t)$  represents the equivalent control component to maintain the ideal sliding motion, and  $u_{sw}(t)$  denotes the discontinuous switching component.

$$u_{eq}(t) = - \left( S\bar{B} \right)^{-1} S\bar{A}\omega(t) \quad (3.49)$$

$$u_{sw}(t) = - \left( S_2\bar{B}_2 \right)^{-1} \rho \frac{\sigma(\omega(t))}{\|\sigma(\omega(t))\|} \quad (3.50)$$

where  $\rho$  is a positive scalar and  $S\bar{B} = S_2\bar{B}_2$  from (3.37) and (3.41).

From the switching function (3.41) and applying control law (3.48) using (3.49)-(3.50) yields

$$\begin{aligned} \dot{\sigma}(t) &= S\dot{\omega}(t) = S \left( \bar{A}\omega(t) + \bar{B}u(t) \right) = S\bar{A}\omega(t) + S\bar{B} \left( u_{eq}(t) + u_{sw}(t) \right) \\ &= -\rho \frac{\sigma(\omega(t))}{\|\sigma(\omega(t))\|} \end{aligned} \quad (3.51)$$

Then, it follows that

$$\sigma^T(t)\dot{\sigma}(t) = -\rho \frac{\sigma^T(t)\sigma(\omega(t))}{\|\sigma(\omega(t))\|} \leq -\rho\|\sigma(\omega(t))\| \quad (3.52)$$

The inequality (3.52) is the so-called *reachability condition* and  $\rho$  is called the *reachability constant* [116, 132]. It is worth mentioning that (3.52) guarantees the system trajectories reach the sliding surface in finite time (i.e., stability of the sliding surface is better than asymptotic convergence behaviour) as the reaching time can be adjusted based on the changes of the designed parameter  $\rho$ .

Moreover, the unit vector  $\sigma(\omega(t))/\|\sigma(\omega(t))\|$  in control (3.48) with (3.50) can also be written as

$$\frac{\sigma(\omega(t))}{\|\sigma(\omega(t))\|} = \text{sgn}(\sigma(\omega(t))) \quad (3.53)$$

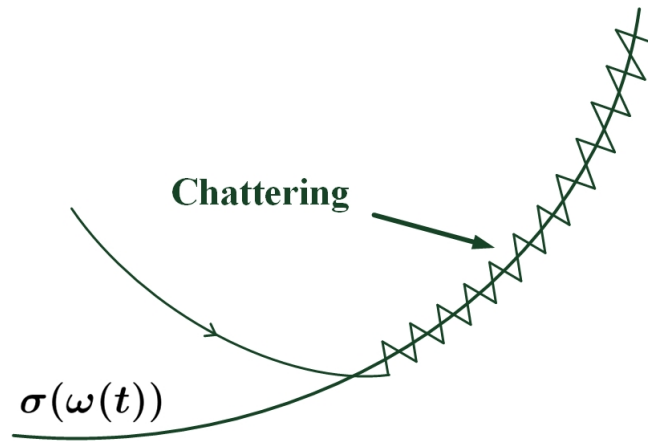


Figure 3.10: The example of chattering phenomenon

where  $sgn(\sigma(\omega(t)))$  is a discontinuous term defined by

$$sgn(\sigma(\omega(t))) = \begin{cases} 1, & \text{if } sgn(\sigma(\omega)) > 0. \\ 0, & \text{if } sgn(\sigma(\omega)) = 0. \\ -1, & \text{if } sgn(\sigma(\omega)) < 0. \end{cases} \quad (3.54)$$

It can be seen that  $sgn(\cdot)$  function is discontinuous, which results in high frequency oscillations when the system trajectories repeatedly cross the sliding surface  $\sigma(\omega(t)) = 0$ . This high frequency motion is referred as *chattering* which is illustrated in Figure 3.10.

Recap the above-mentioned stick balancing example, the control scheme (3.21) can be rewritten using the  $sgn(\cdot)$  function as

$$u(t) = \underbrace{\frac{L}{g}\varpi x_2(t) + x_1(t)}_{u_{eq}(t)} + \underbrace{\frac{L}{g}\delta sgn(\sigma(x(t)))}_{u_{sw}(t)} \quad (3.55)$$

Figure 3.11 shows the time responses of the control law (3.55) for the stick balancing system (3.19). It is obvious to see that the control signal suffers from considerable amount of chattering. Moreover, from the practical engineering perspective, such high frequency oscillations may wear and tear the physical devices, such as motors. For this reason, several chattering-free methods have been proposed to address this issue [135, 136, 137, 138, 139, 116, 140]. The most common approach is to employ a *boundary layer* which approximates the discontinuous  $sgn$  function (3.54) by augmenting a positive scalar in

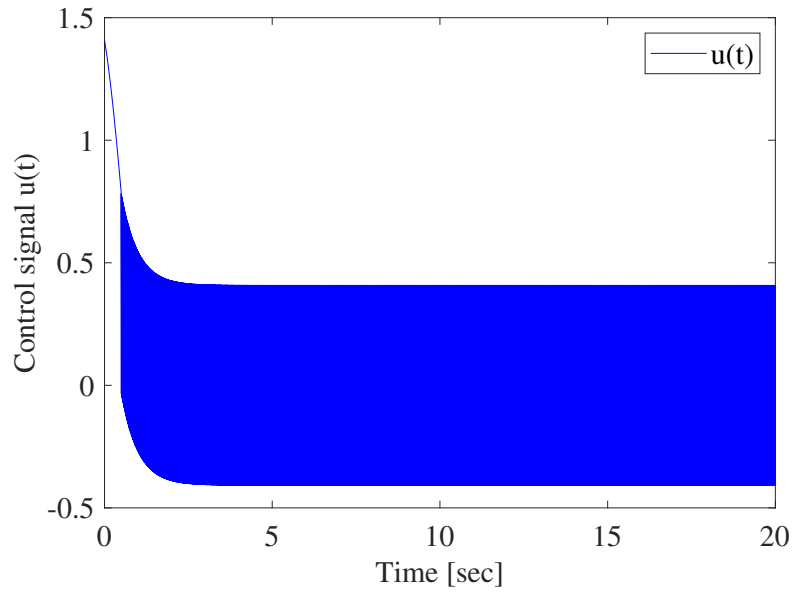


Figure 3.11: The control signal of the stick balancing example with chattering

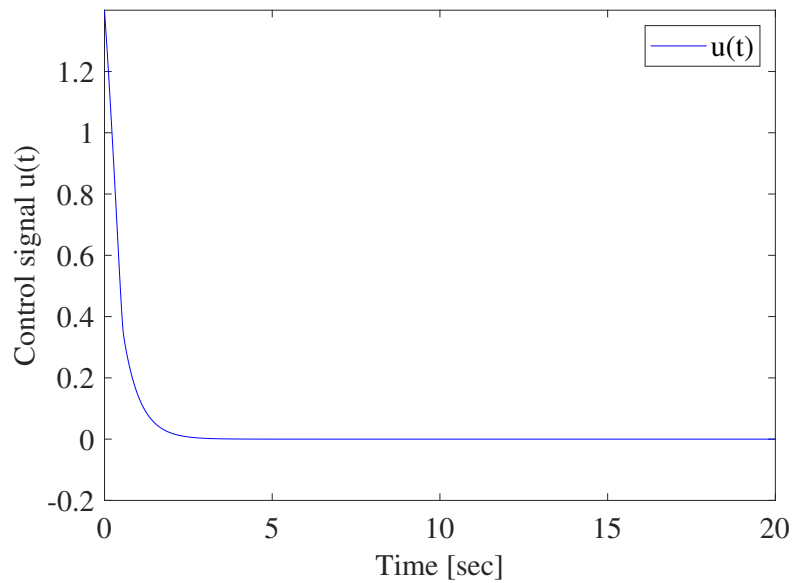


Figure 3.12: The chattering-free control signal of the stick balancing example using smoothing constant  $\eta = 0.05$  in (3.56)

the denominator of the unit vector of (3.53), which is defined by

$$\text{sgn}(\sigma(\cdot)) = \frac{\sigma(\cdot)}{\|\sigma(\cdot)\| + \eta} \quad (3.56)$$

where  $\eta > 0$  is called the smoothing constant.

By replacing the  $\text{sgn}$  function of the control law (3.55) with (3.56) and choosing

$\eta = 0.05$ , the corresponding time response of the chattering-free control signal for the stick balancing example is illustrated in Figure 3.12. It can be seen from Figure 3.12 that the chattering has been significantly reduced.

It is worth mentioning that the smoothing constant  $\eta$  can be selected based on the trial and error technique. Moreover, there is a trade-off between the chattering attenuation and the system performance by the chosen constant  $\eta$ . The larger the value of  $\eta$  is selected, the more the system performance will deteriorate. Therefore,  $\eta$  can be fine tuned for different applications to maximise the performance whilst attenuate chattering as much as possible.

### 3.2.5. CHARACTERISTICS OF THE CONVENTIONAL SMC

From all the background knowledge of SMC described in this section, it is observed that SMC embraces the following characteristics.

- The sliding mode dynamics are a reduced-order system compared to the original system. From the system (3.5), the associated reduced-order sliding mode dynamics using regular form approach is described by (3.44). It can be seen that the dimension of the original system is  $n$ , whereas the order of the sliding mode dynamics is  $n - m$ . Hence, when the sliding motion occurs, the system performance is based solely on the reduced-order sliding mode dynamics, which reduces conservatism from the theoretical point of view.
- In terms of the robustness, the sliding motion is completely insensitive to the matched uncertainty  $\Phi(\cdot)$  from the reduced-order sliding mode dynamics (3.47), which is an excellent feature for dealing with the internal vibrations and noises of the DC motors since the motors can be categorised as the input channels. Moreover, it can be seen from (3.46) that both matched and unmatched uncertainties will affect the reaching phase. Therefore, it is crucial to design robust SMC laws to suppress both uncertainties whilst minimise the time to reach the sliding surface.
- The stability analysis and the design of SMC law comply with the "separation principle". The stability analysis aims to employ the unforced (i.e., independent of control signal) reduced-order sliding mode dynamics to guarantee the performance

when the system moves on the sliding surface. However, the objective of the control design is to drive the system trajectory to the sliding surface in finite time. Therefore, the switching manifold design in sliding phase is usually not dependent on the control scheme. This has advantages when compared to other control methods, such as PID, state and output feedback controls of (3.7) and (3.9). For example, the time responses of the system states are only affected by the reduced-order sliding mode dynamics, which is independent of the control signal. Hence, the performance of the system states can be improved by tuning the parameters of the sliding surface only with the consideration of the sliding mode dynamics rather than the original system. For the reaching phase, the reaching time can be reduced, and the robustness can be enhanced by solely adjusting the design parameters of the SMC law.

### 3.3. NONHOLONOMIC SYSTEMS

This section provides some fundamental knowledge of the nonholonomic systems necessary for the trajectory tracking control in Chapter 4, including the nonholonomic constraint, Pfaffian constraints, and simple example of practical nonholonomic system.

#### 3.3.1. NONHOLONOMIC AND PFAFFIAN CONSTRAINTS

Consider a general electrical or mechanical system as follows.

$$\dot{p}(t) = f(t, p, u) \quad (3.57)$$

where  $p \in \mathbb{R}^n$  and  $u \in \mathbb{R}^m$  represent the vectors of  $n$ -dimensional generalised coordinates and  $m$ -dimensional control input, respectively, which are defined by

$$p = [p_1, p_2, \dots, p_n]^T \quad (3.58)$$

$$u = [u_1, u_2, \dots, u_m]^T \quad (3.59)$$

The corresponding motions of such a system can be expressed as the vector of the

generalised velocities by

$$\dot{p} = [\dot{p}_1, \dot{p}_2, \dots, \dot{p}_n]^T \quad (3.60)$$

Suppose the following form of constraint can be imposed on the system (3.57).

$$g_i(t, p, \dot{p}) = 0, \quad \text{for } i = 1, 2, \dots, m \quad (3.61)$$

The constraint (3.61) is said to be *integrable* if (3.61) can be converted to the following form.

$$G_i(t, p) = 0, \quad \text{for } i = 1, 2, \dots, m \quad (3.62)$$

**Definition 3.2 (Nonholonomic Constraints and Nonholonomic Systems) [141]:** A set of constraints of (3.61) is said to be *nonholonomic constraints* if (3.61) cannot be rendered to (3.62). Otherwise, it is called *holonomic constraints*. Moreover, systems are subject to nonholonomic constraints are said to be *nonholonomic systems*.

The *nonholonomicity* [142] of the system (3.57) arises in several different ways. For example, the number of actuators (control inputs) is less than the number of robot states, i.e.,  $m < n$ , or the robot has redundant degrees of freedom. Moreover, the number of nonholonomicity can be determined from the difference  $n - m$ . For example, a differential-drive TWMR has two motors acting as the control inputs, that is,  $m = 2$ , and three degrees of freedom, that is,  $n = 3$ . Hence, the number of nonholonomic constraints will be  $n - m = 1$ .

**Definition 3.3 (Pfaffian constraints) [141]:** A nonholonomic constraint is called a Pfaffian constraint if it is linear in  $\dot{p}$ , that is, if it can be written as

$$\zeta_i(p)\dot{p} = 0, \quad \text{for } i = 1, 2, \dots, m \quad (3.63)$$

where  $\zeta_i(p)$  are linearly independent row vectors and  $p$  is defined in (3.58).

Moreover, the Pfaffian constraint (3.63) can be described in compact matrix form as

$$M(p)\dot{p} = 0, \quad \text{with } M(p) = \begin{bmatrix} \zeta_1(p) & \zeta_2(p) & \dots & \zeta_m(p) \end{bmatrix} \quad (3.64)$$

Although it has been demonstrated that the nonholonomic systems are controllable [143, 144, 145], the motion control of nonholonomic systems is still challenging. Particularly for the *driftless* nonholonomic system described below.

$$\dot{p}(t) = \sum_{i=1}^m h_i(t, x) u_i(t) \quad (3.65)$$

where  $h_i(t, x) \in \mathbb{R}^n$  is a set of continuously differentiable functions.

Based on Brockett's necessary condition from Lemma 2.3.1, there exists a continuous time-invariant state feedback control scheme for system (3.65) if and only if the numbers of states and inputs are identical (See Theorem 1 in [7]). For the TWMR system, however, the dimension of degrees of freedom is greater than the dimension of the inputs. Hence, the continuous time-invariant state feedback controller is infeasible for the motion control of the driftless system. Therefore, alternative methods have been enormously investigated by employing time-varying, and discontinuous time-invariant control methodologies [56].

### 3.3.2. PRACTICAL EXAMPLE

Having defined the nonholonomic constraints and nonholonomic systems in Section 3.3.1, this section will present a simple bicycle example to illustrate the concepts in details [146].

#### Bicycle

Define the coordinates of the bicycle as  $p = [x, y, \beta, \theta_f]^T$  in Figure 3.13. Since the bicycle system has two control inputs and four degrees of freedom, the number of nonholonomic constraints can be calculated as  $n - m = 2$ . Hence, the non-sliding constraints restrict the vehicle motion at the contact points of the posterior and anterior wheels, which can be written as

$$\dot{x} \sin(\beta + \theta_f) - \dot{y} \cos(\beta + \theta_f) - L \dot{\beta} \cos \theta_f = 0 \quad (3.66)$$

$$\dot{x} \sin \beta - \dot{y} \cos \beta = 0 \quad (3.67)$$

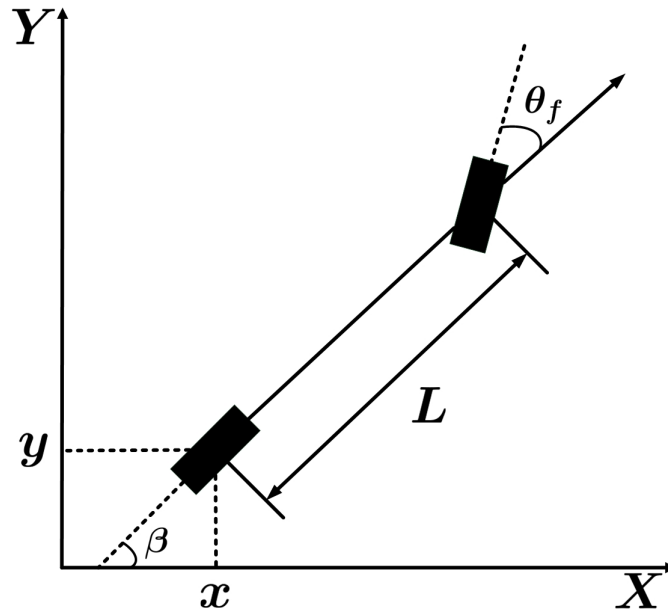


Figure 3.13: The geometry of a bicycle

The corresponding Pfaffian constraint can be described by

$$M(p)\dot{p} = 0 \quad (3.68)$$

where  $M(p)$  is defined in (3.64) as

$$M(p) = \begin{bmatrix} \sin(\beta + \theta_f) & -\cos(\beta + \theta_f) & -L\cos\theta_f & 0 \\ \sin\beta & -\cos\beta & 0 & 0 \end{bmatrix} \quad (3.69)$$

Further, the kinematics of the bicycle can be described as

$$\dot{p} = \Gamma(p)u \quad (3.70)$$

where  $u = [v, \omega]^T$  denotes the control input with linear and angular velocities.  $\Gamma(p)$  is written as

$$\Gamma(p) = \begin{bmatrix} \cos\beta & 0 \\ \sin\beta & 0 \\ \frac{\tan\theta_f}{L} & 0 \\ 0 & 1 \end{bmatrix} \quad (3.71)$$

## 3.4. SUMMARY

In this chapter, the fundamental knowledge of the feedback control concepts, SMC and nonholonomic systems has been reviewed. The state and output feedback controls are discussed with and without the considerations of uncertainties. Moreover, a simple bicycle example has been provided to elucidate nonholonomic constraints and nonholonomic systems. Based on Brockett's necessary condition, it is well-known that the nonholonomic systems cannot be stabilised by the continuous differentiable state feedback time-invariant control law. Therefore, the discontinuous controller, such as SMC, is a decent alternative approach to address this issue. It has been studied that the SMC is an effective method to stabilise the mechanical systems due to the reduced-order property and strong robustness. As a result, the SMC technique is considered the primary methodology for the control design in the rest of the thesis.

## CHAPTER. 4

---

# TRAJECTORY TRACKING CONTROL FOR A TWO-WHEELED MOBILE ROBOT

---

This chapter presents a trajectory tracking SMC design for a TWMR system. The kinematic model of the robot is first derived with the consideration of the nonholonomic constraint. Then the corresponding tracking dynamics are described in Section 4.1. In Section 4.2, a new switching manifold is designed and the reduced-order sliding mode dynamics is generated based on a similar regular form approach of the nonlinear tracking error system, which shows that the resulting sliding motion is asymptotically stable. Further, a SMC law is proposed in Section 4.3 such that the system trajectory is driven to the sliding surface in finite time and maintain on it thereafter. Section 4.4 describes the trajectory tracking control architecture in details. In Section 4.5, both simulation and experiment results demonstrate that the robot is able to track the predefined straight line, circle and lemniscate curve trajectories effectively and robustly in the presence of uncertainties. Lastly, Section 4.6 draws some conclusions.

## 4.1. SYSTEM DESCRIPTION

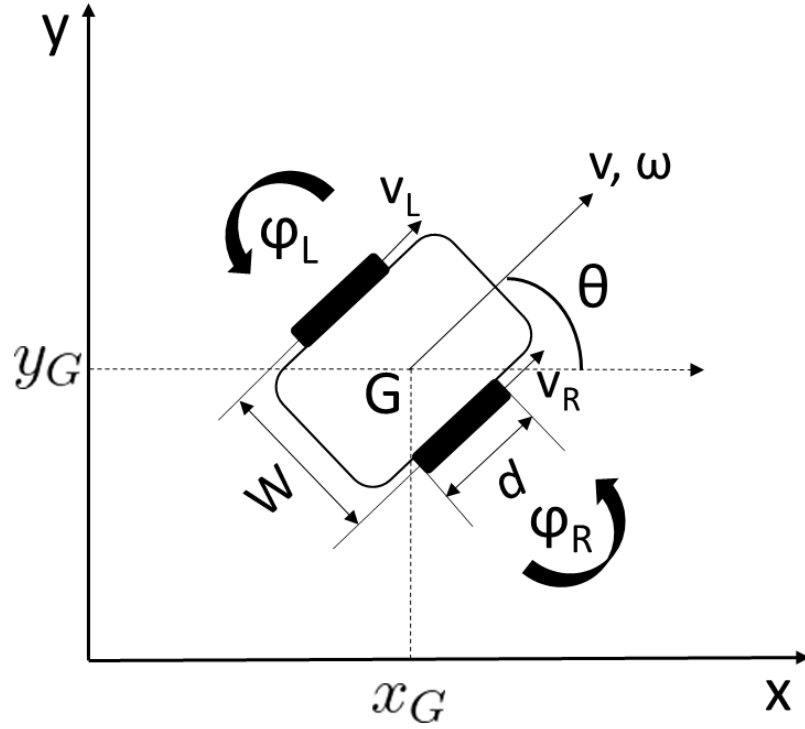


Figure 4.1: Nonholonomic system of a two-wheeled mobile robot

The description of a nonholonomic TWMR is illustrated in Figure 4.1 and its posture  $q \in \mathbb{R}^2 \times \text{SO}(1)$  can be defined with a three degrees of freedom generalised vector coordinates.

$$q(t) = [x_G(t), y_G(t), \theta(t)]^T \quad (4.1)$$

where  $(x_G(t), y_G(t))$  represents the position of the TWMR in the  $x$ - $y$  Cartesian plane,  $\theta(t)$  denotes the orientation angle.

The pure non-slippage rolling assumption states that the TWMR can only drive in the direction perpendicular to the axial of the wheels, which subject to the following Pfaffian nonholonomic constraint (See Section 3.3.1 for more details).

$$\Lambda(q(t))\dot{q}(t) = -\dot{x}_G(t)\sin\theta(t) + \dot{y}_G(t)\cos\theta(t) = 0 \quad (4.2)$$

where

$$\Lambda(q(t)) = [-\sin\theta(t) \quad \cos\theta(t) \quad 0] \quad (4.3)$$

Under assumption from (4.2), the kinematic modelling of the robot can be described by

$$\begin{aligned} \dot{x}_G(t) &= v(t) \cos\theta(t) \\ \dot{y}_G(t) &= v(t) \sin\theta(t) \\ \dot{\theta}(t) &= \omega(t) \end{aligned} \quad (4.4)$$

where  $v(t)$ ,  $\omega(t)$  are the linear and angular velocities of the TWMR respectively.

The equations (4.4) can be rewritten as the first-order kinematic model of the TWMR as follows, which is a linear combination of a matrix  $J(q(t))$  spanning the null space of the matrix  $\Lambda(q(t))$ .

$$\dot{q}(t) = J(q(t)) (u(t) + \Phi(t, q)) + \Psi(t, q) \quad (4.5)$$

where  $u(t) = [v(t), \omega(t)]^T$  is the control input.  $\Phi(t, q) \in \mathbb{R}^2$  represents the matched uncertainty caused by the internal vibrations or noises of the motors and  $\Psi(t, q) \in \mathbb{R}^3$  denotes the unmatched uncertainties due to the slippage caused by the translational movement of the robot.

$$J(q(t)) = \begin{bmatrix} \cos\theta(t) & 0 \\ \sin\theta(t) & 0 \\ 0 & 1 \end{bmatrix} \quad (4.6)$$

**Assumption 4.1.** There exist known continuous non-negative functions  $\varpi(t, q)$  and  $\gamma(t, q)$  such that the matched uncertainty  $\Phi(t, q)$  and unmatched uncertainty  $\Psi(t, q)$  in system (4.5) satisfy

$$\|\Phi(t, q)\| \leq \varpi(t, q) \quad (4.7)$$

$$\|\Psi(t, q)\| \leq \gamma(t, q) \quad (4.8)$$

According to Figure 4.1, the linear and angular velocities of the TWMR are described by

$$v(t) = \frac{v_R(t) + v_L(t)}{2} \quad (4.9)$$

$$\omega(t) = \frac{v_R(t) - v_L(t)}{W} \quad (4.10)$$

$v_L$  and  $v_R$  represents the linear velocities of the left and right wheels.  $W$  is the robot width.

Further,  $v_L(t)$  and  $v_R(t)$  can be written in terms of the angular velocities of the left and right wheels as

$$v_L(t) = \frac{d}{2} \dot{\varphi}_L \quad (4.11)$$

$$v_R(t) = \frac{d}{2} \dot{\varphi}_R \quad (4.12)$$

where  $d$  is the diameter of both driving wheels.

Then, the linear and angular velocities of the TWMR in terms of the angular velocities of the wheels are derived by

$$v(t) = \frac{v_R(t) + v_L(t)}{2} = \frac{\frac{d}{2} \dot{\varphi}_R + \frac{d}{2} \dot{\varphi}_L}{2} = \frac{d(\dot{\varphi}_R + \dot{\varphi}_L)}{4} \quad (4.13)$$

$$\omega(t) = \frac{v_R(t) - v_L(t)}{W} = \frac{\frac{d}{2} \dot{\varphi}_R - \frac{d}{2} \dot{\varphi}_L}{W} = \frac{d(\dot{\varphi}_R - \dot{\varphi}_L)}{2W} \quad (4.14)$$

Hence, based on (4.13) and (4.14), there exists a non-singular coordinate transformation matrix  $T_S$  such that the relationship between the control input  $u$  of the TWMR and the control input  $u_a$  of the motors can be described by the following actuator dynamics.

$$u(t) = T_S u_a(t) \quad (4.15)$$

where

$$T_S = \begin{bmatrix} \frac{d}{4} & \frac{d}{4} \\ -\frac{d}{2W} & \frac{d}{2W} \end{bmatrix} \quad (4.16)$$

$u$  is defined in (4.5) and  $u_a(t) = [\dot{\varphi}_L(t), \dot{\varphi}_R(t)]^T$  is the control input consists of the angular velocities of the left and right actuators respectively.

**Remark 4.1.** It is obvious to notice from (4.16) that  $T_S$  is non-singular and the transformation (4.15) converts the angular velocities  $\dot{\varphi}_L(t)$  and  $\dot{\varphi}_R(t)$  of the wheels to the control input  $u(t)$  represented by the linear and angular velocities  $v(t)$  and  $\omega(t)$  of the TWMR. However, from a practical perspective,  $v(t)$ ,  $\omega(t)$  are designed from the control algorithm and  $\dot{\varphi}_L(t)$ ,  $\dot{\varphi}_R(t)$  act as the real control signals of the actuators. Therefore, the actuator dynamics (4.15) can be rewritten as follows for practical implementation purpose.

$$u_a(t) = T_S^{-1}u(t) \quad (4.17)$$

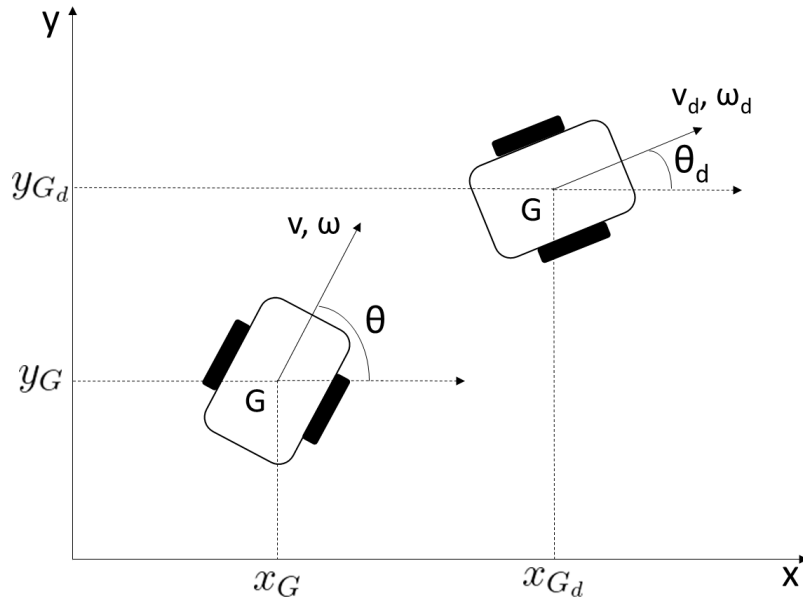


Figure 4.2: Tracking motion of a two-wheeled mobile robot

Consider a desired virtual TWMR with coordinate

$$q_d(t) = [x_{G_d}(t), y_{G_d}(t), \theta_d(t)]^T \quad (4.18)$$

and desired linear and angular velocities  $v_d(t)$ ,  $\omega_d(t)$ . A similar kinematic model of the desired TWMR can be described by

$$\dot{q}_d(t) = \begin{bmatrix} \dot{x}_{G_d}(t) \\ \dot{y}_{G_d}(t) \\ \dot{\theta}_d(t) \end{bmatrix} = \begin{bmatrix} \cos\theta_d(t) & 0 \\ \sin\theta_d(t) & 0 \\ 0 & 1 \end{bmatrix} u_d(t) \quad (4.19)$$

where  $u_d(t) = [v_d(t), \omega_d(t)]^T$  represents the desired control input.

**Remark 4.2.** The desired signals of (4.18) are generated by the dynamics (4.19) using the desired control input  $u_d$  which is given from predefined trajectories.

In order to achieve trajectory tracking control task, the following assumption is imposed on system (4.19).

**Assumption 4.2.** The desired linear velocity  $v_d(t)$  is nonzero and  $v_d(t)$ ,  $\omega_d(t)$  are both bounded by known constants  $v_{d_{max}}$  and  $\omega_{d_{max}}$ , respectively. i.e.,  $\|v_d(t)\| \leq v_{d_{max}}$ ,  $\|\omega_d(t)\| \leq \omega_{d_{max}}$ .

**Remark 4.3.** Assumption 4.2 implies that the reference TWMR does not include motionless configuration due to  $v_d \neq 0$ , similar assumption has been applied in [58] and [59]. Thus, the tracking control can be divided into forward tracking ( $v_d(t) > 0$ ) and backward tracking ( $v_d(t) < 0$ ). In this chapter, without loss of generality, only the forward tracking is considered.

The objective of the trajectory tracking control of the TWMR is to design a control input  $u(t)$  for system (4.5) such that the following equation is satisfied.

$$\lim_{t \rightarrow \infty} \|q_d(t) - q(t)\| = 0 \quad (4.20)$$

where  $q_d(t)$  and  $q(t)$  are the desired and actual states in (4.19) and (4.1), respectively.

Further, consider the local coordinate with respect to the body of the TWMR in Figure 4.2 and introduce a non-singular coordinate transformation matrix  $T_R$  as follows

$$T_R = \begin{bmatrix} \cos\theta(t) & \sin\theta(t) & 0 \\ -\sin\theta(t) & \cos\theta(t) & 0 \\ 0 & 0 & 1 \end{bmatrix} \quad (4.21)$$

Then the tracking error states  $q_e(t) = [x_{G_e}(t), y_{G_e}(t), \theta_e(t)]^T$  can be described by

$$q_e(t) = \begin{bmatrix} x_{G_e}(t) \\ y_{G_e}(t) \\ \theta_e(t) \end{bmatrix} = T_R \begin{bmatrix} x_{G_d}(t) - x_G(t) \\ y_{G_d}(t) - y_G(t) \\ \theta_d(t) - \theta(t) \end{bmatrix} \quad (4.22)$$

where  $(x_{G_e}(t), y_{G_e}(t))$  and  $\theta_e(t)$  are the position and orientation errors of the TWMR respectively.

From (4.5), (4.6), (4.19), (4.21), and (4.22), the dynamics of the tracking error system can be rewritten as

$$\dot{q}_e(t) = M(q_e(t)) + N(q_e(t)) (u(t) + \Phi(t, q_e)) + \widehat{\Psi}(t, q_e) \quad (4.23)$$

where  $q_e(t)$  and  $u(t)$  are defined in (4.22) and (4.5) accordingly and

$$M(q_e(t)) = \begin{bmatrix} v_d(t) \cos\theta_e(t) \\ v_d(t) \sin\theta_e(t) \\ \omega_d(t) \end{bmatrix}, \quad N(q_e(t)) = \begin{bmatrix} -1 & y_{G_e}(t) \\ 0 & -x_{G_e}(t) \\ 0 & -1 \end{bmatrix} \quad (4.24)$$

$$\Phi(t, q_e) := \Phi(t, q) \Big|_{q=q_d - T_R^{-1}q_e} \quad (4.25)$$

$$\widehat{\Psi}(t, q_e) := -T_R \Psi(t, q) \Big|_{q=q_d - T_R^{-1}q_e} \quad (4.26)$$

For further analysis, introduce the following partitions of (4.25) and (4.26).

$$\Phi(t, q_e) = \begin{bmatrix} \Phi_1(t, q_e) \\ \Phi_2(t, q_e) \end{bmatrix} \quad (4.27)$$

$$\widehat{\Psi}(t, q_e) = \begin{bmatrix} \widehat{\Psi}_1(t, q_e) \\ \widehat{\Psi}_2(t, q_e) \end{bmatrix} = \begin{bmatrix} \widehat{\Psi}_{11}(t, q_e) \\ \widehat{\Psi}_{12}(t, q_e) \\ \widehat{\Psi}_2(t, q_e) \end{bmatrix} \quad (4.28)$$

where  $\Phi_1(\cdot) \in \mathbb{R}$ ,  $\Phi_2(\cdot) \in \mathbb{R}$ ,  $\widehat{\Psi}_1(\cdot) \in \mathbb{R}^2$ , and  $\widehat{\Psi}_{11}(\cdot) \in \mathbb{R}$ .

From Assumption 4.1 and (4.25)-(4.26), it follows that

$$\|\Phi(t, q_e)\| \leq \varpi(t, q_e) \quad (4.29)$$

$$\|\widehat{\Psi}(t, q_e)\| \leq \gamma(t, q_e) \quad (4.30)$$

It is worth mentioning that the tracking control problem based on the kinematic systems (4.5) and (4.19) is equivalent to the problem of designing a control  $u(t)$  such that the controlled system (4.23) is asymptotically stable.

## 4.2. STABILITY ANALYSIS OF THE SLIDING MOTION

Since the tracking error dynamics (4.23) and (4.24) are nonlinear and strong coupled, the regular form approach, introduced in Section 3.2.3 to derive the sliding mode dynamics and further analyze the stability of the sliding motion, cannot be readily obtained.

Consider the switching function

$$\sigma(q_e(t)) = \begin{bmatrix} \sigma_1(q_e(t)) \\ \sigma_2(q_e(t)) \end{bmatrix} = \begin{bmatrix} x_{G_e}(t) \\ K_1\theta_e(t) + K_2\tan^{-1}(y_{G_e}(t)) \end{bmatrix} \quad (4.31)$$

where  $K_1$  and  $K_2$  are the design parameters satisfying  $K_1 > 0$ ,  $K_2 > 0$ .

Then the corresponding sliding surface is described by

$$\sigma(q_e(t)) = \begin{bmatrix} \sigma_1(q_e(t)) \\ \sigma_2(q_e(t)) \end{bmatrix} = \begin{bmatrix} x_{G_e}(t) \\ K_1\theta_e(t) + K_2\tan^{-1}(y_{G_e}(t)) \end{bmatrix} = \begin{bmatrix} 0 \\ 0 \end{bmatrix} \quad (4.32)$$

When the system trajectory is restricted to the sliding surface (4.32), it follows that

$$x_{G_e}(t) = 0 \quad (4.33)$$

$$\theta_e(t) = -\frac{K_2}{K_1}\tan^{-1}(y_{G_e}(t)) \quad (4.34)$$

Based on (4.23)-(4.26), (4.33)-(4.34), by direct computation, the reduced-order sliding mode dynamic when limited to the sliding surface  $\sigma(t) = 0$  can be described by

$$\dot{y}_{G_e}(t) = v_d \sin\left(-\frac{K_2}{K_1}\tan^{-1}(y_{G_e}(t))\right) + \Theta \widehat{\Psi}_1(t, q_e) \quad (4.35)$$

where  $\widehat{\Psi}_1(\cdot)$  is given in (4.28) and  $\Theta \in \mathbb{R}^{1 \times 2}$  is defined by

$$\Theta = \begin{bmatrix} \sin(\theta_d - \theta_e) & -\cos(\theta_d - \theta_e) \end{bmatrix} \quad (4.36)$$

The following result is ready to be presented.

**Theorem 4.1.** Suppose Assumptions 4.1 and 4.2 are satisfied, the sliding mode dynamic (4.35) corresponding to the sliding surface (4.33)-(4.34) is asymptotically stable if  $v_d > 0$

and the following condition is satisfied

$$v_d - \|\Theta\| \gamma(t, q_e) > 0 \quad (4.37)$$

*Proof.* For system (4.35), consider the Lyapunov candidate function

$$V(y_{G_e}(t)) = \frac{1}{2} y_{G_e}^2(t) \quad (4.38)$$

Based on (4.30), the time derivative of  $V$  along the trajectories of sliding mode dynamic (4.35) is given by

$$\begin{aligned} \dot{V}|_{(4.35)} &= y_{G_e} \dot{y}_{G_e} \\ &= - \left( v_d \sin \left( \frac{K_2}{K_1} \tan^{-1}(y_{G_e}(t)) \right) - \Theta \widehat{\Psi}_1(t, q_e) \right) y_{G_e}(t) \\ &\leq - \left( v_d \left| \sin \left( \frac{K_2}{K_1} \tan^{-1}(y_{G_e}(t)) \right) \right| - \|\Theta\| \|\widehat{\Psi}_1(t, q_e)\| \right) |y_{G_e}(t)| \\ &\leq - \left( v_d - \|\Theta\| \gamma(t, q_e) \right) |y_{G_e}(t)| \end{aligned} \quad (4.39)$$

Consequently, the derivative of the selected Lyapunov function (4.38) is negative definite if (4.37) is satisfied and  $y_{G_e} \neq 0$ . Moreover, the equality is held if and only if  $y_{G_e} = 0$ .

Therefore, the conclusion follows.  $\square$

### 4.3. REACHABILITY ANALYSIS

The aim now is to design a SMC law such that the reachability condition mentioned in Section 3.2.4

$$\sigma^T(t) \dot{\sigma}(t) \leq -\eta \|\sigma(t)\| \quad (4.40)$$

is satisfied for the positive reaching gain  $\eta$  and  $\sigma(t)$  is the switching function given in (4.31).

Based on the error states (4.22) and the desired control input in (4.19), the following SMC law is proposed

$$u(t) = -\Lambda^{-1}(q_e) \left\{ \Gamma(q_e) \begin{bmatrix} v_d \cos \theta_e \\ v_d \sin \theta_e \\ \omega_d \end{bmatrix} + \left( \|\Lambda(q_e)\| \varpi(t, q_e) + \|\Xi(q_e)\| \gamma(t, q_e) + \rho \right) \text{sgn}(\sigma(q_e)) \right\} \quad (4.41)$$

where  $\rho$  is a positive constant and  $\sigma$  is given in (4.31)

$$\Gamma(q_e(t)) = \begin{bmatrix} 1 & 0 & 0 \\ 0 & \frac{K_2}{1+y_{G_e}^2} & K_1 \end{bmatrix} \quad (4.42)$$

$$\Lambda(q_e(t)) = \begin{bmatrix} -1 & y_{G_e} \\ 0 & -\left(K_1 + \frac{K_2 x_{G_e}}{1+y_{G_e}^2}\right) \end{bmatrix} \quad (4.43)$$

$$\Xi(q_e(t)) = \begin{bmatrix} -\cos(\theta_d - \theta_e) & -\sin(\theta_d - \theta_e) & 0 \\ \frac{K_2}{1+y_{G_e}^2} \sin(\theta_d - \theta_e) & -\frac{K_2}{1+y_{G_e}^2} \cos(\theta_d - \theta_e) & -K_1 \end{bmatrix} \quad (4.44)$$

**Theorem 4.2.** Consider the error dynamics (4.23) in the domain  $\Pi$  where

$$\Pi = \left\{ (x_{G_e}, y_{G_e}, \theta_e) \left| \begin{array}{l} x_{G_e} \neq -\frac{K_1}{K_2}(1 + y_{G_e}^2) \\ y_{G_e} \in \mathbb{R} \\ |\theta_e| \leq \pi \end{array} \right. \right\} \quad (4.45)$$

Suppose Assumptions 4.1 and 4.2 are satisfied. Then the control law (4.41) is able to drive the system (4.23) to the sliding surface (4.32) in finite time and maintain a sliding motion on it thereafter.

*Proof.* From the switching manifold (4.31) and error dynamics (4.23), (4.24), it follows that

$$\dot{\sigma} = \begin{bmatrix} \dot{\sigma}_1 \\ \dot{\sigma}_2 \end{bmatrix} = \Gamma(q_e) \begin{bmatrix} v_d \cos \theta_e \\ v_d \sin \theta_e \\ \omega_d \end{bmatrix} + \Lambda(q_e) (u(t) + \Phi(t, q_e)) + \Xi(t, q_e) \widehat{\Psi}(t, q_e) \quad (4.46)$$

where  $u = [v, \omega]^T$  is given in (4.5) and  $\Gamma(\cdot)$ ,  $\Lambda(\cdot)$ , and  $\Xi(\cdot)$  are defined in (4.42)-(4.44).  $\widehat{\Psi}(\cdot)$  is defined in (4.26).

Applying the control law (4.41) in (4.46) yields

$$\begin{aligned} \dot{\sigma}(q_e) = & - \left( \|\Lambda(q_e)\| \varpi(t, q_e) + \|\Xi(q_e)\| \gamma(t, q_e) + \rho \right) \text{sgn}(\sigma(q_e(t))) \\ & + \Lambda(q_e) \Phi(t, q_e) + \Xi(q_e) \Psi(t, q_e) \end{aligned} \quad (4.47)$$

Hence

$$\begin{aligned} \sigma^T \dot{\sigma} = & \sigma^T \left[ - \left( \|\Lambda(q_e)\| \varpi(t, q_e) + \|\Xi(q_e)\| \gamma(t, q_e) + \rho \right) \text{sgn}(\sigma(q_e(t))) \right. \\ & \left. + \Lambda(q_e) \Phi(t, q_e) + \Xi(q_e) \Psi(t, q_e) \right] \\ \leq & - \|\sigma(q_e)\| \left[ \|\Lambda(q_e)\| \varpi(t, q_e) + \|\Xi(q_e)\| \gamma(t, q_e) + \rho - \Lambda(q_e) \Phi(t, q_e) - \Xi(q_e) \Psi(t, q_e) \right] \\ \leq & - \|\sigma(q_e)\| \left[ \|\Lambda(q_e)\| \varpi(t, q_e) + \|\Xi(q_e)\| \gamma(t, q_e) + \rho - \|\Lambda(q_e)\| \|\Phi(t, q_e)\| \right. \\ & \left. - \|\Xi(q_e)\| \|\Psi(t, q_e)\| \right] \\ \leq & - \|\sigma(q_e)\| \left[ \|\Lambda(q_e)\| \varpi(t, q_e) + \|\Xi(q_e)\| \gamma(t, q_e) + \rho - \|\Lambda(q_e)\| \varpi(t, q_e) \right. \\ & \left. - \|\Xi(q_e)\| \gamma(t, q_e) \right] \\ \leq & -\rho \|\sigma(q_e)\| \end{aligned} \quad (4.48)$$

where  $\rho$  is defined in (4.41).

Therefore, it follows that the reachability condition (4.40) is satisfied.  $\square$

**Remark 4.4.** The condition of  $x_{G_e}$  in the domain  $\Pi$  from (4.45) guarantees the existence of the invertible matrix  $\Lambda(\cdot)$  in (4.41). Moreover, since  $|\tan^{-1}(y_{G_e})| < 0.5\pi$ , from (4.34),  $|\theta_e| = \left| \frac{K_2}{K_1} \tan^{-1}(y_{G_e}) \right| < \frac{0.5K_2}{K_1} \pi$ . Therefore, the condition  $K_1 \geq 0.5K_2$  must be held to satisfy  $|\theta_e| \leq \pi$  of the domain  $\Pi$ .

**Remark 4.5.** It is worth noting that the limitation of  $v_d(t) > 0$  in Theorem 4.1 indicates that the robot only moves forward during the entire trajectory tracking control. For the case of driving backwards (i.e.,  $v_d(t) < 0$ ), the similar design can be achieved by slightly modifying the sliding function (4.31) and the control law (4.41), respectively.

**Remark 4.6.** It should be mentioned that chattering may appear in the SMC because of the discontinuity characteristic in control (4.41). To attenuate this high frequency oscillation, a smoothing constant ( $\delta > 0$ ) is normally augmented as a continuous term  $\sigma/(\|\sigma\| + \delta)$  to replace  $\sigma/\|\sigma\|$  of (4.41) both in simulation and practical implementation [116]. The detailed explanation of the chattering effect can be referred to Section 3.2.4.

**Remark 4.7.** It is obvious to see from (4.41) that the control law employs the known bounds of matched and unmatched uncertainties  $\varpi(\cdot)$  and  $\gamma(\cdot)$  to reduce the system disturbances.

**Remark 4.8.** According to the SMC concept, Theorems 4.1 and 4.2 together show that the closed-loop system formed by employing the control law (4.41) to the error system (4.23) is asymptotically stable and thus  $q_e(t) \rightarrow 0$  as  $t \rightarrow \infty$ . It follows from (4.22) that

$$q_d(t) - q(t) = \begin{bmatrix} x_{G_d}(t) - x_G(t) \\ y_{G_d}(t) - y_G(t) \\ \theta_d(t) - \theta(t) \end{bmatrix} = T_R^{-1} q_e(t) \quad (4.49)$$

where  $T_R$  is defined in (4.21).

Hence, the objective of the trajectory tracking control (4.20) is achieved.

## 4.4. DESCRIPTION OF CONTROL ARCHITECTURE

This section describes the trajectory tracking SMC architecture illustrated in Figure 4.5 which consists of two main sections, namely the software section on the left and the hardware section to the right.

- **Software section:** The software section, illustrated in the control architecture of Figure 4.5, involves two separate parts, the one-time off-line pre-configuration and the recurrently real-time trajectory tracking controls. Further, four sub-modules are enumerated to briefly elucidate the processes of the overall trajectory tracking

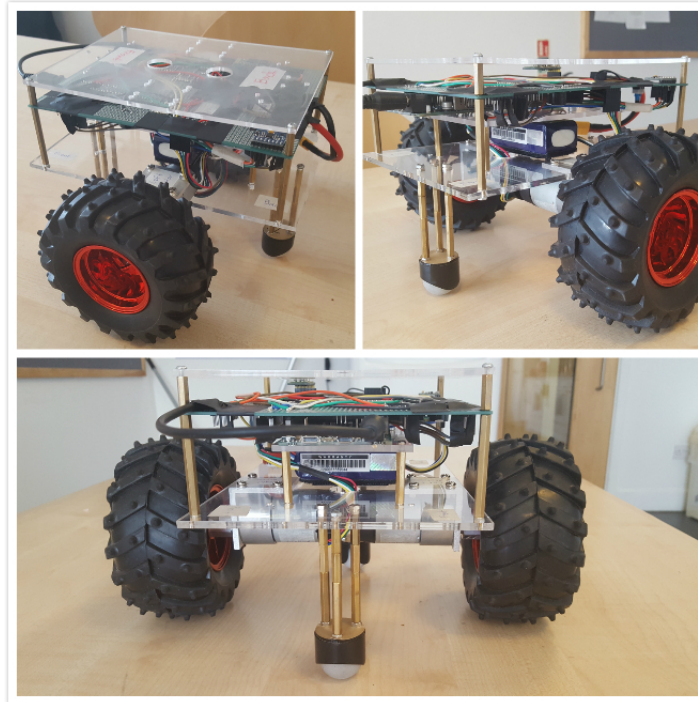


Figure 4.3: Prototype of the two-wheeled mobile robot for sliding mode trajectory tracking control

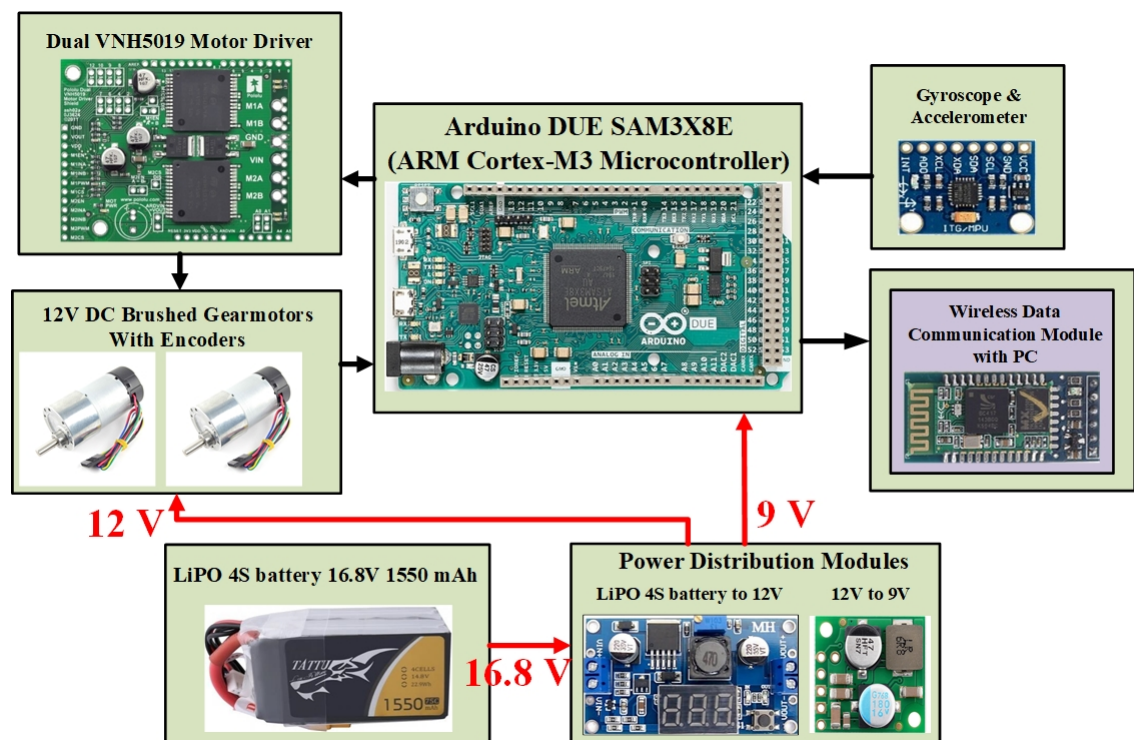


Figure 4.4: Hardware architecture of the two-wheeled mobile robot

Table 4.1: Parameters of the TWMR, sliding surfaces and control law

Symbols with units	Definitions	Values
$d$ [m]	Diameter of the wheel	0.12
$W$ [m]	Distance between the two wheels	0.23
$v_{d_{max}}$ [m/s]	Maximum desired linear velocity	0.5
$\omega_{d_{max}}$ [rad/s]	Maximum desired angular velocity	1
$K_1$ [N/A]	Design parameter 1 of the sliding surface	7
$K_2$ [N/A]	Design parameter 2 of the sliding surface	10
$\rho$ [N/A]	Reaching gain	4
$\delta$ [N/A]	Smoothing constant	0.6
$K_p$ [N/A]	Proportional gain of the PID controller	30
$K_i$ [N/A]	Integral gain of the PID controller	5
$K_d$ [N/A]	Derivative gain of the PID controller	2.5

control task. In addition, the software-related descriptions are detailed in Appendix C. The four sub-modules are explained below

1. **Off-line initial configuration:** It is crucial to pre-configure the initial posture  $q_d(t_0)$  in (4.18) and  $q(t_0)$  in (4.1) of the desired and actual TWMRs along with the desired linear and angular velocities  $(v_d, \omega_d)$  prior to the real-time trajectory tracking control. It is worth mentioning that once the initial posture of the desired robot is configured properly, the initial posture of the actual robot cannot be placed arbitrarily due to the consideration of forward tracking described in Remark 4.3 and the local condition of  $|\theta_e| \leq \pi$  in (4.45).
2. **Real-time desired and actual posture generators:** As described in Remark 4.2, the desired posture is generated from (4.19) with the predefined  $v_d$  and  $\omega_d$ . However, the posture of the actual robot is computed from the triad data  $(v, \omega$  and  $\theta)$  based on the TWMR dynamics (4.4). It can be seen from Figure 4.5 that  $v$  is calculated from the left and right encoders data. The angular velocity  $\omega$  is obtained after the calibration and filtration processes of the original IMU

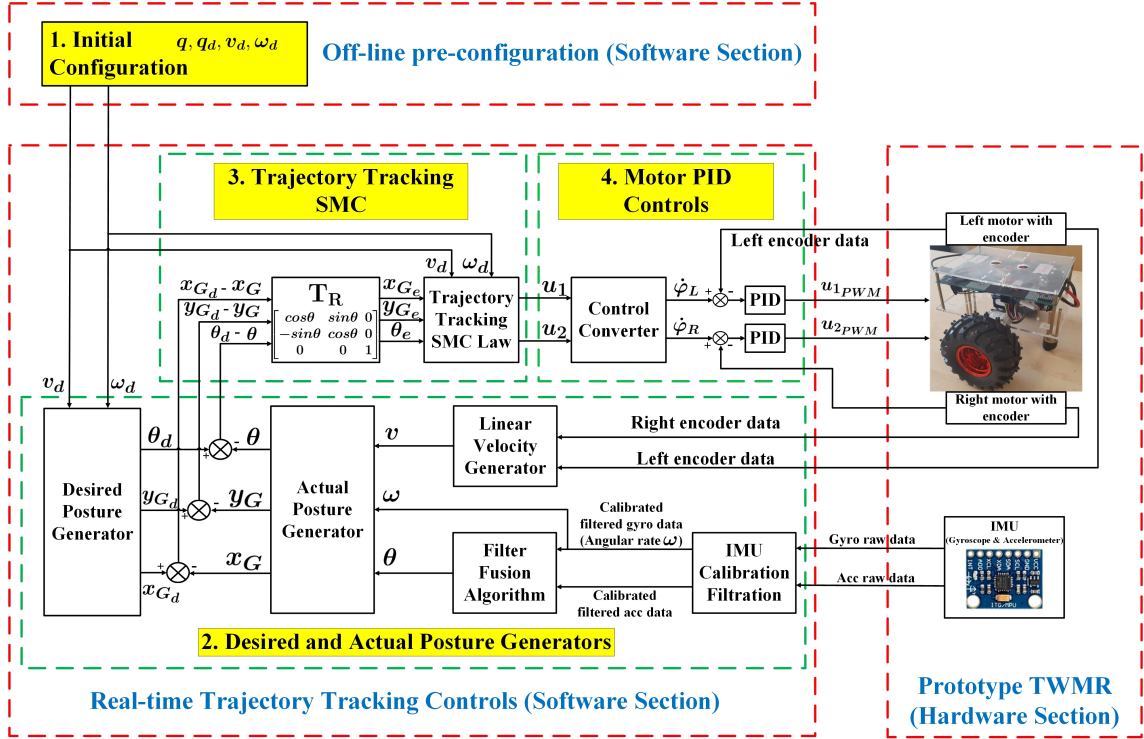


Figure 4.5: Trajectory Tracking Sliding Mode Control Architecture of a Two-wheeled Mobile Robot

raw data. Lastly, the heading angle of the TWMR is determined based on a Mahony filter fusion algorithm. Moreover, the detailed IMU calibration, filtration procedures and Mahony filter fusion algorithm with results are described in Appendix C.2.1.

- 3. Real-time trajectory tracking SMC:** Having collected all the information from the desired and actual robots. The aim of the trajectory tracking SMC is to stabilise the error posture in (4.22), which is equivalent to achieve the objective in (4.20). It should be noted that the outputs of the trajectory tracking SMC laws  $u_1$  and  $u_2$  in Figure 4.5 and (4.41) act as the desired linear and angular velocities of the actual robot to chase the posture of the reference robot, which cannot be applied directly as control inputs to the DC motors in practice.
- 4. Real-time motor PID controls:** To tackle the above-mentioned issue and once the trajectory tracking SMC laws are generated from part 3, two PID controllers are applied to the DC motors to regulate the real-time angular ve-

locities (data from two encoder sensors) of the motors to the reference angular velocities converted based on the actuator dynamics (4.17) of the trajectory tracking SMC laws in Remark 4.1. In addition, the appropriate PID parameter values  $K_P$ ,  $K_I$  and  $K_D$  are provided in Table 4.1.

Further, having finished all the processes of part 1 to 4, the procedure will be repeated from part 2 to generate the desired and actual postures of the robots then execute the trajectory tracking SMC and PID controllers of the motors recurrently to achieve the objective of (4.20).

- **Hardware section:** The prototype wheeled robot has been built and assembled, which has two differentially driven wheels from both sides and two caster wheels mounted on the front and rear of the robot, respectively, as depicted in Figure 4.3. The dimension of this TWMR is 0.22m length  $\times$  0.23m width  $\times$  0.17m height, and it weighs 0.674 kg in total. The detailed parameters of this robot are provided in Table 4.1. Moreover, the primary hardware components involved in the physical TWMR system design are illustrated in Figure 4.4. The central microcontroller unit is employed by a prevalent ARM Cortex-M3 Arduino DUE board. The board is primarily for collecting the sensors data from IMU and quadrature encoders, executing the proposed SMC law, sending the corresponding PWM commands to the motor driver board for actuators control and transmitting the real-time postures data of the desired and actual robots to PC MATLAB via the wireless module. Moreover, the IMU consists of a 3-axis gyroscope and a 3-axis accelerometer, which outputs the required orientation (heading) angular rate and the non-gravitational force per unit mass of the TWMR. Further, the raw angular velocity and accelerometer data are calibrated and filtered, then feed into a Mahony filter fusion algorithm [147] (See also Appendix C.2.1) to retrieve the heading (Euler yaw) angle of the robot. It is worth mentioning that the calibration and filtration processes significantly reduce the misalignment errors, offsets of both triads and noises from the raw outputs of the gyroscope and accelerometer sensors. The filter fusion algorithm [147] also addresses the zero drifting issue caused by the gyroscope sensor for better tracking performance. In terms of actuators of the TWMR, two 12V brushed DC motors,

with a 30:1 metal speed reduction gearbox and two quadrature encoders attached on the rear protrusion of the motors, are driven by a dual motor driver module using PWM signals. The detailed hardware descriptions are provided in Appendix B.

## 4.5. SIMULATION AND EXPERIMENTAL RESULTS

In this section, three different trajectories are employed to demonstrate the feasibility and effectiveness of the proposed SMC scheme (4.41) in simulation and practice with the comparison to a conventional PID control law [148]. The design parameters of the sliding surfaces and SMC law are listed in Table 4.1, which are tuned based on the trial and error technique. Moreover, three cases of predefined reference trajectories are configured as follows.

### Case 1: Line

$$\left( x_{G_d}(t), y_{G_d}(t) \right) = \left( f_l t - 0.5, f_l t - 0.5 \right) \quad (4.50)$$

### Case 2: Circle

$$\left( x_{G_d}(t), y_{G_d}(t) \right) = \left( 0.25 \cos(f_c t) - 0.25, 0.25 \sin(f_c t) \right) \quad (4.51)$$

### Case 3: Lemniscate curve

$$\left( x_{G_d}(t), y_{G_d}(t) \right) = \left( f_{lc} \sin\left(\frac{t}{5}\right), f_{lc} \sin\left(\frac{t}{10}\right) \right) \quad (4.52)$$

where  $f_l$ ,  $f_c$  and  $f_{lc}$  represent the linear velocity tuning factors of the line, circle and lemniscate curve trajectories, respectively.

Further, the desired control input  $u_d(t) = [v_d(t), \omega_d(t)]$  in (4.19) can be generated based on the following commands [8].

$$v_d(t) = \sqrt{\dot{x}_{G_d}^2(t) + \dot{y}_{G_d}^2(t)} \quad (4.53)$$

$$\omega_d(t) = \frac{-\ddot{x}_{G_d}(t)\dot{y}_{G_d}(t) + \ddot{y}_{G_d}(t)\dot{x}_{G_d}(t)}{\dot{x}_{G_d}^2(t) + \dot{y}_{G_d}^2(t)} \quad (4.54)$$

**Remark 4.9.** It is worth mentioning that the robot tracking speed can be adjusted by increasing or decreasing the linear velocity tuning factors  $f_l$ ,  $f_c$  and  $f_{lc}$  in (4.50)-(4.52)

on conditions from Assumption 4.2 that  $\|v_d(t)\| \leq v_{d_{max}}$ ,  $\|\omega_d(t)\| \leq \omega_{d_{max}}$  where  $v_{d_{max}}$  and  $\omega_{d_{max}}$  are configured in Table 4.1. From the practical implementation perspective, however, it should be pointed out that there is a trade-off between the tracking speed and the tracking accuracy in which the higher the configured speed, the lower the tracking precision might be. Hence, to achieve decent tracking performance with relatively accepted robot velocity, the factors  $f_l$ ,  $f_c$  and  $f_{lc}$  can be fine tuned according to the trial and error method.

Based on Assumption 4.1 and (4.29)-(4.30), the matched and unmatched uncertainties of (4.7) and (4.8) satisfy

$$\|\Phi(t, q_e)\| \leq \underbrace{0.8\|q_e\| + 0.5|v_d\omega_d|}_{\varpi(t, q_e)} \quad (4.55)$$

$$\|\Psi(t, q_e)\| \leq \underbrace{0.1\sin^2(\theta_e)}_{\gamma(t, q_e)} \quad (4.56)$$

#### 4.5.1. SIMULATION RESULTS

**Case 1:** The initial postures of the desired and actual TWMR, red and cyan triangles illustrated in Figure 4.6, are configured as  $q_d = [0, 0, 0.7854]^T$  and  $q = [-0.2, -0.2, 1.5708]^T$  where the reference robot is located at (0, 0) with the orientation angle 0.7854 radian (45 degrees) facing northeast. The actual robot begins at (-0.2, -0.2) heading north with the orientation angle 1.5708 radian (90 degrees). From (4.50) with  $f_l = 0.1414$ , by direct calculation using (4.53)-(4.54), the reference linear and angular velocities can be computed as  $v_d = 0.2$  m/s and  $\omega_d = 0$  rad/s, respectively. Since  $v_d = 0.2$  is greater than zero, the forward tracking is performed as mentioned in Remark 4.3. The simulation results of line tracking are showed in Figures 4.6, 4.8, and 4.10. Figure 4.6 demonstrates the simulated motion of the line trajectory in  $x_G$ - $y_G$  plane via PID and proposed SMC laws. As noticed from Figure 4.6, the proposed SMC has better tracking precision compared to the PID counterpart. In Figure 4.8, the comparisons of tracking errors show that both control methods are able to drive the error signals to zero asymptotically. However, the proposed SMC scheme has preferable tracking convergence time, which is approximately 4 seconds compared to 8 seconds using PID control. Lastly, the corresponding linear and angular velocities of control signals are illustrated in Figure 4.10.

**Case 2:** The initial postures of the reference and actual robots are configured as  $q_d = [0, 0, 1.5708]^T$  and  $q = [0.28, -0.25, 2.18]^T$  where the reference TWMR resides at (0, 0) heading north with 90 degrees whereas the actual robot starts outside the trajectory at coordinate (0.28, -0.25) towards northwest with the orientation angle 2.18 radian (approximately 125 degrees). From (4.51) and commands (4.53)-(4.54) with  $f_c = 0.8$ , the desired linear and angular velocities can be calculated as  $v_d = 0.2$  m/s and  $\omega_d = 0.8$  rad/s, respectively. It can be seen from (4.51) that the radius and centre coordinate of the circular trajectory is 0.25 metre and  $(-0.25, 0)$  accordingly. Figures 4.12, 4.14, and 4.16 illustrate the simulation results of circular trajectory tracking. Figure 4.12 shows that the proposed SMC is able to track the circle trajectory slightly accurate in contrast to PID one. From Figure 4.14, it can be seen that the tracking errors are converged to the equilibrium points within 2 seconds using proposed SMC algorithm as opposed to the PID method which takes roughly 7 seconds. In Figure 4.16, the actual control signals also demonstrate the velocities tracking rate using proposed SMC outperform the ones via PID control.

**Case 3:** The desired robot starts from the origin with  $\theta_d = 1.3963$  rad (80 degrees) and the actual robot begins at  $(-0.6, -0.5)$  heading 0.7854 rad (45 degrees) towards the direction of northeast. From (4.52), (4.53) and (4.54) with the configuration of velocity tuning factor  $f_{lc} = 0.6$ , the reference linear and angular velocities for generating lemniscate curve can be described by

$$v_d(t) = 0.6\sqrt{0.04\cos^2(0.2t) + 0.01\cos^2(0.1t)} \quad (4.57)$$

$$\omega_d(t) = \frac{4\sin(0.2t)\cos(0.1t) - 2\sin(0.1t)\cos(0.2t)}{40\cos^2(0.2t) + 10\cos^2(0.1t)} \quad (4.58)$$

The initial velocities when  $t = 0$  are  $v_d(0) = 0.1342$  m/s and  $\omega_d(0) = 0$  rad/s. A complete cycle of tracking the lemniscate curve is finished in roughly  $2\pi \times 10 = 63$  seconds. Figure 4.18 shows the tracking motion of the lemniscate curve. Similar to the simulation results of line and circular trajectories, this type of trajectory can be tracked more precisely by applying the proposed SMC law against the PID method, even around the smooth corners. Moreover, the tracking errors illustrated in Figure 4.20 also demonstrates that the proposed SMC law is superior in terms of the errors convergence rate. It can be seen that the settling time of designed SMC is approximately 3 seconds, whereas nearly 20 seconds to reach the steady-state via PID controller.

Overall, since  $\|\Theta\| = 1$  from (4.36), with the configured  $v_d$  from three different trajectories and the uncertainty satisfying the bound  $\gamma(t, q_e)$  in (4.56), it is straightforward to verify that the condition (4.37) is satisfied in Theorem 4.1. Moreover, the proposed SMC methodology achieves better trajectory tracking performance than the PID counterpart in terms of the accuracy, convergence rate and settling time among all three different trajectory types under simulation environment.

### 4.5.2. EXPERIMENTAL RESULTS

Having verified the effectiveness of the proposed SMC law in simulation, the tracking control of reference trajectories (4.50)-(4.52) are going to be demonstrated on a physical TWMR platform as well. The experiment configurations of line, circle, and lemniscate curve tracking scenarios are identical to the simulation's counterparts. Figures 4.7, 4.9 and 4.11 show the experiment results of line trajectory tracking. The performance of proposed SMC and PID laws of circular tracking is demonstrated in Figures 4.13, 4.15, and 4.17. Moreover, Figures 4.19, 4.21, and 4.23 illustrate the comparison results on a lemniscate curve between PID and proposed SMC scheme. It is noticeable from experimentally tracking motions of Figures 4.7, 4.13 and 4.19 that the designed SMC law achieves better tracking performance with minimum deviations compared to the PID control under the tracking of line and lemniscate curve trajectories and the results are considerably similar on circular tracking. As concerns the convergence rate and settling time, Figure 4.9 shows comparable tracking error results by employing these two controllers with improved convergence rate and less settling time using the proposed SMC method. Furthermore, it can be seen from Figures 4.15 and 4.21 that the time responses of circular and lemniscate curve trajectories tracking errors are sluggish by applying PID loop compared to the proposed SMC law. Lastly, although the tracking control signals are similar under line and lemniscate curve trajectory tracking in Figures 4.11 and 4.23. It can be noticed from Figure 4.17 of circular tracking that there exists a roughly 60% overshoot of the linear velocity tracking signal via PID algorithm, and the convergence rates of linear and angular velocities are improved significantly by using the proposed SMC law.

In summary, the experiment results, obtained from the validation on a physical TWMR

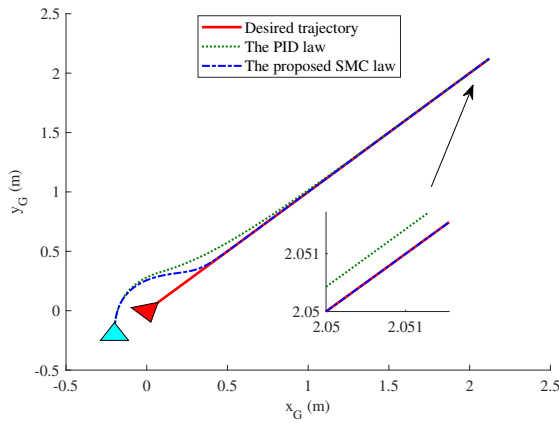


Figure 4.6: Simulation results of trajectory motion under line tracking in  $x_G$ - $y_G$  plane

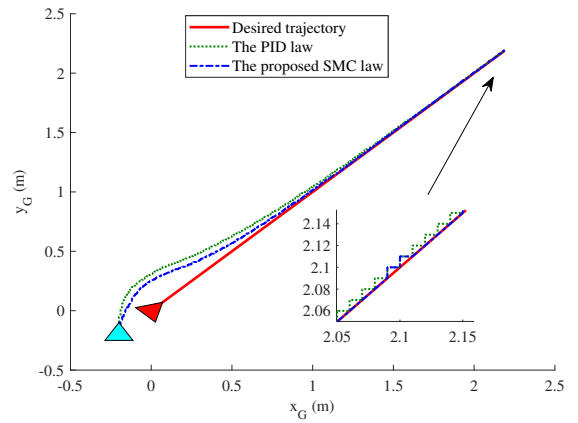


Figure 4.7: Experiment results of trajectory motion under line tracking in  $x_G$ - $y_G$  plane

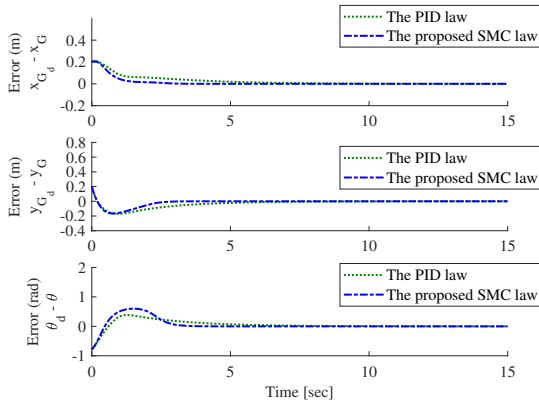


Figure 4.8: Simulation results of error signals  $(x_{G_d} - x_G, y_{G_d} - y_G, \theta_d - \theta)$  under line tracking

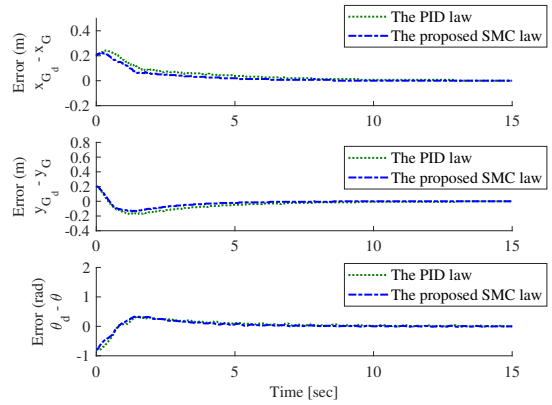


Figure 4.9: Experiment results of error signals  $(x_{G_d} - x_G, y_{G_d} - y_G, \theta_d - \theta)$  under line tracking

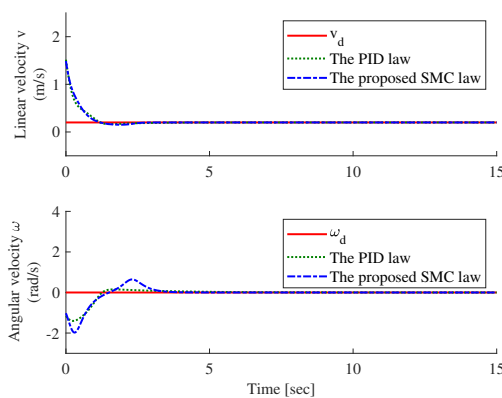


Figure 4.10: Simulation results of control signals  $(v, \omega)$  under line tracking

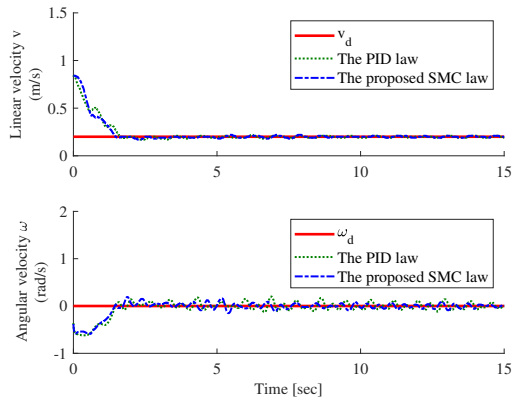


Figure 4.11: Experiment results of control signals  $(v, \omega)$  under line tracking

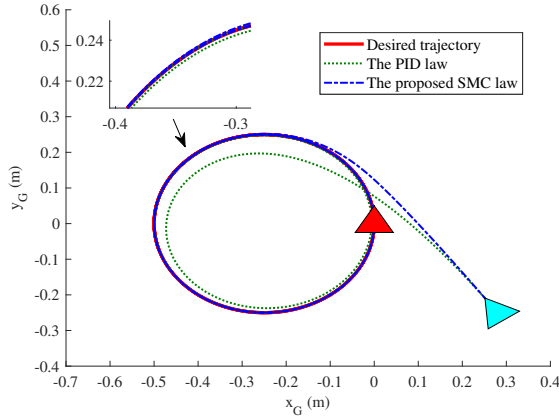


Figure 4.12: Simulation results of trajectory motion under circular tracking in  $x_G$ - $y_G$  plane

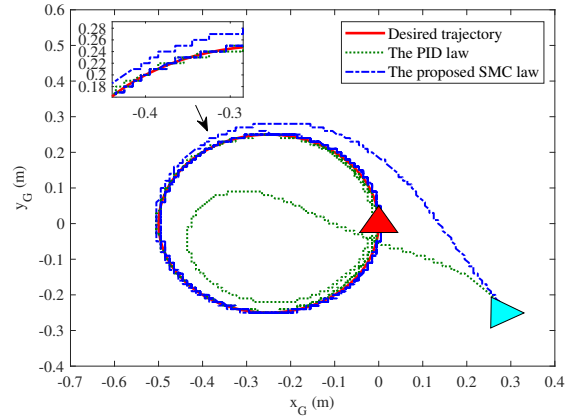


Figure 4.13: Experiment results of trajectory motion under circular tracking in  $x_G$ - $y_G$  plane

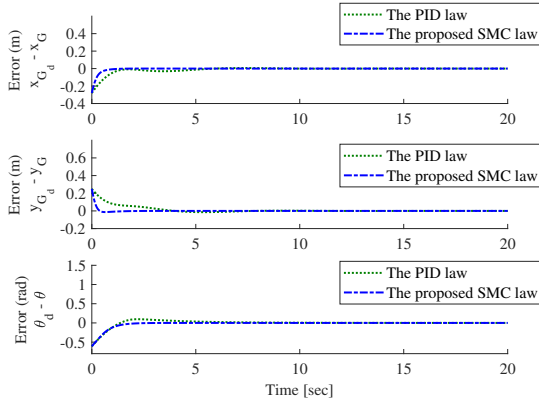


Figure 4.14: Simulation results of error signals  $(x_{G_d} - x_G, y_{G_d} - y_G, \theta_d - \theta)$  under circular tracking

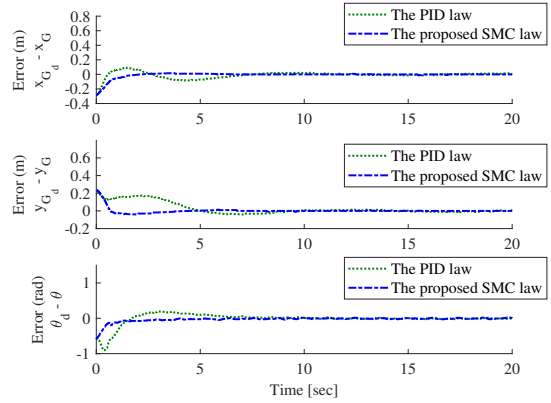


Figure 4.15: Experiment results of error signals  $(x_{G_d} - x_G, y_{G_d} - y_G, \theta_d - \theta)$  under circular tracking

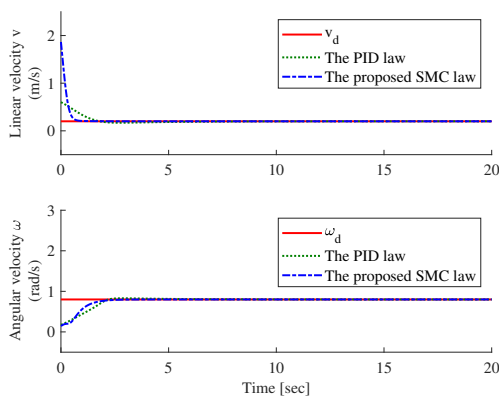


Figure 4.16: Simulation results of control signals  $(v, \omega)$  under circular tracking

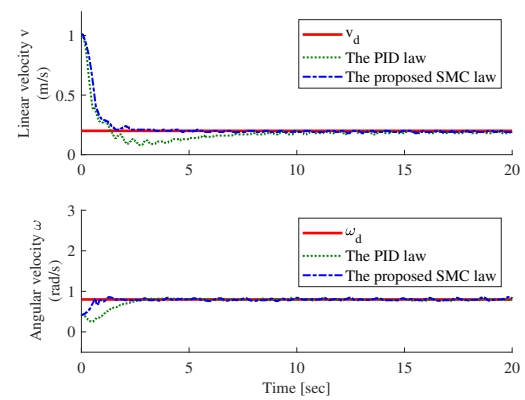


Figure 4.17: Experiment results of control signals  $(v, \omega)$  under circular tracking

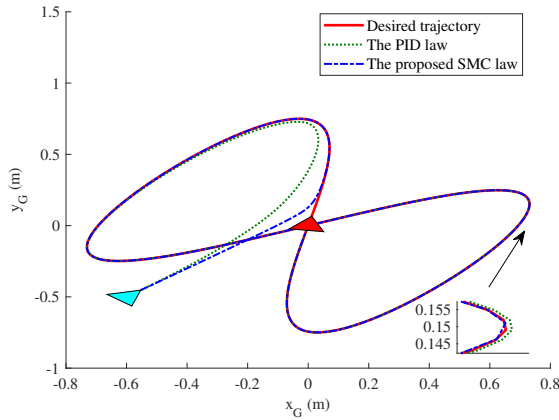


Figure 4.18: Simulation results of trajectory motion under lemniscate tracking in  $x_G$ - $y_G$  plane

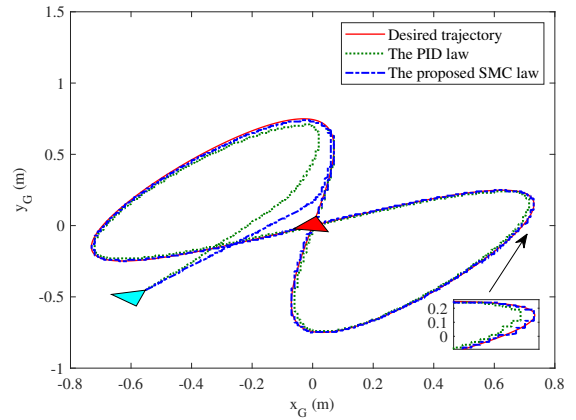


Figure 4.19: Experiment results of trajectory motion under lemniscate tracking in  $x_G$ - $y_G$  plane

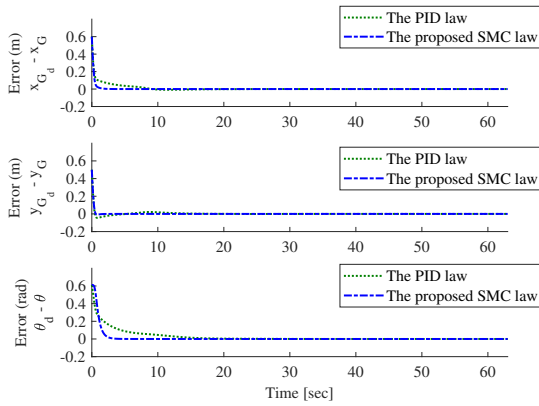


Figure 4.20: Simulation results of error signals  $(x_{G_d} - x_G, y_{G_d} - y_G, \theta_d - \theta)$  under lemniscate tracking

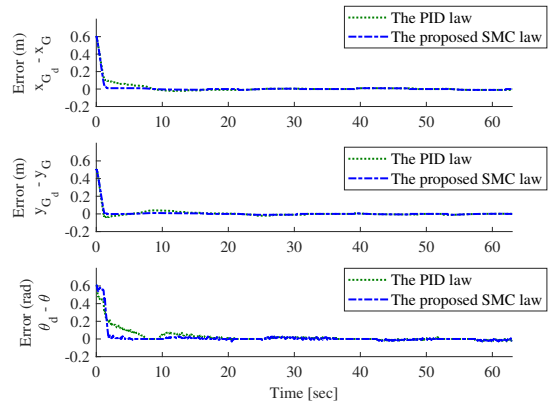


Figure 4.21: Experiment results of error signals  $(x_{G_d} - x_G, y_{G_d} - y_G, \theta_d - \theta)$  under lemniscate tracking

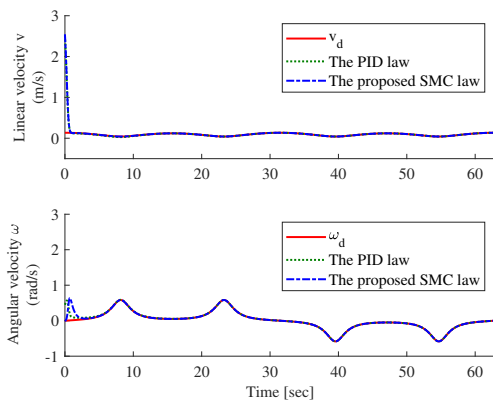


Figure 4.22: Simulation results of control signals  $(v, \omega)$  under lemniscate tracking

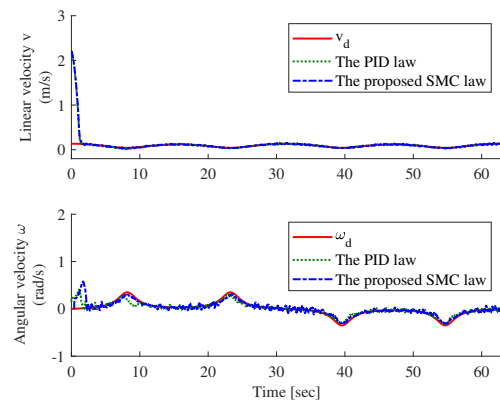


Figure 4.23: Experiment results of control signals  $(v, \omega)$  under lemniscate tracking

---

platform, also demonstrate the feasibility and effectiveness of the proposed SMC scheme. The designed SMC achieves better tracking performance than the PID one, consistent with the simulation results.

## 4.6. CONCLUSION

In this chapter, a nonlinear SMC law is proposed for the trajectory tracking of a TWMR system. A particular structure of a sliding surface is designed to help deriving the sliding mode reduced-order dynamic to facilitate the stability analysis. It shows that the tracking errors are asymptotically stable both in simulation and experiment. Finally, the results demonstrate the effectiveness and robustness of the designed SMC law in the presence of the matched and unmatched uncertainties and the tracking performance is better than the PID control method.

## CHAPTER. 5

---

# STATE FEEDBACK CONTROL OF A TWO-WHEELED INVERTED PENDULUM

---

In this chapter, a regular-form based state feedback SMC law is proposed to stabilise a TWIP dynamic system under assumption that all system states are available in the control design. In Section 5.1, A Lagrangian-based dynamics are employed for a TWIP system with the consideration of unknown matched and unmatched uncertainties which are bounded by known nonlinear functions. Then the model is linearised and further transformed into a regular form to facilitate the analysis and design. A sliding surface is designed and the stability and reachability analyses are carried out in Section 5.2. Section 5.3 presents the control architecture for regulating the TWIP system, followed by the designed description of a RTOS-based software architecture implemented for the TWIP platform. Finally, Section 5.5 verifies the designed control scheme on the TWIP system both in simulation and experiment and the results demonstrate the effectiveness and robustness of the regulation control. Finally, some conclusions are drawn in Section 5.6.

## 5.1. SYSTEM DESCRIPTION AND PRELIMINARIES

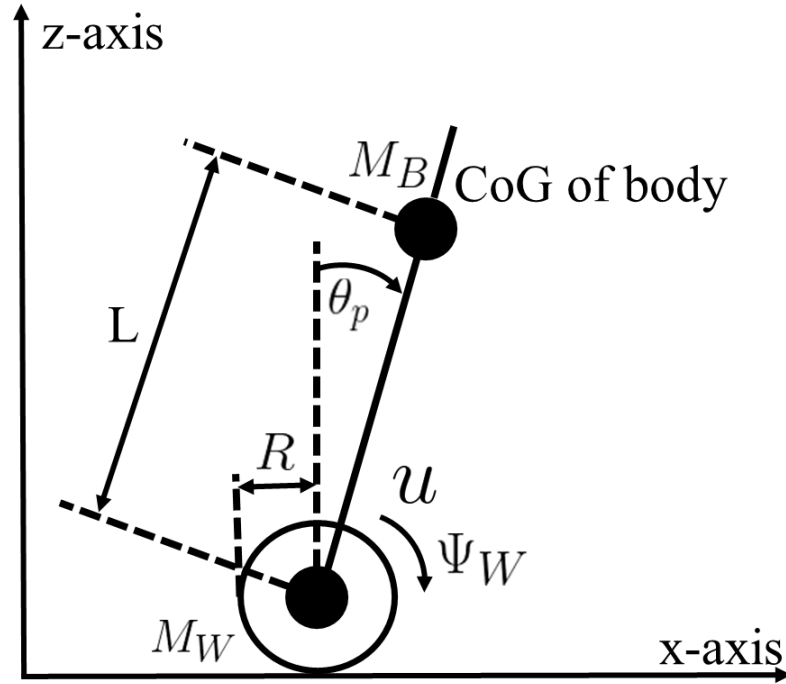


Figure 5.1: Model of a two-wheeled inverted pendulum

The longitudinal motion analysis of the TWIP is considered in this chapter, which is illustrated in Figure 5.1.

The dynamics of the system is described based on the derivations of the TWIP modelling from Appendix A by simply configuring the inclination angle of the ramp  $\alpha$  to zero.

$$\begin{cases} n_1 \ddot{\theta}_p + n_2 \cos \theta_p \ddot{\Psi}_W - n_3 \sin \theta_p = -u - \tau_B \\ n_4 \ddot{\Psi}_W + n_2 \cos \theta_p \ddot{\theta}_p - n_2 \sin \theta_p \dot{\theta}_p^2 = u + \tau_B - \tau_W \end{cases} \quad (5.1)$$

where  $n_i$  for  $i = 1, 2, 3, 4$  are constants and defined by

$$\begin{cases} n_1 = M_B L^2 + J_{\theta_p}, & n_2 = 2M_B L R, & n_3 = M_B g L \\ n_4 = 4(M_B + M_W) R^2 + J_w \end{cases} \quad (5.2)$$

$\theta_p$  is the attitude pitch angle of the TWIP body,  $L$  is the length between the wheel axis and the centre of gravity (CoG) of the body,  $R$  is the radius of the wheel,  $\Psi_W$  is the angular displacement of the wheel,  $M_B$ ,  $M_W$  are the masses of the TWIP body and wheel respectively,  $J_{\theta_p}$  is the moment of inertia of the body w.r.t y-axis, and  $J_w$  is the moment of inertia of the wheel. Moreover,  $\tau_B$ ,  $\tau_W$  are the friction torque forces related to the TWIP body and the ground,  $u$  represents the total torque (control input) applied to the wheels.

The nonlinear system (5.1) can be further rewritten in state-space representation (See Section 3.1.1) as follows

$$\dot{x}(t) = \mathcal{F}(x(t)) + \mathcal{G}(x(t))(u(t) + f_m(t, x)) + f_{u_1}(t, x) \quad (5.3)$$

where

$$\mathcal{F}(x) = \begin{bmatrix} x_2 \\ -\frac{n_2 n_3 \cos x_3 \sin x_3}{n_1 n_4 - n_2^2 \cos^2(x_3)} + \frac{n_1 n_2 \sin x_3}{n_1 n_4 - n_2^2 \cos^2(x_3)} x_4^2 \\ x_4 \\ \frac{n_3 n_4 \sin x_3}{n_1 n_4 - n_2^2 \cos^2(x_3)} - \frac{n_2^2 \sin x_3 \cos x_3}{n_1 n_4 - n_2^2 \cos^2(x_3)} x_4^2 \end{bmatrix} \quad (5.4)$$

$$\mathcal{G}(x) = \begin{bmatrix} 0 \\ \frac{n_1 + n_2 \cos x_3}{n_1 n_4 - n_2^2 \cos^2(x_3)} \\ 0 \\ -\frac{n_2 \cos x_3 + n_4}{n_1 n_4 - n_2^2 \cos^2(x_3)} \end{bmatrix}, \quad f_{u_1} = \begin{bmatrix} 0 \\ -\frac{n_1}{n_1 n_4 - n_2^2 \cos^2(x_3)} \\ 0 \\ \frac{n_2 \cos x_3}{n_1 n_4 - n_2^2 \cos^2(x_3)} \end{bmatrix} \tau_W$$

$$f_m = \tau_B$$

$x(t) = [x_1, x_2, x_3, x_4]^T = [\Psi_W, \dot{\Psi}_W, \theta_p, \dot{\theta}_p]^T$  is defined as the state vector,  $f_m$  represents the internal joint friction which can be treated as the input channel of the control signal and categorised to the unknown matched uncertainty.  $f_{u_1}$  is the unknown unmatched uncertainty which is the correlation between the ground and the wheels, such as the slippage caused by the translational movement of the robot.

For given desired signals  $x_d(t) = [x_{1_d}, x_{2_d}, x_{3_d}, x_{4_d}]^T$ . The problem considered in this chapter is to design a SMC law such that the system (5.3) is able to track the desired signals, that is

$$\lim_{t \rightarrow \infty} \|x_i(t) - x_{i_d}(t)\| = 0 \quad \text{for } i = 1, 2, 3, 4 \quad (5.5)$$

For simplification purpose, system (5.3) can be linearised around the desired signals  $x_d(t)$  as

$$\dot{x}(t) = \mathcal{A}x(t) + \mathcal{B}(u(t) + f_m(t, x)) + f_{u_2}(t, x) \quad (5.6)$$

where  $\mathcal{A}$  and  $\mathcal{B}$  are constant matrices defined by

$$\mathcal{A} = \left. \frac{\partial \mathcal{F}(x)}{\partial x} \right|_{x=x_d} = \begin{bmatrix} 0 & 1 & 0 & 0 \\ 0 & 0 & \frac{-n_2 n_3}{n_1 n_4 - n_2^2} & 0 \\ 0 & 0 & 0 & 1 \\ 0 & 0 & \frac{n_3 n_4}{n_1 n_4 - n_2^2} & 0 \end{bmatrix} \quad (5.7)$$

$$\mathcal{B} = \left. \frac{\partial \mathcal{G}(x)}{\partial u} \right|_{x=x_d} = \begin{bmatrix} 0 \\ \frac{n_1 + n_2}{n_1 n_4 - n_2^2} \\ 0 \\ -\frac{n_2 + n_4}{n_1 n_4 - n_2^2} \end{bmatrix}$$

$f_m$  is defined in (5.4) and  $f_{u_2}$  is given by

$$f_{u_2} = \begin{bmatrix} 0 \\ -\frac{n_1}{n_1 n_4 - n_2^2} \\ 0 \\ \frac{n_2}{n_1 n_4 - n_2^2} \end{bmatrix} \tau_W \quad (5.8)$$

Further, the following assumptions are imposed on system (5.6).

**Assumption 5.1.** For this model, the matrix pair  $(\mathcal{A}, \mathcal{B})$  is controllable.

**Assumption 5.2.** There exist known continuous nonlinear functions  $\beta(t, x)$  and  $\gamma(t, x)$  such that the unknown matched and unmatched uncertainties  $f_m(t, x)$ ,  $f_{u_2}(t, x)$  are bounded and satisfy ( See [149] )

$$\begin{aligned} \|f_m(t, x)\| &\leq \beta(t, x) \\ \|f_{u_2}(t, x)\| &\leq \gamma(t, x) \end{aligned} \quad (5.9)$$

**Remark 5.1.** In this chapter, the upper bounds of  $\|f_m(t, x)\|$  and  $\|f_{u_2}(t, x)\|$  in Assumption 5.2 are required to be known functions, which will be employed in the control design to reduce or reject the system uncertainties.

According to the objective from (5.5), define the error states to be  $e = [e_1, e_2, e_3, e_4]^T = [x_1 - x_{1_d}, x_2 - x_{2_d}, x_3 - x_{3_d}, x_4 - x_{4_d}]^T$  and error dynamics of the longitudinal system based on (5.6) can be described by

$$\dot{e}(t) = \mathcal{A}e(t) + \mathcal{B}(u(t) + f_m(t, e + x_d)) + f_{u_3}(t, e + x_d) \quad (5.10)$$

where  $f_m$ ,  $\mathcal{A}$ ,  $\mathcal{B}$  are defined in (5.4) and (5.7), the unmatched uncertainty  $f_{u_3}(t, e + x_d) = f_{u_2}(t, e + x_d) + \mathcal{A}x_d - \dot{x}_d$ .

From Assumption 5.2,  $f_m(t, e + x_d)$  and  $f_{u_3}(t, e + x_d)$  satisfy

$$\begin{aligned} \|f_m(t, e + x_d)\| &\leq \beta(t, e + x_d) \\ \|f_{u_3}(t, e + x_d)\| &\leq \gamma(t, e + x_d) + \|\mathcal{A}\| \|x_d\| + \|\dot{x}_d\| \end{aligned} \quad (5.11)$$

## 5.2. SLIDING MODE ANALYSIS AND CONTROL DESIGN

Since the error dynamics (5.10) is not constructed in a well-known regular form, which is not readily apparent for stability analysis of SMC. Introduce a new coordinate transformation.

$$\omega(t) = [\omega_1, \omega_2, \omega_3, \omega_4]^T = T_r e(t) \quad (5.12)$$

$$T_r = \begin{bmatrix} 1 & 0 & 0 & 0 \\ 0 & 1 & 0 & \frac{n_1+n_2}{n_2+n_4} \\ 0 & 0 & 1 & 0 \\ 0 & 0 & 0 & 1 \end{bmatrix} \quad (5.13)$$

It is clear that  $T_r$  is non-singular.

Hence, system (5.10) can be described in regular form in terms of the new coordinates  $\omega(t)$  as

$$\dot{\omega}(t) = \bar{\mathcal{A}}\omega(t) + \bar{\mathcal{B}}(u(t) + f_m(t, \omega)) + f_{u_4}(t, \omega) \quad (5.14)$$

where

$$\bar{\mathcal{A}} = \begin{bmatrix} 0 & 1 & 0 & -\frac{n_1+n_2}{n_2+n_4} \\ 0 & 0 & \frac{n_3}{n_2+n_4} & 0 \\ 0 & 0 & 0 & 1 \\ 0 & 0 & \frac{n_3n_4}{n_1n_4-n_2^2} & 0 \end{bmatrix}, \quad \bar{\mathcal{B}} = \begin{bmatrix} 0 \\ \mathcal{B}_2 \end{bmatrix} = \begin{bmatrix} 0 \\ 0 \\ 0 \\ -\frac{n_2+n_4}{n_1n_4-n_2^2} \end{bmatrix} \quad (5.15)$$

$f_m(t, \omega)$  and  $f_{u_4}(t, \omega)$  are the matched and unmatched uncertainties in  $\omega$ -system.

The following assumption is imposed on system (5.14).

**Assumption 5.3.** The term  $\mathcal{B}_2$  is non-zero.

Based on Assumption 5.2 and (5.11), (5.12),

$$\begin{aligned} \|f_m(t, \omega)\| &\leq \beta(t, T_r^{-1}\omega + x_d) \\ \|f_{u_4}(t, \omega)\| &\leq \gamma(t, T_r^{-1}\omega + x_d) + \|\mathcal{A}\| \|x_d\| + \|\dot{x}_d\| \end{aligned} \quad (5.16)$$

For further analysis, partition  $f_{u_4}(t, \omega)$  into

$$f_{u_4}(t, \omega) = \begin{bmatrix} 0 \\ f_{u_{41}}(t, \omega) \\ 0 \\ f_{u_{42}}(t, \omega) \end{bmatrix} \quad (5.17)$$

Consider the switching function

$$\sigma(t) = \delta_1\omega_1(t) + \delta_2\omega_2(t) + \delta_3\omega_3(t) + \omega_4(t) \quad (5.18)$$

where  $\delta_1, \delta_2, \delta_3$  are design parameters.

Then, the sliding surface is described by

$$\sigma(t) = \delta_1\omega_1(t) + \delta_2\omega_2(t) + \delta_3\omega_3(t) + \omega_4(t) = 0 \quad (5.19)$$

Hence, when sliding motion occurs,  $\omega_4(t)$  can be expressed in terms of  $\omega_1(t), \omega_2(t)$ , and  $\omega_3(t)$  as

$$\omega_4(t) = -\delta_1\omega_1(t) - \delta_2\omega_2(t) - \delta_3\omega_3(t) \quad (5.20)$$

### 5.2.1. STABILITY ANALYSIS OF SLIDING MOTION

From (5.14), (5.15), and (5.20), it is straightforward to see that the reduced-order sliding mode system when confined to the sliding surface  $\sigma(t) = 0$  can be derived as

$$\dot{\omega}_s(t) = \underbrace{\begin{bmatrix} \left(\frac{n_1+n_2}{n_2+n_4}\right)\delta_1 & \left(\frac{n_1+n_2}{n_2+n_4}\right)\delta_2 + 1 & \left(\frac{n_1+n_2}{n_2+n_4}\right)\delta_3 \\ 0 & 0 & \frac{n_3}{n_2+n_4} \\ -\delta_1 & -\delta_2 & -\delta_3 \end{bmatrix}}_{\tilde{\mathcal{A}}_{11}^s} \omega_s(t) + \underbrace{\begin{bmatrix} 0 \\ f_{u_{41}} \\ 0 \end{bmatrix}}_{\tilde{f}_{u_{41}}} \quad (5.21)$$

where  $\omega_s(t) = [\omega_1(t), \omega_2(t), \omega_3(t)]^T$ .

The following assumption is imposed on system (5.21).

**Assumption 5.4.**  $\frac{n_3}{n_2+n_4}$  of  $\tilde{\mathcal{A}}_{11}^s$  is a non-zero constant.

**Lemma 5.1.** Consider the reduced-order sliding mode dynamics (5.21), and suppose Assumptions 5.1, 5.2 and 5.4 are satisfied,  $\tilde{\mathcal{A}}_{11}^s$  is Hurwitz stable if the following inequalities hold for  $\delta_1$ ,  $\delta_2$  and  $\delta_3$ .

$$\delta_1 > 0, \quad \delta_2 > \frac{\delta_1}{\delta_3 - \left(\frac{n_1+n_2}{n_2+n_4}\right)\delta_1}, \quad \delta_3 > \left(\frac{n_1+n_2}{n_2+n_4}\right)\delta_1 \quad (5.22)$$

*Proof.* The characteristic equation of  $\tilde{\mathcal{A}}_{11}^s$  can be described by

$$z^3 + \left[\delta_3 - \left(\frac{n_1+n_2}{n_2+n_4}\right)\delta_1\right]z^2 + \frac{n_3}{n_2+n_4}\delta_2z + \frac{n_3}{n_2+n_4}\delta_1 = 0 \quad (5.23)$$

The corresponding coefficients of the first column of the Routh-hurwitz array are determined as

$$\begin{aligned} a_0 &= 1, \quad a_1 = \delta_3 - \left(\frac{n_1+n_2}{n_2+n_4}\right)\delta_1 \\ b_1 &= \frac{\frac{n_3\delta_2}{n_2+n_4} \left[\delta_3 - \left(\frac{n_1+n_2}{n_2+n_4}\right)\delta_1\right] - \frac{n_3}{n_2+n_4}\delta_1}{\delta_3 - \left(\frac{n_1+n_2}{n_2+n_4}\right)\delta_1} \\ c_1 &= \frac{n_3}{n_2+n_4}\delta_1 \end{aligned} \quad (5.24)$$

By direct calculation, it follows that  $a_0$ ,  $a_1$ ,  $b_1$  and  $c_1$  in (5.24) are positive if the inequalities in (5.22) hold. Then under Assumption 5.4 and based on the Routh-Hurwitz stability criterion, the matrix  $\tilde{\mathcal{A}}_{11}^s$  is stable. ■

From Lemma 5.1, if  $\delta_1$ ,  $\delta_2$  and  $\delta_3$  satisfy (5.22),  $\tilde{\mathcal{A}}_{11}^s$  is stable, which implies that for any symmetric positive definite matrix  $Q \in \mathbb{R}^{3 \times 3}$ , there exists a unique symmetric positive definite matrix  $P \in \mathbb{R}^{3 \times 3}$  satisfying the Lyapunov equation

$$\tilde{\mathcal{A}}_{11}^{sT} P + P \tilde{\mathcal{A}}_{11}^s = -Q \quad (5.25)$$

**Theorem 5.1.** Under the conditions of Lemma 5.1, the state  $\omega_s(t)$  of the sliding mode dynamics (5.21) is uniformly ultimately bounded.

*Proof.* For system (5.21), consider a candidate Lyapunov function

$$V(\omega_s) = \omega_s^T P \omega_s$$

Then, the time derivative of  $V$  along the trajectories of sliding mode dynamics (5.21) is given by

$$\begin{aligned} \dot{V} &= \dot{\omega}_s^T P \omega_s + \omega_s^T P \dot{\omega}_s \\ &= \left( \tilde{\mathcal{A}}_{11}^s \omega_s + \tilde{f}_{u_{41}}(t, \omega) \right)^T P \omega_s + \omega_s^T P \left( \tilde{\mathcal{A}}_{11}^s \omega_s + \tilde{f}_{u_{41}}(t, \omega) \right) \\ &= \omega_s^T \tilde{\mathcal{A}}_{11}^{sT} P \omega_s + \tilde{f}_{u_{41}}^T(t, \omega) P \omega_s + \omega_s^T P \tilde{\mathcal{A}}_{11}^s \omega_s + \omega_s^T P \tilde{f}_{u_{41}}(t, \omega) \\ &= \omega_s^T \left( \tilde{\mathcal{A}}_{11}^{sT} P + P \tilde{\mathcal{A}}_{11}^s \right) \omega_s + 2\omega_s^T P \tilde{f}_{u_{41}}(t, \omega) \end{aligned} \quad (5.26)$$

From (5.25), it follows that

$$\begin{aligned} \dot{V} &= -\omega_s^T Q \omega_s + 2\omega_s^T P \tilde{f}_{u_{41}}(t, \omega) \\ &\leq -\omega_s^T Q \omega_s + 2\|P\omega_s\| \|\tilde{f}_{u_{41}}(t, \omega)\| \\ &\leq -\lambda_{\min}(Q) \|\omega_s\|^2 + 2\lambda_{\max}(P) \|\omega_s\| \|\tilde{f}_{u_{41}}(t, \omega)\| \\ &\leq -\lambda_{\max}(P) \|\omega_s\| \left( \frac{\lambda_{\min}(Q)}{\lambda_{\max}(P)} \|\omega_s\| - 2 \left( \gamma(t, T_r^{-1}\omega + x_d) \right. \right. \\ &\quad \left. \left. + \|\mathcal{A}\| \|x_d\| + \|\dot{x}_d\| \right) \right) \end{aligned} \quad (5.27)$$

where the condition (5.16) is used above.

Consequently,  $\dot{V} \leq 0$  if

$$\|\omega_s\| \geq \frac{2 \left( \gamma(t, T_r^{-1}\omega + x_d) + \|\mathcal{A}\| \|x_d\| + \|\dot{x}_d\| \right)}{\lambda_{\min}(Q) / \lambda_{\max}(P)}$$

Hence, the conclusion follows. ■

**Remark 5.2.** It is obvious to notice from (5.21) that the sliding motion is only affected by the unmatched uncertainty  $\tilde{f}_{u_{41}}(t, \omega)$ , which is mentioned in the SMC's characteristics of Section 3.2.5.

### 5.2.2. SLIDING MODE CONTROL DESIGN

The objective of this section is to design a controller such that the reachability condition described in Section 3.2.4

$$\sigma^T(t)\dot{\sigma}(t) \leq -\rho\|\sigma(t)\| \quad (5.28)$$

is satisfied for some positive constant  $\rho$ , where  $\sigma(t)$  is the switching function defined in (5.18).

The following SMC law is proposed

$$\begin{aligned} u(t) = & -\mathcal{B}_2^{-1} \left\{ \delta_1 \omega_2 + \left( \frac{n_3 n_4}{n_1 n_4 - n_2^2} + \frac{n_3}{n_2 + n_4} \delta_2 \right) \omega_3 \right. \\ & + \left[ \delta_3 - \left( \frac{n_1 + n_2}{n_2 + n_4} \right) \delta_1 \right] \omega_4 + \left[ |\mathcal{B}_2| \beta(t, T_r^{-1} \omega + x_d) \right. \\ & + (|\delta_2| + 1) \left( \gamma(t, T_r^{-1} \omega + x_d) + \|\mathcal{A}\| \|x_d\| + \|\dot{x}_d\| \right) \\ & \left. \left. + \rho \frac{\sigma(t)}{\|\sigma(t)\|} \right\} \end{aligned} \quad (5.29)$$

where  $\beta(\cdot)$  and  $\gamma(\cdot)$  are given in (5.16).

**Theorem 5.2.** Consider the system in (5.14), the control (5.29) is able to drive system (5.14) to the sliding surface (5.19) in finite time and maintain a sliding motion on it thereafter.

*Proof.* From the definition of  $\sigma(t)$  in (5.18), it follows that

$$\begin{aligned} \dot{\sigma}(t) = & \delta_1 \omega_2 + \left( \frac{n_3 n_4}{n_1 n_4 - n_2^2} + \frac{n_3}{n_2 + n_4} \delta_2 \right) \omega_3 \\ & + \left[ \delta_3 - \left( \frac{n_1 + n_2}{n_2 + n_4} \right) \delta_1 \right] \omega_4 + \mathcal{B}_2 \left( u(t) + f_m(t, \omega) \right) \\ & + \delta_2 f_{u_{41}}(t, \omega) + f_{u_{42}}(t, \omega) \end{aligned} \quad (5.30)$$

Substituting the designed control law (5.29) into (5.30) yields

$$\begin{aligned} \dot{\sigma}(t) = & - \left[ |\mathcal{B}_2| \beta(t, T_r^{-1} \omega + x_d) + (|\delta_2| + 1) \right. \\ & \times \left( \gamma(t, T_r^{-1} \omega + x_d) + \|\mathcal{A}\| \|x_d\| + \|\dot{x}_d\| \right) + \rho \left. \right] \\ & \times \frac{\sigma(t)}{\|\sigma(t)\|} + \mathcal{B}_2 f_m(t, \omega) + \delta_2 f_{u_{41}}(t, \omega) + f_{u_{42}}(t, \omega) \end{aligned} \quad (5.31)$$

Therefore,

$$\begin{aligned} \sigma^T(t) \dot{\sigma}(t) \leq & -\|\sigma\| \left\{ \left[ |\mathcal{B}_2| \beta(t, T_r^{-1} \omega + x_d) + (|\delta_2| + 1) \right. \right. \\ & \times \left( \gamma(t, T_r^{-1} \omega + x_d) + \|\mathcal{A}\| \|x_d\| + \|\dot{x}_d\| \right) + \rho \left. \right] \\ & - |\mathcal{B}_2| \|f_m(t, \omega)\| - |\delta_2| \|f_{u_{41}}(t, \omega)\| \\ & \left. - \|f_{u_{42}}(t, \omega)\| \right\} \\ \leq & -\|\sigma\| \left\{ \left[ |\mathcal{B}_2| \beta(t, T_r^{-1} \omega + x_d) + (|\delta_2| + 1) \right. \right. \\ & \times \left( \gamma(t, T_r^{-1} \omega + x_d) + \|\mathcal{A}\| \|x_d\| + \|\dot{x}_d\| \right) + \rho \left. \right] \\ & - |\mathcal{B}_2| \beta(t, T_r^{-1} \omega + x_d) - |\delta_2| \left( \gamma(t, T_r^{-1} \omega + x_d) \right. \\ & \left. + \|\mathcal{A}\| \|x_d\| + \|\dot{x}_d\| \right) - \left( \gamma(t, T_r^{-1} \omega + x_d) \right. \\ & \left. + \|\mathcal{A}\| \|x_d\| + \|\dot{x}_d\| \right) \left. \right\} \\ \leq & -\rho \|\sigma(t)\| \end{aligned} \quad (5.32)$$

where  $\rho$  is defined in (5.28). Inequality (5.32) shows that the reaching condition (5.28) is satisfied. Hence the result follows.  $\blacksquare$

**Remark 5.3.** Based on SMC theory, Theorems 5.1 and 5.2 together show that the closed-loop system formed by applying the control (5.29) to the system (5.14) is uniformly ultimately bounded. From (5.12), it follows that

$$e(t) = T_r^{-1} \omega(t) \quad (5.33)$$

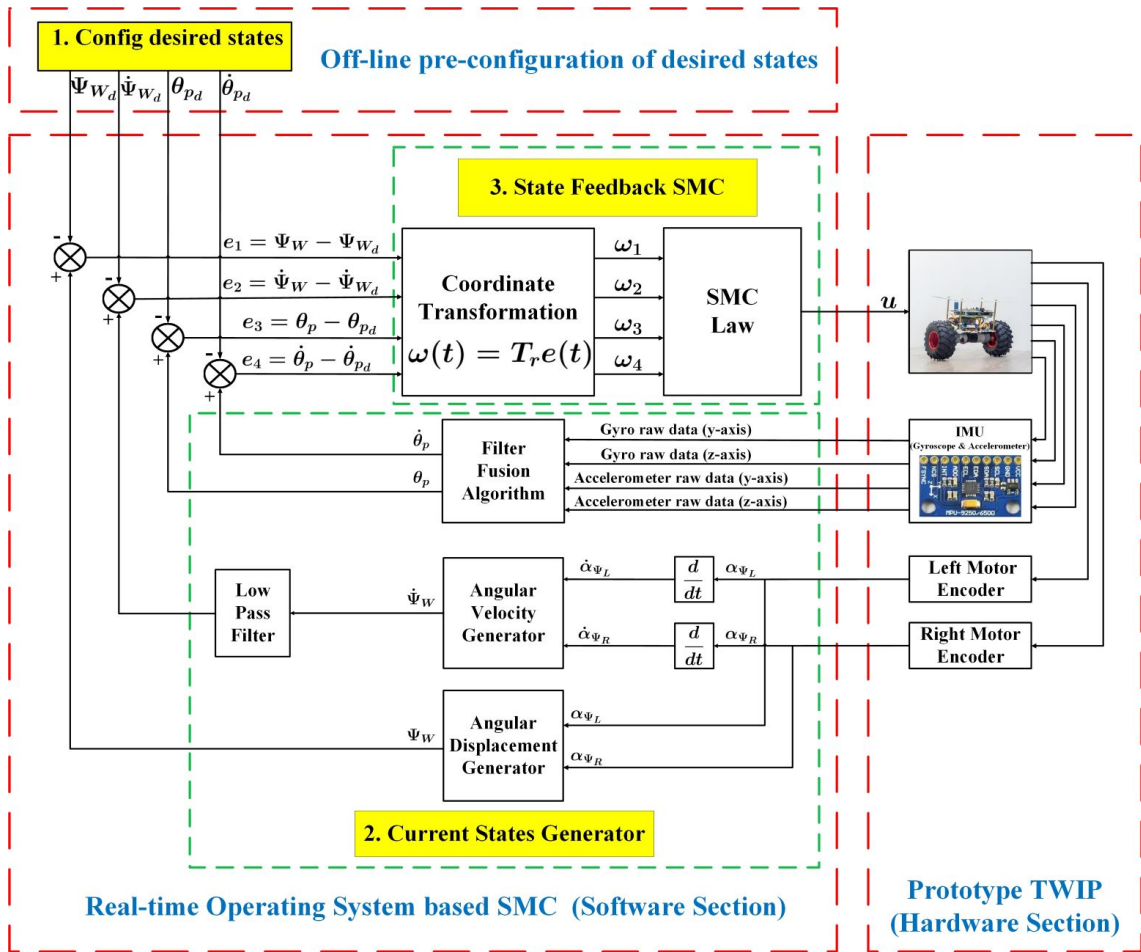


Figure 5.2: State Feedback Sliding Mode Control Architecture of a Two-wheeled Inverted Pendulum

where  $T_r$  is defined in (5.13).

Therefore, the tracking error  $e(t)$  is also uniformly ultimately bounded.

## 5.3. DESCRIPTION OF CONTROL ARCHITECTURE

This section describes the state feedback SMC architecture illustrated in Figure 5.2 similar to the one presented in Section 4.4, which also contains the software and hardware sections.

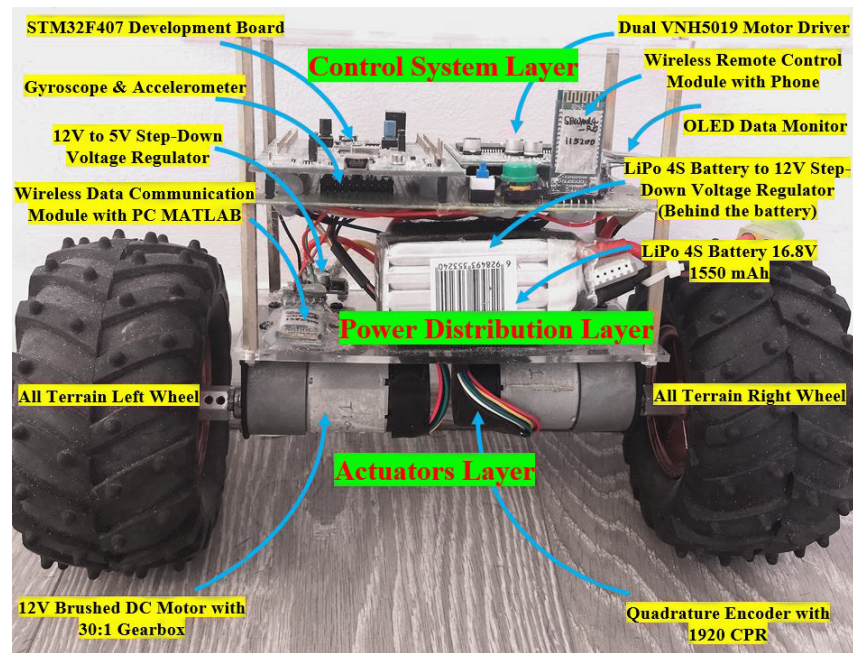


Figure 5.3: The prototype of the TWIP platform

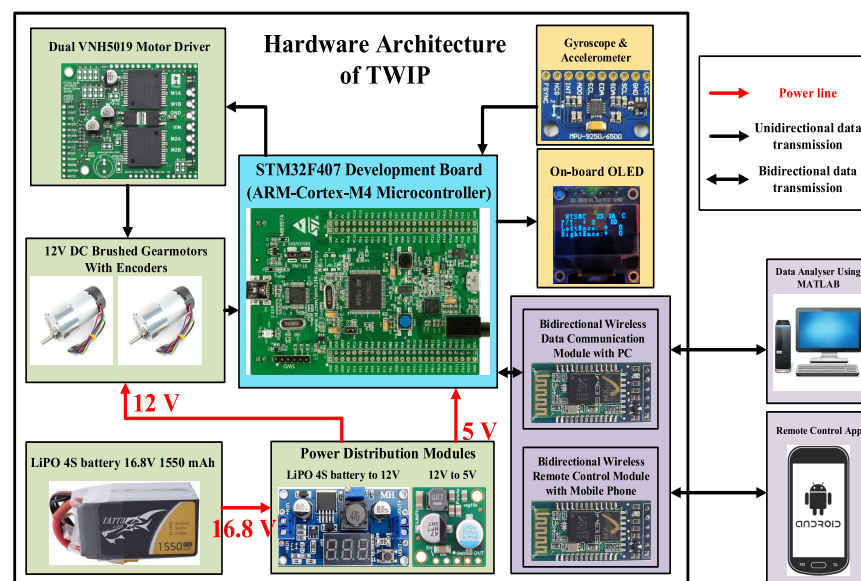


Figure 5.4: Hardware architecture of the Two-wheeled Inverted Pendulum

- **Software section:** The software section involves two features, the former is an standalone off-line pre-configuration process, and the latter is the combination of a current states generator and a state feedback SMC, which are implemented based on a self-developed light-weight cooperative RTOS framework. The detailed architecture is elucidated in Section 5.4.

Table 5.1: Model parameters for the TWIP

Symbols with units	Definitions	Values
$M_B$ [kg]	Mass of body	1.008
$M_W$ [kg]	Mass of wheel	0.179
$R$ [m]	Radius of wheel	0.06
$L$ [m]	Length to CoG	0.09
$J_W$ [kg.m <sup>2</sup> ]	Inertial of wheel	0.001032
$J_{P_\theta}$ [kg.m <sup>2</sup> ]	y-axis inertial of body	0.0027

1. **Off-line pre-configuration of desired states:** The desired states are often configured prior to the execution of control law to indicate that at what equilibrium points the TWIP system is supposed to be controlled.
2. **Real-time current states generator:** Having configured the desired states in part 1, the objective of this chapter in (5.5) can be achieved by determining the actual states of the TWIP system in real time. In Figure 5.2, the state of angular displacement of the robot can be directly computed from the angular positions  $\alpha_{\Psi_L}$  and  $\alpha_{\Psi_R}$  of the two encoders. The corresponding angular velocity state of the TWIP system is obtained from the derivatives of encoder outputs. Because of the noises occurring from the differentiation of the angular position signals of the encoders, a low pass filter is augmented to the system to eliminate as much noises as possible for better performance. To obtain the attitude states, the same IMU sensor is employed as in Chapter 4 to retrieve the self-balancing pitch angle and angular rate respectively using the filter fusion algorithm described in Appendix C.2.1. Then all the state variables are to be compared to the desired states and the associated error state  $e(t)$  is fed into the coordinate transformation block  $\omega(t) = T_r e(t)$  of (5.12) for the execution of control law.
3. **Real-time state feedback SMC:** The SMC law in (5.29) employs the output  $\omega$  states to generate the necessary control signal for regulating the  $\omega$  state

uniformly ultimately bounded based on Theorem 5.1. Further, from Remark 5.3, the inverse coordinate transformation  $e(t) = T_r^{-1}\omega(t)$  indicates that the control objective (5.5) is achieved.

The procedures of aforementioned part 2 and 3 will be performed repeatedly in real time to satisfy the control goal of (5.5) for the TWIP system.

- **Hardware section:** A prototype TWIP platform has been fabricated as illustrated in Figure 5.3, which is designed in three layers, namely Control System Layer (CSL), Power Distribution Layer (PDL), and Actuators Layer (AL) from top to bottom. The dimension of this TWIP is 0.29m x 0.153m x 0.192m (width x depth x height), and it weighs 1.366 kg in total, including the body and two wheels. The parameters of the TWIP is provided in Table 5.1. It is worth mentioning that the process of retrieving the moment of inertia  $J_W$  is described in Appendix C.2.2. Moreover, the general hardware architecture is depicted in Figure 5.4. The raw attitude data and the proposed control scheme are sampled and executed in CSL, the former are collected using a 9-axis IMU, which is further filtered by a Mahony algorithm [147] to retrieve the Euler angles (See Figure C.7 in Section C.2.1) and the latter is implemented based on the presented control law (5.29). All data are transmitted to both PC MATLAB and mobile phone via wireless Bluetooth modules for validity and performance analysis. Moreover, PDL consists of a LiPo 4S battery as the primary external power source and a power distribution module for allocating different voltages to actuators and microcontroller board. In addition, Two 12V DC motors with two 1920 counts per revolution quadrature encoders are attached in the AL. It should be noted that the motors are driven independently by two motor driver carriers with the function of supporting up to 20 kHz PWM signals generated from an ARM-based STM32F407 microcontroller board. Finally, the primary sampling period for data collection, filtration and control execution is 10 ms within a light-weight cooperative RTOS. The detailed hardware specifications and RTOS software architecture are described in Appendix B and Section 5.4, respectively.

## 5.4. REAL-TIME OPERATING SYSTEM BASED EMBEDDED ARCHITECTURE DESIGN FOR CONTROL OF THE TWO-WHEELED INVERTED PENDULUM

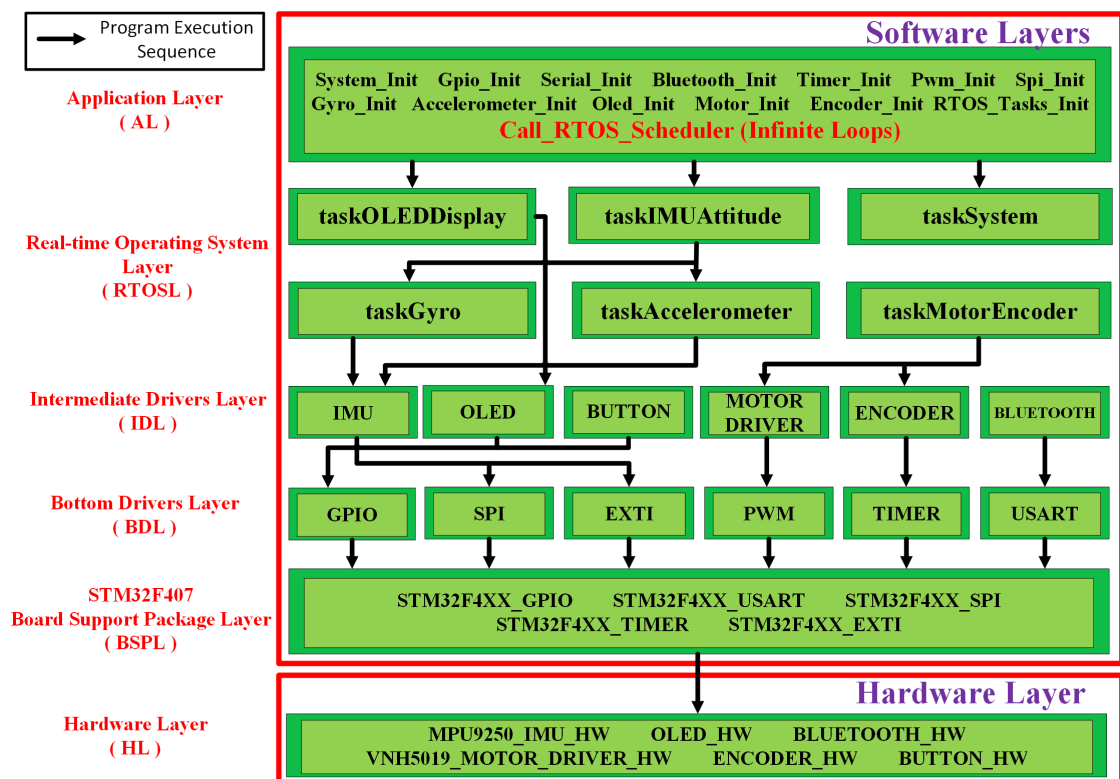


Figure 5.5: Real-time Operating System Based Software Architecture of the TWIP System

This section introduces an embedded architecture for controlling the TWIP system based on a self-developed lightweight cooperative time-driven RTOS. RTOS is a software program that rapidly switches between pre-allocated tasks, giving the illusion that multiple missions are being executed simultaneously on a single processing unit. RTOS is prevailing in robotics because it provides a deterministic hard real-time response than the soft response of distributed operating systems, for example, Linux, Windows. Figure 5.5 illustrates the software architecture implemented on the STM32F407 microcontroller board

(See Figure B.1 (b) in Appendix B.1) of the TWIP robot, which consists of five different layers, namely STM32F407 board support package layer (BSPL), Bottom Drivers Layer (BDL), Intermediate Drivers Layer (IDL), Real-time Operating System Layer (RTOSL), and Application Layer (AL).

- **STM32F407 board support package layer (BSPL)** provides the low-level register-based hardware-specific drivers by the ST company that allow upper layer routines to exchange the data information with the onboard hardware peripherals. It should be pointed out that BSPL is customisable based on different hardware resources of the embedded board. In this thesis, for the STM32F407 board of the TWIP platform, the minimum required BSP drivers are the general-purpose input/output (GPIO), Universal Synchronous/Asynchronous Receiver/Transmitter (USART), Serial Peripheral Interface (SPI), Timer, and External Interrupt as illustrated in Figure 5.5.
- **Bottom Drivers Layer (BDL)** is a self-developed generic hardware abstraction layer (HAL) above the BSPL, primary for managing and allocating different hardware related resources whilst invoking the application programming interface (API) of BSPL to communicate with the onboard hardware. For example, BDL employs the 'struct' data type of 'ioPortDefs' variable to bundle all the GPIO ports together, such as GPIOA up to GPIOF and the 'struct' of 'uartDevice\_t' to deal with all available USART resources. Moreover, this layer also provides useful APIs for its upper layer, for example, the `getIOByPinNum(uint8_t pinNum)` API returns all the I/O information related to an input specific I/O pin number. The `serialWrite(serialPort_t *instance, uint8_t ch)` transmit a particular character 'ch' to a configured serial port. It should be emphasised that the purpose of designing a BDL as a universal layer is for code reusability, which is implemented not only for the TWIP system but also for all other applications using the STM32F407 board.
- **Intermediate Drivers Layer (IDL)** is another self-developed platform-specific driver layer which is designed solely for the TWIP system of this thesis. IDL contains the necessary drivers for control and data communication of the TWIP, including IMU driver, motor driver, encoder driver, bluetooth driver, etc.

- **Real-time Operating System Layer (RTOSL)** is yet another self-developed core layer consisting of multiple predefined tasks which can be executed simultaneously by a cooperative time-driven scheduler to improve system performance. The details of each task, illustrated in Figure 5.5, with the corresponding task execution period are described as follows.
  - taskSystem, running at 100 ms, calculates the CPU and tasks utilisations of the overall system.
  - taskGyro, running at 125  $\mu$ s, uses the SPI interface to retrieve the raw gyroscope data using the maximum potential output data rate, which is mentioned in Appendix B.3.
  - taskAccelerometer, running at 1 ms, obtains the raw accelerometer data.
  - taskIMUAttitude, running at 10 ms, employs the raw data from the gyroscope and accelerometer tasks and feed into the Mahony filter fusion algorithm [147] to retrieve the Euler angles (See Appendix C.2.1) for the control implementation.
  - taskMotorEncoder, running at 10 ms, requests the data from gyroscope and IMU attitude tasks, then executes the SMC law to regulate the TWIP system.
  - taskOLEDDisplay, running at 50 ms, displays pitch and yaw angle information, the angular displacement of both wheels, etc on an onboard OLED device for debugging purposes. Moreover, this task also transmits the real-time data to the PC Matlab for data display and logging.
- **Application Layer (AL)** is the self-developed top layer for initialising the required hardware resources and RTOS tasks of the TWIP system, for example, the initialisations of the numbers of allocated GPIO pins, gyroscope, accelerometer, timer, PWM for motor control, SPI for IMU data transmission, etc. After initialising all the compulsory processes, most importantly, AL invokes the RTOS scheduler algorithm to start running the pre-allocated tasks concurrently.

## 5.5. SIMULATION AND EXPERIMENT RESEARCH

The verification of the proposed control law is conducted under both simulation and experiment, which will be elaborated in this section.

### 5.5.1. NUMERICAL SIMULATION

The simulation is tested under the scenario with which the TWIP is driven on a flat surface. The control aim is to balance the TWIP to the desired equilibrium  $x_d = [0, 0, 0, 0]^T$ . By using the data from Table 5.1, the corresponding system can be described based on (5.6), (5.7) and (5.8) as

$$\dot{x}(t) = \underbrace{\begin{bmatrix} 0 & 1 & 0 & 0 \\ 0 & 0 & -137.0893 & 0 \\ 0 & 0 & 0 & 1 \\ 0 & 0 & 219.2744 & 0 \end{bmatrix}}_{\mathcal{A}} x(t) + \underbrace{\begin{bmatrix} 0 \\ 307.7729 \\ 0 \\ -400.4251 \end{bmatrix}}_{\mathcal{B}} (u(t) + f_m(t, x)) + \underbrace{\begin{bmatrix} 0 \\ -153.7336 \\ 0 \\ 154.0393 \end{bmatrix}}_{f_{u_2}(t, x)} \tau_W \quad (5.34)$$

It can be verified that the matrix pair  $(\mathcal{A}, \mathcal{B})$  is controllable. Therefore, Assumption 5.1 is satisfied.

Based on Assumption 5.2 and system (5.34), the unknown signals  $f_m(t, x)$  and

$f_{u_2}(t, x)$ , defined in (5.4) and (5.8), satisfy

$$\begin{aligned} \|f_m(t, x)\| &= \|\tau_B\| \leq \underbrace{\frac{1}{40}|x_4| + \frac{7}{200}\sin^2(x_4)}_{\beta(t,x)} \\ \|f_{u_2}(t, x)\| &= \left\| \begin{bmatrix} 0 \\ -153.7336 \\ 0 \\ 154.0393 \end{bmatrix} \right\| \|\tau_W\| \\ &\leq \underbrace{217.6284 \left( \frac{11}{200}|x_2| + \frac{6}{125}\sin^2(x_2) \right)}_{\gamma(t,x)} + 5.0 \end{aligned} \quad (5.35)$$

Choose  $\delta_1 = 6.9$ ,  $\delta_2 = 2.2$  and  $\delta_3 = 13.7$  satisfying the conditions (5.22) of Lemma 5.1. The corresponding switching function is determined as

$$\sigma(t) = 6.9\omega_1(t) + 2.2\omega_2(t) + 13.7\omega_3(t) + \omega_4(t) \quad (5.36)$$

Further, based on the system in (5.14), it follows that the regular form of (5.34) can be described by

$$\begin{aligned} \dot{\omega}(t) &= \underbrace{\begin{bmatrix} 5.3034 & 2.6910 & 10.53 & 0 \\ 0 & 0 & 31.4484 & 0 \\ -6.9 & -2.2 & -13.7 & 0 \\ 0 & 0 & 219.2744 & 0 \end{bmatrix}}_{\bar{A}} \omega(t) \\ &+ \underbrace{\begin{bmatrix} 0 \\ 0 \\ 0 \\ -400.4251 \end{bmatrix}}_{\bar{B}} \left( u(t) + f_m(t, \omega) \right) + \underbrace{\begin{bmatrix} 0 \\ f_{u_{41}}(t, \omega) \\ 0 \\ f_{u_{42}}(t, \omega) \end{bmatrix}}_{f_{u_4}(t, \omega)} \end{aligned} \quad (5.37)$$

It is noticeable from (5.37) that  $\mathcal{B}_2 = -400.4251 \neq 0$ . Hence, Assumption 5.3 is held.

According to the coordinate transformation (5.12) and the conditions of (5.11), (5.16), (5.35), it follows that  $f_m(t, \omega)$  and  $f_{u_4}(t, \omega)$  in (5.37) satisfy

$$\begin{aligned} \|f_m(t, \omega)\| &\leq \underbrace{\frac{1}{40}|\omega_4(t) + x_{4_d}(t)| + \frac{7}{200}\sin^2(\omega_4(t) + x_{4_d}(t))}_{\beta(t, T_r^{-1}\omega + x_d)} \\ \|f_{u_4}(t, \omega)\| &\leq \underbrace{217.6284\left(\frac{11}{200}|\omega_2 - 0.7686\omega_4 + x_{2_d}|\right.}_{\gamma(t, T_r^{-1}\omega + x_d)} \\ &\quad \left. + \frac{6}{125}\sin^2(\omega_2 - 0.7686\omega_4 + x_{2_d})\right) + 5.0 \end{aligned} \quad (5.38)$$

From the system matrix  $\bar{A}$  in (5.37) and the matrix  $\tilde{A}_{11}^s$  defined in (5.21), it follows that

$$\tilde{A}_{11}^s = \begin{bmatrix} 5.3034 & 2.6910 & 10.53 \\ 0 & 0 & 31.4484 \\ -6.9 & -2.2 & -13.7 \end{bmatrix} \quad (5.39)$$

It is straightforward to check that  $\frac{n_3}{n_2+n_4} = 31.4484 \neq 0$ . Hence, Assumption 5.4 is satisfied, and  $\tilde{A}_{11}^s$  is Hurwitz stable.

Therefore, for  $Q = I_3$ , the solution of Lyapunov equation (5.25) is

$$P = \begin{bmatrix} 2.9859 & 0.4012 & 2.3675 \\ 0.4012 & 0.2210 & 0.7180 \\ 2.3675 & 0.7180 & 3.5043 \end{bmatrix} \quad (5.40)$$

The designed SMC control law is

$$\begin{aligned} u(t) = 0.0025 &\left\{ 6.9\omega_2 + 288.4607\omega_3 + 8.3966\omega_4 + \left[ 400.4251\left(\frac{1}{40}|\omega_4(t) + x_{4_d}(t)| \right. \right. \right. \\ &\quad \left. \left. + \frac{7}{200}\sin^2(\omega_4(t) + x_{4_d}(t))\right) + 3.2\left(217.6284\left(\frac{11}{200}|\omega_2(t) + x_{2_d}(t) - 0.7686\omega_4(t)| \right. \right. \right. \\ &\quad \left. \left. + \frac{6}{125}\sin^2(\omega_2(t) - 0.7686\omega_4(t) + x_{2_d}(t))\right) + 5.0\right] \frac{\sigma(t)}{\|\sigma(t)\|} \right\} \end{aligned} \quad (5.41)$$

For simulation purpose, the initial condition is chosen as  $x_0 = [0.02, 0, 0.4363, 0]^T$ , which implies that the initial position is 0.02 metre and the initial attitude angle is

0.4363 in radian. Moreover, the control design parameter  $\rho = 5.0$ . The time responses of the system states and errors are shown in Figure 5.6 and Figure 5.7, respectively, and the control signal, described in PWM signal under 12V, is shown in Figure 5.8. The results demonstrate the effectiveness and robustness of the controller, which are uniformly ultimately bounded as proved in Theorem 5.1.

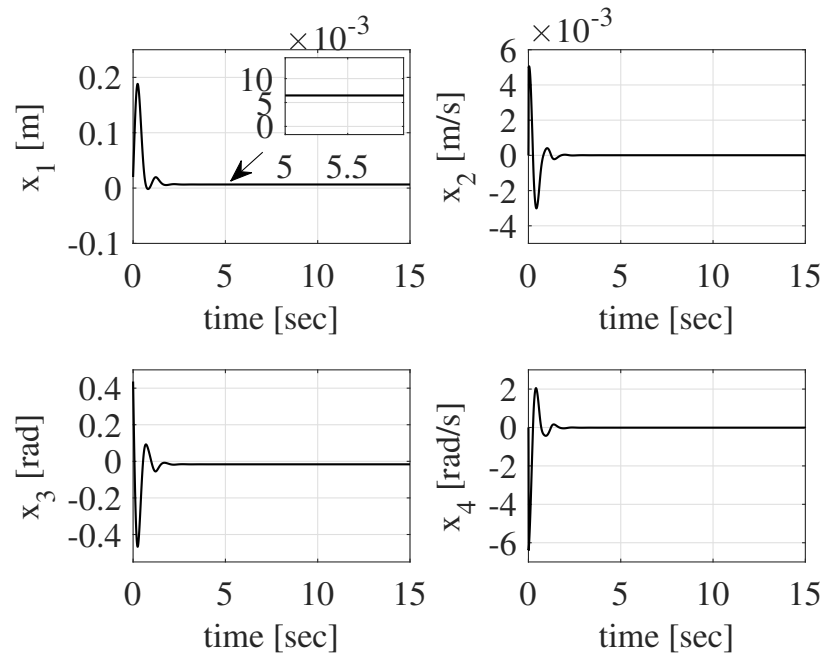


Figure 5.6: The responses of the system states under simulation

### 5.5.2. EXPERIMENTAL RESULTS

In this section, the TWIP is placed stationary on a flat surface and tilted with initial attitude angle  $x_3 = 0.4363$  rad and the initial position at  $x_1 = 0.02$  metre. Figures 5.9 and 5.10 show the time responses of the system states and errors, respectively. Figure 5.11 illustrates the control signal to balance the TWIP to the equilibrium status. The experimentation demonstrates that the obtained practical results are in consistence with the corresponding simulation ones.

**Remark 5.4.** From engineering perspective, it is worth mentioning that the majorities of the noises for a TWIP system come from the motor vibrations. Moreover, the backlash, caused by the gearboxes, might also influence the robustness of the control. However,

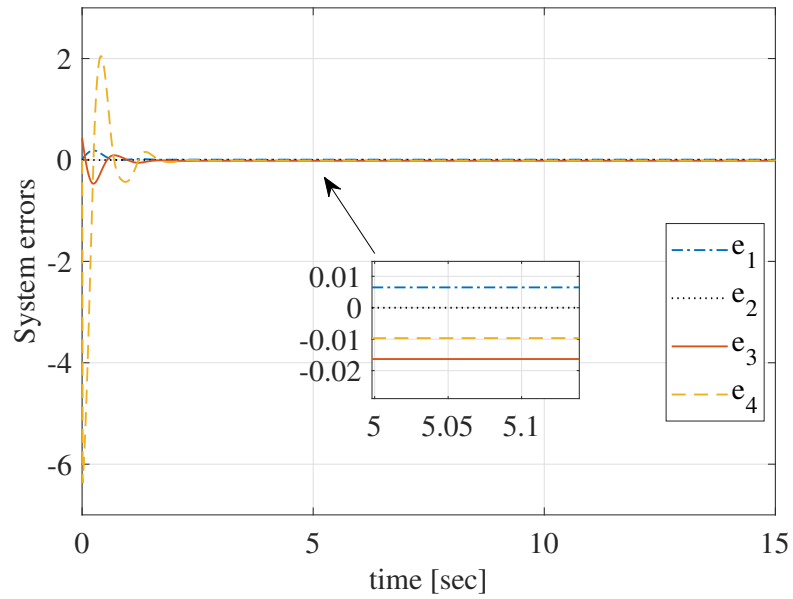


Figure 5.7: The responses of the error system under simulation

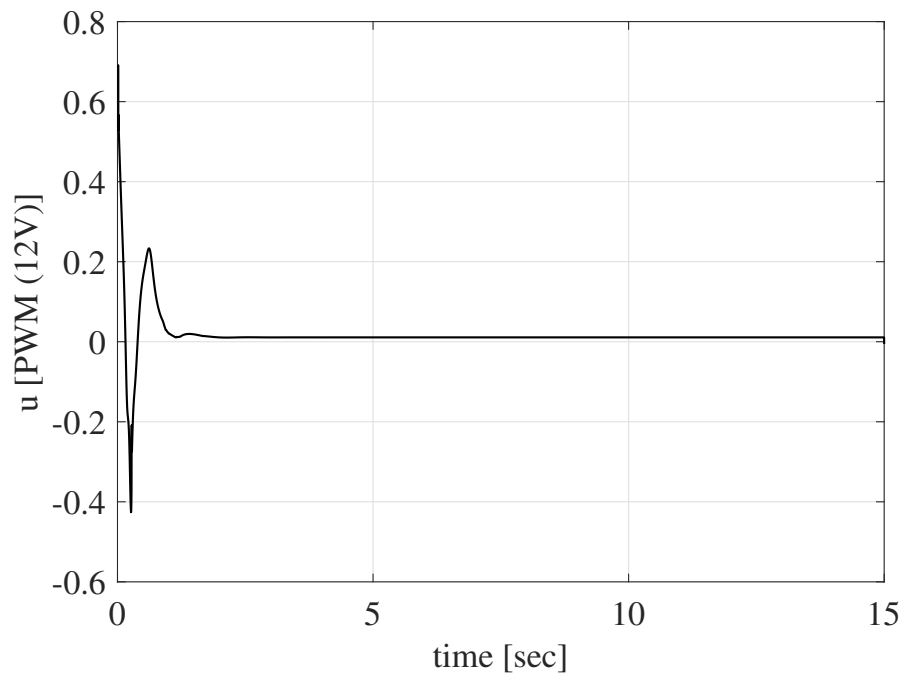


Figure 5.8: The response of the control under simulation

the negative effects of motor noises and backlash are all be able to classified as matched uncertainties, which can be completely nullified by the SMC during sliding motion to improve the system performance.

**Remark 5.5.** For the practical implementation of the TWIP, the SMC law (5.29), de-

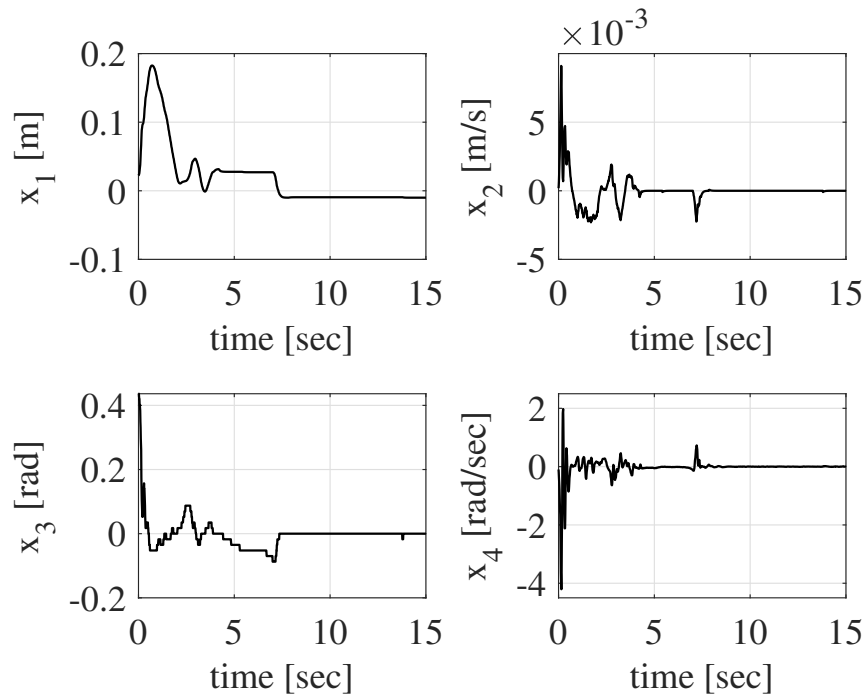


Figure 5.9: The responses of the system states on a practical TWI platform

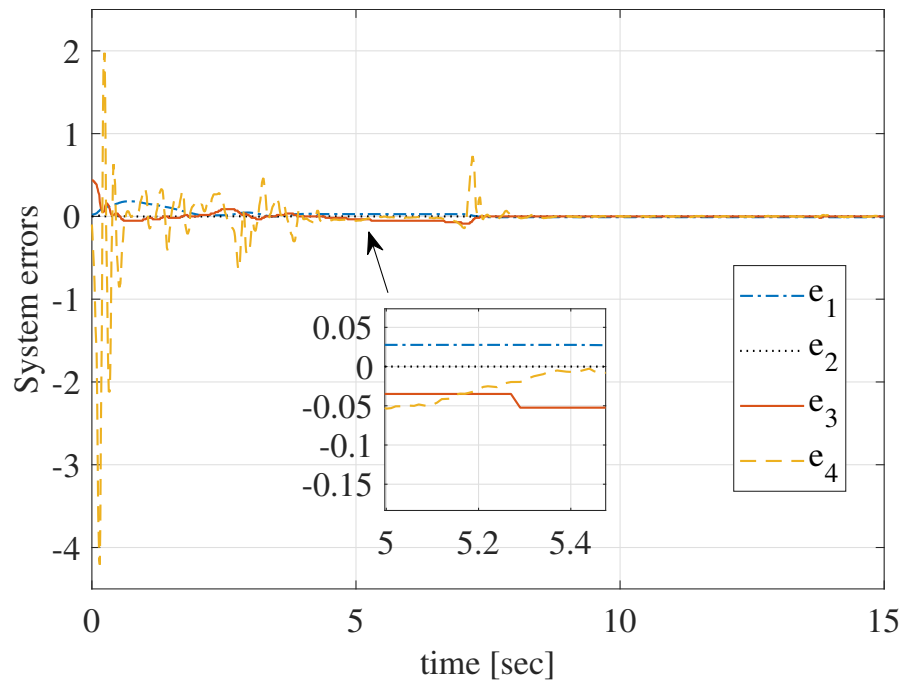


Figure 5.10: The responses of the error system on a practical TWIP platform

signed based on the linearised model (5.6), is applied to the nonlinear system model (5.3) rather than the linearised dynamics (5.6) to demonstrate the effectiveness and robustness of the control. The results in Figures 5.9, 5.10 and 5.11 show that the proposed control

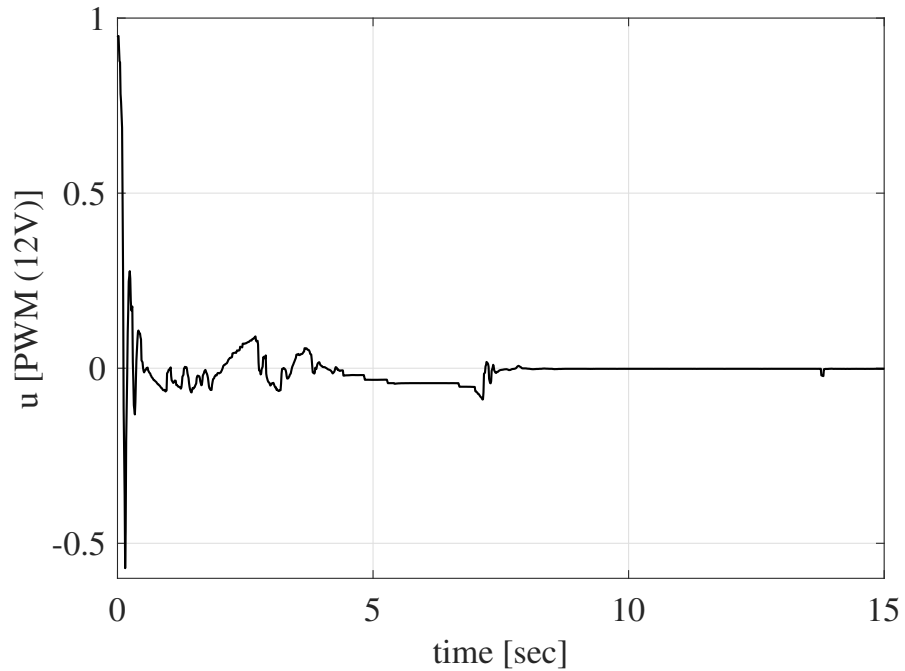


Figure 5.11: The response of the control on a practical TWIP platform

scheme is able to stabilise the TWIP properly even in the presence of the matched and unmatched uncertainties. In addition, both the simulation and experiment indicate that the results are uniformly ultimately bounded. These confirm the theoretical results obtained in Theorems 5.1 and 5.2.

## 5.6. CONCLUSION

In this chapter, the proposed SMC scheme employs the full-state vector to control the TWIP system. However, state variables are not always available due to the absence of transducers, imprecise measurement of the sensing devices, unaffordable equipment, etc. Therefore, the next chapter will present a static output feedback SMC law to regulate the TWIP system using only output information.

## CHAPTER. 6

---

# STATIC OUTPUT FEEDBACK CONTROL OF A TWO-WHEELED INVERTED PENDULUM

---

This chapter presents a static output feedback SMC scheme to regulate the TWIP system using partial state information. Section 6.1 describes the TWIP system based on the Lagrangian approach with the considerations of unknown matched and unmatched uncertainties. Then the model is linearised and further transformed into a regular form to facilitate the stability analysis and control design. Next, a sliding surface is designed and the stability and reachability analyses are carried out in Section 6.2. Section 6.3 verifies the designed control scheme on the TWIP system under simulation. Finally, Section 6.4 draws some conclusions.

## 6.1. PROBLEM FORMULATION AND PRELIMINARIES

### 6.1.1. SYSTEM DESCRIPTIONS

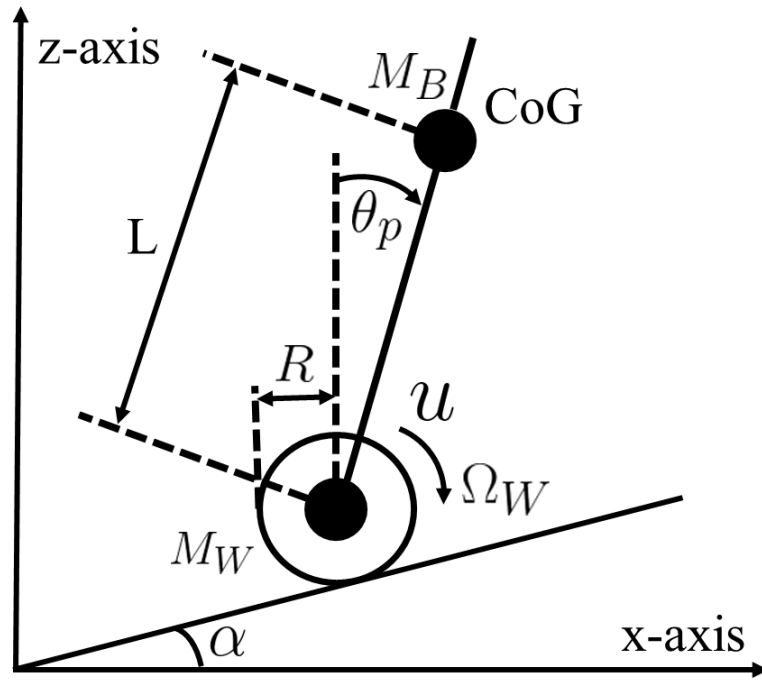


Figure 6.1: Description of a two-wheeled inverted pendulum

Consider the longitudinal Lagrangian dynamics of the TWIP system [109].

$$\left\{ \begin{array}{l} c_1 \ddot{\theta}_p + c_2 \cos(\theta_p + \alpha) \ddot{\Omega}_W - c_3 \sin \theta_p = -u - c_b \dot{\theta}_p - \tau_M \\ c_4 \ddot{\Omega}_W + c_2 \cos(\theta_p + \alpha) \ddot{\theta}_p - c_2 \sin(\theta_p + \alpha) \dot{\theta}_p^2 + c_5 \\ = u + c_b \dot{\theta}_p - c_r \dot{\Omega}_W + \tau_M - \tau_W \end{array} \right. \quad (6.1)$$

where  $c_1, c_2, c_3, c_4, c_5$  are constants and defined by

$$\begin{aligned} c_1 &= M_B L^2 + J_{\theta_p}, \quad c_2 = 2M_B L R \\ c_3 &= M_B g L, \quad c_4 = 4(M_B + M_W) R^2 + J_w \\ c_5 &= 2gR(M_B + M_W) \sin \alpha \end{aligned} \quad (6.2)$$

$L$  is the length between the wheel axis and the centre of gravity (CoG) of the body,  $\theta_p$  represents the attitude pitch angle,  $R$  and  $\Omega_W$  denote the radius and angular displacement of the wheels, respectively,  $M_B$ ,  $M_W$  are the masses of the TWIP body and wheel accordingly,  $\alpha$  is a positive known constant, which denotes the inclination angle of a slope.  $J_{\theta_p}$  is the moment of inertia of the body w.r.t  $y$  axis, and  $J_w$  is the moment of inertia of the wheel. In addition,  $c_b$  and  $c_r$  correspond to the driving and rolling friction coefficients of the body and wheels, respectively.  $u$  is defined as the control input applied to the actuators. Moreover,  $\tau_M$  denotes the matched uncertainties caused by the internal frictions of the motors.  $\tau_W$  is the unmatched uncertainties which are the correlation between the ground and the wheels, such as the slippage caused by the translational movement of the TWIP system.

**Remark 6.1.** The TWIP system in [109] is modelled based on the kinetic energy and potential energy of the Lagrangian method. However, it is inevitable to involve the dissipation energy in real systems [150]. Hence, the dynamics (6.1) is an improvement of the modelling in [109] by considering the dissipation energy caused by the frictions of TWIP body and rolling wheels.

The nonlinear dynamics (6.1) can be further derived as

$$\dot{x}(t) = F(t, x) + G(t, x)(u(t) + \Phi(t, x)) + \Psi(t, x) \quad (6.3)$$

where

$$F(\cdot) = \begin{bmatrix} x_3 \\ x_4 \\ \frac{f_1}{c_1 c_4 - c_2^2 \cos^2(x_2 + \alpha)} \\ \frac{f_2}{c_1 c_4 - c_2^2 \cos^2(x_2 + \alpha)} \end{bmatrix}, \quad G(\cdot) = \begin{bmatrix} 0 \\ 0 \\ \frac{c_1 + c_2 \cos(x_2 + \alpha)}{c_1 c_4 - c_2^2 \cos^2(x_2 + \alpha)} \\ -\frac{c_4 + c_2 \cos(x_2 + \alpha)}{c_1 c_4 - c_2^2 \cos^2(x_2 + \alpha)} \end{bmatrix}, \quad \Psi(\cdot) = \begin{bmatrix} 0 \\ 0 \\ -\frac{c_1}{c_1 c_4 - c_2^2 \cos^2(x_2 + \alpha)} \\ \frac{c_2 \cos(x_2 + \alpha)}{c_1 c_4 - c_2^2 \cos^2(x_2 + \alpha)} \end{bmatrix} \tau_W$$

$$\Phi(\cdot) = \tau_M$$

$$\begin{aligned} f_1 &= -c_2 c_3 \cos(x_2 + \alpha) \sin x_2 - c_1 c_5 - c_1 c_r x_3 \\ &\quad + c_b (c_1 + c_2 \cos(x_2 + \alpha)) x_4 + c_1 c_2 \sin(x_2 + \alpha) x_4^2 \\ f_2 &= c_3 c_4 \sin x_2 - c_2^2 \sin(x_2 + \alpha) \cos(x_2 + \alpha) x_4^2 \\ &\quad - c_b (c_4 + c_2 \cos(x_2 + \alpha)) x_4 + c_2 c_5 \cos(x_2 + \alpha) \\ &\quad + c_2 c_r \cos(x_2 + \alpha) x_3 \end{aligned} \tag{6.4}$$

$x(t) = [x_1, x_2, x_3, x_4]^T = [\Omega_W, \theta_p, \dot{\Omega}_W, \dot{\theta}_p]^T$  represents the state vector. The uncertainties  $\Phi(\cdot)$  and  $\Psi(\cdot)$  are used to denote matched and unmatched nonlinear disturbances, respectively.

Based on the approximate linearisation approach, dynamics (6.3) can be linearised around the desired signals  $x_d(t) = [x_{1_d}, x_{2_d}, x_{3_d}, x_{4_d}]^T = [\Omega_{W_d}, \theta_{p_d}, \dot{\Omega}_{W_d}, \dot{\theta}_{p_d}]^T$  as

$$\dot{x}(t) = Ax(t) + B(u(t) + \Phi(t, x)) + E\Delta\Psi(t, x) \tag{6.5}$$

$$y(t) = Cx(t) \tag{6.6}$$

where  $A$ ,  $B$ ,  $C$  and  $E$  are constant matrices defined by

$$\begin{aligned}
 A &= \begin{bmatrix} 0 & 0 & 1 & 0 \\ 0 & 0 & 0 & 1 \\ 0 & A_{32} & A_{33} & A_{34} \\ 0 & A_{42} & A_{43} & A_{44} \end{bmatrix}, \quad B = \begin{bmatrix} 0 \\ 0 \\ \frac{c_1+c_2(\cos\alpha-x_{2_d}\sin\alpha)}{c_1c_4-c_2^2\cos^2(x_{2_d}+\alpha)} \\ -\frac{c_4+c_2(\cos\alpha-x_{2_d}\sin\alpha)}{c_1c_4-c_2^2\cos^2(x_{2_d}+\alpha)} \end{bmatrix} \\
 C &= \begin{bmatrix} 1 & 0 & 0 & 0 \\ 0 & 1 & 0 & 0 \\ 0 & 0 & 0 & 1 \end{bmatrix}, \quad E = \begin{bmatrix} E_1 \\ E_2 \end{bmatrix} = \begin{bmatrix} 0 \\ 0 \\ -\frac{c_1}{c_1c_4-c_2^2\cos^2(x_{2_d}+\alpha)} \\ \frac{c_2(\cos\alpha-x_{2_d}\sin\alpha)}{c_1c_4-c_2^2\cos^2(x_{2_d}+\alpha)} \end{bmatrix} \\
 A_{32} &= \frac{-c_2c_3\cos\alpha + 2c_2c_3x_{2_d}\sin\alpha}{c_1c_4 - c_2^2\cos^2(x_{2_d} + \alpha)}, & A_{33} &= \frac{-c_1c_r}{c_1c_4 - c_2^2\cos^2(x_{2_d} + \alpha)} \\
 A_{34} &= \frac{c_b(c_1 + c_2\cos\alpha) - c_2c_dx_{2_d}\sin\alpha}{c_1c_4 - c_2^2\cos^2(x_{2_d} + \alpha)}, & A_{42} &= \frac{c_3c_4 - c_2c_5\sin\alpha - c_2c_r x_{3_d}\sin\alpha}{c_1c_4 - c_2^2\cos^2(x_{2_d} + \alpha)} \\
 A_{43} &= \frac{c_r c_2(\cos\alpha - x_{2_d}\sin\alpha)}{c_1c_4 - c_2^2\cos^2(x_{2_d} + \alpha)}, & A_{44} &= \frac{-c_b(c_4 + c_2\cos\alpha - c_2x_{2_d}\sin\alpha)}{c_1c_4 - c_2^2\cos^2(x_{2_d} + \alpha)}
 \end{aligned} \tag{6.7}$$

Suppose the angular velocity  $\dot{\Omega}_W$  of the wheels are not available. Then, the output state can be represented as  $y = [y_1, y_2, y_3]^T = [\Omega_W, \theta_p, \dot{\theta}_p]^T$ . Moreover,  $\Delta\Psi(\cdot) = \tau_W$  denote the unmatched uncertainties.  $E$  is employed to describe the structural characteristics of the unmatched uncertainty  $\Delta\Psi(\cdot)$ .

### 6.1.2. ANALYSIS OF THE ATTITUDE EQUILIBRIUM

When systems (6.5)-(6.6) reach the equilibrium point, the linear velocity, linear acceleration, the attitude angular velocity, acceleration and the friction torque related to the ground  $\tau_W$  are all zero. i.e.,  $x_3 = \dot{\Omega}_W = 0$ ,  $\dot{x}_3 = \ddot{\Omega}_W = 0$ ,  $x_4 = \dot{\theta}_p = 0$ ,  $\dot{x}_4 = \ddot{\theta}_p = 0$ , and  $\tau_W = 0$ . Hence, system (6.1) can be reduced as follows

$$\begin{aligned}
 -c_3\sin x_{2_d} &= -u - \tau_M \\
 c_5 &= u + \tau_M
 \end{aligned} \tag{6.8}$$

By simplifying (6.8), the desired attitude  $x_{2_d}$  can be derived as

$$x_{2_d} = \arcsin \left[ \frac{2R(M_B + M_W)}{M_B L} \sin\alpha \right] \tag{6.9}$$

**Remark 6.2.** It is worth mentioning that when the TWIP is travelled on a flat surface, i.e.,  $\alpha = 0$ , the desired attitude equilibrium is configured to zero (i.e.,  $x_{2_d} = 0$ ) in despite of the configurations of other parameters in (6.9). However, when the TWIP is driven on a slanted surface, i.e.,  $\alpha > 0$ ,  $x_{2_d}$  is not only dependent on the nominal parameters of the TWIP but also the inclined slope angle  $\alpha$ .

### 6.1.3. BASIC ASSUMPTIONS

The following assumptions are imposed on the system (6.5)-(6.6).

**Assumption 6.1.** The matrix pair  $(A, B)$  is completely controllable. Hence, according to [116], there exists a non-singular coordinate transformation  $\tilde{x} = \tilde{T}x$  such that the system triple  $(A, B, C)$  with respect to the new coordinates has the following structure matrices

$$\begin{aligned} \tilde{A} &= \begin{bmatrix} \tilde{A}_{11} & \tilde{A}_{12} \\ \tilde{A}_{21} & \tilde{A}_{22} \end{bmatrix}, & \tilde{B} &= \begin{bmatrix} 0 \\ \tilde{B}_2 \end{bmatrix} \\ \tilde{C} &= \begin{bmatrix} 0 & \tilde{C}_2 \end{bmatrix}, & \tilde{E} &= \begin{bmatrix} \tilde{E}_1 \\ \tilde{E}_2 \end{bmatrix} \end{aligned} \quad (6.10)$$

where  $\tilde{A}_{11} \in \mathbb{R}^{3 \times 3}$ ,  $\tilde{B}_2 \in \mathbb{R}$ ,  $\tilde{C}_2 \in \mathbb{R}^{3 \times 3}$  and  $\tilde{E}_1 \in \mathbb{R}^3$ .

**Assumption 6.2.** For the triple  $(\tilde{A}_{11}, \tilde{A}_{12}, \tilde{C}_2)$  with  $\tilde{C}_2 = [0_{2 \times 1} \ I_2]$ , there exists a positive constant matrix  $K = \begin{bmatrix} K_1 & K_2 \end{bmatrix} \in \mathbb{R}^{1 \times 2}$  such that  $\tilde{A}_{11} + \tilde{A}_{12}K\tilde{C}_2$  is stable.

**Remark 6.3.** Assumptions 6.1 and 6.2 together guarantee the existence of an output sliding surface for the triple  $(A, B, C)$  [116].

Further, consider a coordinate transformation  $z = \hat{T}\tilde{x}$  with the matrix  $\hat{T}$  defined by

$$\hat{T} = \begin{bmatrix} I_3 & 0 \\ K\tilde{C}_2 & I \end{bmatrix} \quad (6.11)$$

And let

$$T = \hat{T}\tilde{T} \quad (6.12)$$

be a composite nonsingular matrix.

It follows from above analysis that in the new coordinate transformation  $z = Tx$ , systems (6.5)-(6.6) with the triple  $(A, B, C)$  has the following regular form

$$\dot{z} = \begin{bmatrix} \hat{A}_{11} & \hat{A}_{12} \\ \hat{A}_{21} & \hat{A}_{22} \end{bmatrix} z + \begin{bmatrix} 0 \\ \hat{B}_2 \end{bmatrix} (u + \Phi(t, T^{-1}z)) \quad (6.13)$$

$$+ \begin{bmatrix} \tilde{E}_1 \\ K\bar{C}_2\tilde{E}_1 + \tilde{E}_2 \end{bmatrix} \Delta\Psi(t, T^{-1}z) \\ y = \begin{bmatrix} 0 & \hat{C}_2 \end{bmatrix} z \quad (6.14)$$

where  $\hat{A}_{11} = \tilde{A}_{11} + \tilde{A}_{12}K\bar{C}_2$  is Hurwitz stable,  $\hat{B}_2 \in \mathbb{R}$  and  $\hat{C}_2 \in \mathbb{R}^{3 \times 3}$  is nonsingular.

$$\begin{bmatrix} \hat{A}_{11} & \hat{A}_{12} \\ \hat{A}_{21} & \hat{A}_{22} \end{bmatrix} = TAT^{-1}, \quad \begin{bmatrix} 0 \\ \hat{B}_2 \end{bmatrix} = TB \quad (6.15)$$

$$\begin{bmatrix} 0 & \hat{C}_2 \end{bmatrix} = CT^{-1}, \quad \begin{bmatrix} \tilde{E}_1 \\ K\bar{C}_2\tilde{E}_1 + \tilde{E}_2 \end{bmatrix} = TE \quad (6.16)$$

**Remark 6.4.** According to the results of the preceding analysis, systems (6.5)-(6.6) can be transformed into systems (6.13)-(6.14) using a linear non-singular transformation  $z = Tx$ . It can be seen that systems (6.13) and (6.14) are in well-known canonical form, which will be employed subsequently for generating regular form based error dynamics to underpin the designs of sliding surface and control law.

For further system analysis, partition  $\hat{C}_2$  and  $T^{-1}$  as

$$\hat{C}_2 = \begin{bmatrix} \hat{C}_{21} & \hat{C}_{22} \end{bmatrix} \quad (6.17)$$

$$T^{-1} = \begin{bmatrix} \Lambda_1 & \Lambda_2 \end{bmatrix} \quad (6.18)$$

where  $\hat{C}_{21} \in \mathbb{R}^{3 \times 2}$  and  $\Lambda_1 \in \mathbb{R}^{4 \times 3}$ .

Then, systems (6.13) and (6.14) can be rewritten as

$$\dot{z}_1 = \hat{A}_{11}z_1 + \hat{A}_{12}z_2 + \tilde{E}_1\Delta\Psi(t, T^{-1}z) \quad (6.19)$$

$$\dot{z}_2 = \hat{A}_{21}z_1 + \hat{A}_{22}z_2 + \hat{B}_2(u + \Phi(t, T^{-1}z)) \\ + (K\bar{C}_2\tilde{E}_1 + \tilde{E}_2)\Delta\Psi(t, T^{-1}z) \quad (6.20)$$

$$y = \hat{C}_{21}z_{12} + \hat{C}_{22}z_2 \quad (6.21)$$

where  $z = [z_1 \ z_2]^T$  with  $z_1 \in \mathbb{R}^3$  and  $z_2 = [z_{11} \ z_{12}]^T$  with  $z_{11} \in \mathbb{R}$ .

**Assumption 6.3.** There exist known nonlinear  $\mathcal{C}^1$  functions (See Definition 2.3.1 in Section 2.3)  $\zeta_1$ ,  $\xi_1$ ,  $\zeta_2$  and  $\xi_2$  such that in the vicinity of the origin, the unknown matched and unmatched uncertainties  $\Phi$ ,  $\Delta\Psi$  are bounded by

$$\|\Phi(t, x)\| \leq \zeta_1(t, x) + \zeta_2(t, y) \quad (6.22)$$

$$\|\Delta\Psi(t, x)\| \leq \xi_1(t, x) + \xi_2(t, y) \quad (6.23)$$

where  $\zeta_1$  and  $\xi_1$  are Lipschitz with respect to  $x$  in the vicinity of the origin.

**Remark 6.5.** Assumption 6.3 states that the bounds on the matched and mismatched uncertainties are nonlinear and required to be known in order to reject the disturbances in the control design.

#### 6.1.4. CONTROL OBJECTIVE

The objective of this chapter is, for a given output signal  $y_d(t) = [y_{1_d}(t), y_{2_d}(t), y_{3_d}(t)]^T = [\Omega_{W_d}, \theta_{p_d}, \dot{\theta}_{p_d}]^T$ , to design a SMC scheme such that the system outputs of  $y(t)$  can track the desired signals  $y_d(t)$

$$\lim_{t \rightarrow \infty} \|y_i(t) - y_{i_d}(t)\| = 0 \quad \text{for } i = 1, 2, 3 \quad (6.24)$$

From the system and desired states  $x(t)$  and  $x_d(t)$  mentioned above, define the error states to be

$$e_x(t) = x(t) - x_d(t) \quad (6.25)$$

and the corresponding error outputs  $e_y(t) = [e_{y_1}, e_{y_2}, e_{y_3}]^T$  can be represented as

$$e_y(t) = y(t) - y_d(t) = Ce_x(t) \quad (6.26)$$

Then, the dynamics of the error states can be described by

$$\begin{aligned} \dot{e}_x(t) &= Ae_x + B(u + \Phi(t, e_x + x_d)) + Ax_d - \dot{x}_d \\ &\quad + E\Delta\Psi(t, e_x + x_d) \end{aligned} \quad (6.27)$$

$$y = Ce_x + Cx_d \quad (6.28)$$

It follows from Assumption 6.3 that  $\Phi(t, e_x + x_d)$  and  $\Psi(t, e_x + x_d)$  satisfy

$$\|\Phi(t, e_x + x_d)\| \leq \zeta_1(t, e_x + x_d) + \zeta_2(t, y) \quad (6.29)$$

$$\|\Delta\Psi(t, e_x + x_d)\| \leq \xi_1(t, e_x + x_d) + \xi_2(t, y) \quad (6.30)$$

## 6.2. SLIDING MODE ANALYSIS AND CONTROL DESIGN

Section 6.1 shows that there exists coordinate transformations  $z = Tx$  such that the TWIP system (6.5)-(6.6) can be described in (6.13)-(6.14) in the new coordinate  $z$ . In this section, a sliding surface will be designed and the corresponding stability will be analysed based on the reduced-order sliding mode dynamics.

Under Assumptions 6.1 and 6.2, consider an output dependent switching function

$$\sigma(e_y) = \Gamma e_y \quad (6.31)$$

where  $\Gamma \in \mathbb{R}^{1 \times 3}$  is a design matrix, which can be obtained from [116].

Hence, the corresponding sliding surface is described by

$$\sigma(e_y) = \Gamma e_y = 0 \quad (6.32)$$

Based on the transformation matrix (6.12), it follows from (6.19)-(6.21) and (6.27) that the error systems

$$e_z = T e_x = z - z_d \quad (6.33)$$

in  $z$  coordinate can be described by

$$\begin{aligned} \dot{e}_{z_1} = & \hat{A}_{11}e_{z_1} + \hat{A}_{12}e_{z_2} + \tilde{E}_1\Delta\Psi(t, T^{-1}(e_z + z_d)) \\ & + \hat{A}_{11}z_{1d} + \hat{A}_{12}z_{2d} - \dot{z}_{1d} \end{aligned} \quad (6.34)$$

$$\begin{aligned} \dot{e}_{z_2} = & \hat{A}_{21}e_{z_1} + \hat{A}_{22}e_{z_2} + \hat{B}_2(u + \Phi(t, T^{-1}(e_z + z_d))) \\ & + (K\bar{C}_2\tilde{E}_1 + \tilde{E}_2)\Delta\Psi(t, T^{-1}(e_z + z_d)) + \hat{A}_{21}z_{1d} \\ & + \hat{A}_{22}z_{2d} - \dot{z}_{2d} \end{aligned} \quad (6.35)$$

$$y = \hat{C}_{21}e_{z_1} + \hat{C}_{22}e_{z_2} + \hat{C}_{21}z_{1d} + \hat{C}_{22}z_{2d} \quad (6.36)$$

where  $e_z = [e_{z_1} \ e_{z_2}]^T$  with  $e_{z_1} \in \mathbb{R}^3$  and  $e_{z_2} = [e_{z_{11}} \ e_{z_{12}}]^T$  with  $e_{z_{11}} \in \mathbb{R}$ . Moreover,  $z_d = [z_{1_d} \ z_{2_d}]^T$  and  $z_{1_d} = [z_{11_d} \ z_{12_d}]^T$  are the desired signals of  $z$  and  $z_{1_d}$ , respectively.

According to (6.31), the new switching manifold in terms of the  $e_z$  dynamics becomes

$$\Gamma e_y = \Gamma C e_x = \Gamma C T^{-1} T e_x = \Gamma \underbrace{\begin{bmatrix} 0 & \hat{C}_2 \end{bmatrix}}_{C T^{-1}} \underbrace{e_z}_{T e_x} = \Gamma \hat{C}_2 e_{z_2} \quad (6.37)$$

Therefore, the associated sliding surface (6.32) can be rewritten as

$$\sigma(e_z) = e_{z_2} = 0 \quad (6.38)$$

### 6.2.1. STABILITY ANALYSIS OF THE SLIDING MODE

Based on the structure of system (6.34)-(6.36), the sliding motion of system (6.27)-(6.28) based on the sliding surface (6.38) is dominated by system (6.34). When (6.34) is restricted to the sliding surface (6.38), it follows that

$$\begin{aligned} \dot{e}_{z_1} = & \hat{A}_{11} e_{z_1} + \tilde{E}_1 \Delta \Psi(t, \Lambda_1(e_{z_1} + z_{1_d}) + \Lambda_2 z_{2_d}) + \hat{A}_{11} z_{1_d} \\ & + \hat{A}_{12} z_{2_d} - \dot{z}_{1_d} \end{aligned} \quad (6.39)$$

**Remark 6.6.** System (6.39) represents the reduced-order sliding mode dynamics of systems (6.27)-(6.28) associated with the sliding surface (6.38). It is worth noting that the matched uncertainty  $\Phi(\cdot)$  has no effect on the stability of the sliding mode system. Moreover, the sliding mode dynamics (6.39) and unmatched uncertainty  $\Delta \Psi(\cdot)$  only depend on partial error state  $e_{z_1}$  rather than  $e_z$ . Therefore, the conservatism is reduced compared to other existing works [37, 109] which utilise full-state variables in stability analyses.

Since  $\hat{A}_{11}$  of (6.34) is stable, for any symmetric positive definite matrix  $Q_{z_1}$ , there exists a symmetric positive definite matrix  $P_{z_1}$  satisfying the Lyapunov equation

$$\hat{A}_{11}^T P_{z_1} + P_{z_1} \hat{A}_{11} = -Q_{z_1} \quad (6.40)$$

The following theorem can now be presented.

**Theorem 6.1.** Under Assumptions 6.1-6.3. The sliding motion of systems (6.34)-(6.36) associated with the sliding surface (6.38), governed by the sliding mode dynamics (6.39)

is uniformly ultimately bounded if the following condition is satisfied

$$\begin{aligned} \frac{1}{2}\underline{\lambda}(Q_{z_1})\|e_{z_1}\|^2 &> \|P_{z_1}e_{z_1}\| \left( \|\tilde{E}_1\|(\xi_1(t, \Lambda_1(e_{z_1} + z_{1d}) \right. \\ &\quad \left. + \Lambda_2 z_{2d}) + \xi_2(t, \hat{C}_{21}(e_{z_{12}} + z_{12d}) \right. \\ &\quad \left. + \hat{C}_{22}z_{2d})) + \|\hat{A}_{11}z_{1d} + \hat{A}_{12}z_{2d} - \dot{z}_{1d}\| \right) \end{aligned} \quad (6.41)$$

where  $\underline{\lambda}(Q_{z_1})$  is the minimum eigenvalue of matrix  $Q_{z_1}$ .

*Proof:* For the reduced-order sliding mode dynamics (6.39), consider the Lyapunov function candidate

$$V(e_{z_1}) = e_{z_1}^T P_{z_1} e_{z_1} \quad (6.42)$$

Based on (6.40), the time derivative of  $V$  along the trajectories of sliding mode dynamics (6.39) is given by

$$\begin{aligned} \dot{V}|_{(6.39)} &= -e_{z_1}^T Q_{z_1} e_{z_1} + 2e_{z_1}^T P_{z_1} (\tilde{E}_1 \Delta\Psi(\Lambda_1(e_{z_1} + z_{1d}) \\ &\quad + \Lambda_2 z_{2d}) + \hat{A}_{11}z_{1d} + \hat{A}_{12}z_{2d} - \dot{z}_{1d}) \\ &\leq -\underline{\lambda}(Q_{z_1})\|e_{z_1}\|^2 + 2\|P_{z_1}e_{z_1}\|(\|\tilde{E}_1\| \\ &\quad \times \|\Delta\Psi(\Lambda_1(e_{z_1} + z_{1d}) + \Lambda_2 z_{2d})\| + \|\hat{A}_{11}z_{1d} \\ &\quad + \hat{A}_{12}z_{2d} - \dot{z}_{1d}\|) \end{aligned} \quad (6.43)$$

From (6.18), (6.23), (6.30), (6.33) and (6.36)

$$\begin{aligned} \dot{V}|_{(6.39)} &\leq -\underline{\lambda}(Q_{z_1})\|e_{z_1}\|^2 + 2\|P_{z_1}e_{z_1}\|(\|\tilde{E}_1\| \\ &\quad \times (\xi_1(t, \Lambda_1(e_{z_1} + z_{1d}) + \Lambda_2 z_{2d}) + \xi_2(t, \hat{C}_{21}(e_{z_{12}} \\ &\quad + z_{12d}) + \hat{C}_{22}z_{2d})) + \|\hat{A}_{11}z_{1d} + \hat{A}_{12}z_{2d} - \dot{z}_{1d}\|) \end{aligned} \quad (6.44)$$

It follows from (6.41) that the time derivative of  $V(e_{z_1})$  along the trajectories of systems (6.39) is negative definite. Therefore, the conclusion follows.  $\blacksquare$

### 6.2.2. REACHABILITY ANALYSIS

The aim now is to design an output feedback SMC such that the system states of  $e_x(t)$  are driven to the sliding surface (6.31) in finite time.

In order to design the control law, the following partitions are introduced

$$e_z = Te_x = \begin{bmatrix} (Te_x)_1 \\ (Te_x)_2 \end{bmatrix} \quad (6.45)$$

$$T^{-1} = \begin{bmatrix} \Theta_1 & \Theta_2 \end{bmatrix} \quad (6.46)$$

where  $(Te_x)_1 \in \mathbb{R}$  and  $\Theta_1 \in \mathbb{R}^{4 \times 1}$ .

**Remark 6.7.** It is worth mentioning that the partition in (6.46) is different from the one showed in (6.18). The partition in (6.18) is related to the design of the sliding surface to facilitate the stability analysis of the sliding motion whereas the partition of (6.46) is correlated with the dimension of the output matrix for control design and reachability analysis.

From (6.14), (6.25) and (6.45), it follows that

$$(Te_x)_2 = \widehat{C}_2^{-1}y - (Tx_d)_2 \quad (6.47)$$

From (6.33), (6.45)-(6.47) that

$$\begin{aligned} e_x &= T^{-1}e_z = T^{-1} \begin{bmatrix} (Te_x)_1 \\ \widehat{C}_2^{-1}y - (Tx_d)_2 \end{bmatrix} \\ &= \Theta_1(Te_x)_1 + \Theta_2(\widehat{C}_2^{-1}y - (Tx_d)_2) \end{aligned} \quad (6.48)$$

Further, assuming  $\|\Theta_1(Te_x)_1\| \leq \delta$  is bounded in the vicinity of the origin. Then the control scheme can now be proposed

$$\begin{aligned} u(t) &= -(\Gamma CB)^{-1} \left\{ \Gamma CA\Theta_2\widehat{C}_2^{-1}y - \Gamma CA\Theta_2(Tx_d)_2 \right. \\ &\quad + \Gamma CAx_d - \Gamma C\dot{x}_d + \frac{\sigma(e_y)}{\|\sigma(e_y)\|} \left[ \|\Gamma CB\|(\zeta_1(t, \Theta_2(\widehat{C}_2^{-1}y \right. \\ &\quad \left. - (Tx_d)_2) + x_d) + \zeta_2(t, y)) + \|\Gamma CE\|(\xi_1(t, \Theta_2(\widehat{C}_2^{-1}y \right. \\ &\quad \left. - (Tx_d)_2) + x_d) + \xi_2(t, y)) + (\|\Gamma CB\|\mathcal{L}_{\zeta_1} \right. \\ &\quad \left. + \|\Gamma CE\|\mathcal{L}_{\xi_1} + \|\Gamma CA\|)\delta + \rho \right] \left. \right\} \end{aligned} \quad (6.49)$$

where  $\mathcal{L}_{\zeta_1}$  and  $\mathcal{L}_{\xi_1}$  denote the Lipschitz constants of function  $\zeta_1$  and  $\xi_1$  of (6.22)-(6.23) in the vicinity of the origin, respectively.  $\rho$  is a positive scalar.

**Remark 6.8.** It is obvious to note from (6.49) that the control law contains the known bounds of the uncertainties described from Assumption 6.3. However, if the uncertainty bounds are unknown, a neural network approach [151] can be applied to approximate the unknown nonlinear bounds and utilised in the control design.

The following conclusion is ready to be presented.

**Theorem 6.2.** Consider systems (6.34)-(6.36), under Assumptions 6.1-6.3 and the boundedness condition  $\|\Theta_1(Te_x)_1\| \leq \delta$  in the vicinity of the origin, the control law (6.49) is able to drive the system (6.34)-(6.36) to the sliding surface (6.32) in finite time and maintains motion on it afterwards.

*Proof:* From (6.26), (6.27), (6.31) and (6.48), it follows that

$$\begin{aligned} \dot{\sigma} = & \Gamma CA\Theta_1(Te_x)_1 + \Gamma CA\Theta_2(\widehat{C}_2^{-1}y - (Tx_d)_2) \\ & + \Gamma CBu + \Gamma CB\Phi(t, e_x + x_d) + \Gamma CE\Delta\Psi(t, e_x + x_d) \\ & + \Gamma CAx_d - \Gamma C\dot{x}_d \end{aligned} \quad (6.50)$$

Applying control law (6.49) to (6.50) yields

$$\begin{aligned} \dot{\sigma} = & \Gamma CA\Theta_1(Te_x)_1 - \frac{\sigma(e_y)}{\|\sigma(e_y)\|} \left[ \|\Gamma CB\|(\zeta_1(t, \Theta_2(\widehat{C}_2^{-1}y - (Tx_d)_2) + x_d) + \zeta_2(t, y)) \right. \\ & + \|\Gamma CE\|(\xi_1(t, \Theta_2(\widehat{C}_2^{-1}y - (Tx_d)_2) + x_d) + \xi_2(t, y)) + (\|\Gamma CB\|\mathcal{L}_{\zeta_1} + \|\Gamma CE\|\mathcal{L}_{\xi_1} \\ & \left. + \|\Gamma CA\|)\delta + \rho \right] + \Gamma CE\Delta\Psi(t, e_x + x_d) + \Gamma CB\Phi(t, e_x + x_d) \end{aligned} \quad (6.51)$$

It follows from (6.29), (6.30), (6.48) and (6.51) that

$$\begin{aligned}
\sigma^T \dot{\sigma} &\leq \|\sigma\| \left[ \|\Gamma CA\| \|\Theta_1(Te_x)_1\| + \|\Gamma CB\| \|\Phi(t, e_x + x_d)\| + \|\Gamma CE\| \|\Delta\Psi(t, e_x + x_d)\| \right. \\
&\quad - \|\Gamma CB\| (\zeta_1(t, \Theta_2(\widehat{C}_2^{-1}y - (Tx_d)_2) + x_d) + \zeta_2(t, y)) - \|\Gamma CE\| (\xi_1(t, \Theta_2(\widehat{C}_2^{-1}y \\
&\quad - (Tx_d)_2) + x_d) + \xi_2(t, y)) - \|\Gamma CB\| \mathcal{L}_{\zeta_1} \delta - \|\Gamma CE\| \mathcal{L}_{\xi_1} \delta - \|\Gamma CA\| \delta - \rho \left. \right] \\
&\leq \|\sigma\| \left[ \|\Gamma CB\| (\zeta_1(t, e_x + x_d) + \zeta_2(t, y)) + \|\Gamma CE\| (\xi_1(t, e_x + x_d) + \xi_2(t, y)) - \|\Gamma CB\| \right. \\
&\quad \times (\zeta_1(t, \Theta_2(\widehat{C}_2^{-1}y - (Tx_d)_2) + x_d) + \zeta_2(t, y)) - \|\Gamma CE\| (\xi_1(t, \Theta_2(\widehat{C}_2^{-1}y - (Tx_d)_2) \\
&\quad + x_d) + \xi_2(t, y)) - \|\Gamma CB\| \mathcal{L}_{\zeta_1} \delta - \|\Gamma CE\| \mathcal{L}_{\xi_1} \delta - \rho \left. \right] \\
&\leq \|\sigma\| \left[ \|\Gamma CB\| (\zeta_1(t, e_x + x_d) - \zeta_1(t, \Theta_2(\widehat{C}_2^{-1}y - (Tx_d)_2) + x_d)) + \|\Gamma CE\| (\xi_1(t, e_x + x_d) \right. \\
&\quad - \xi_1(t, \Theta_2(\widehat{C}_2^{-1}y - (Tx_d)_2) + x_d)) - \|\Gamma CB\| \mathcal{L}_{\zeta_1} \delta - \|\Gamma CE\| \mathcal{L}_{\xi_1} \delta - \rho \left. \right] \\
&\leq \|\sigma\| \left[ \|\Gamma CB\| \mathcal{L}_{\zeta_1} (e_x - \Theta_2(\widehat{C}_2^{-1}y - (Tx_d)_2)) + \|\Gamma CE\| \mathcal{L}_{\xi_1} (e_x - \Theta_2(\widehat{C}_2^{-1}y - (Tx_d)_2)) \right. \\
&\quad - \|\Gamma CB\| \mathcal{L}_{\zeta_1} \delta - \|\Gamma CE\| \mathcal{L}_{\xi_1} \delta - \rho \left. \right] \\
&\leq \|\sigma\| \left[ -\|\Gamma CB\| \mathcal{L}_{\zeta_1} \delta - \|\Gamma CE\| \mathcal{L}_{\xi_1} \delta - \rho + \|\Gamma CB\| \mathcal{L}_{\zeta_1} \|\Theta_1(Te_x)_1\| \right. \\
&\quad \left. + \|\Gamma CE\| \mathcal{L}_{\xi_1} \|\Theta_1(Te_x)_1\| \right] \\
&\leq -\rho \|\sigma\|
\end{aligned} \tag{6.52}$$

Therefore, the reachability condition, described in Section 3.2.4, is satisfied and the result follows. ■

**Remark 6.9.** The combination of Theorems 6.1 and 6.2 show that the states in the closed-loop system generated from (6.34)-(6.36) of  $e_z$  dynamics are uniformly ultimately bounded. Since  $e_z(t) = Te_x(t)$  is a nonsingular coordinate transformation, it is straightforward to see from (6.26) that  $e_y(t) = Ce_x(t) = CT^{-1}e_z(t)$  is also uniformly ultimately bounded. Thus, the control objective (6.24) is achieved.

## 6.3. SIMULATION STUDY

This section demonstrates the static output feedback SMC to balance a TWIP system under simulation. The parameters of the robot are provided in Table 6.1. The TWIP

is tested on an inclined surface with the slope angle  $\alpha = 5^\circ$ . According to (6.9), the desired attitude angle  $x_{2_d}$  can be calculated as  $x_{2_d} = 0.1368$  rad. Then, the initial and desired output states are configured as  $y_0 = [0.2, 0.3142, 0]^T$  and  $x_d = [0, 0.1368, 0]^T$ , respectively. The matrices of dynamics (6.5)-(6.6) can be described by

$$\begin{aligned}
 A &= \begin{bmatrix} 0 & 0 & 1 & 0 \\ 0 & 0 & 0 & 1 \\ 0 & -113.12 & -63.612 & 50.483 \\ 0 & 190.91 & 62.595 & -67.085 \end{bmatrix}, \quad B = \begin{bmatrix} 0 \\ 0 \\ 252.41 \\ -335.42 \end{bmatrix} \\
 C &= \begin{bmatrix} 1 & 0 & 0 & 0 \\ 0 & 1 & 0 & 0 \\ 0 & 0 & 0 & 1 \end{bmatrix}, \quad E = \begin{bmatrix} 0 \\ 0 \\ -127.22 \\ 125.19 \end{bmatrix}
 \end{aligned} \tag{6.53}$$

Table 6.1: Model parameters for the TWIP

Symbols with units	Definitions	Values
$M_B$ [kg]	Mass of body	1.036
$M_W$ [kg]	Mass of wheel	0.18
$R$ [m]	Radius of wheel	0.06
$L$ [m]	Length to CoG	0.09
$J_W$ [kg.m <sup>2</sup> ]	Inertial of wheel	0.001032
$J_{P_\theta}$ [kg.m <sup>2</sup> ]	y-axis inertial of body	0.0027
$c_b$ [N/A]	Driving friction coefficient of the body	0.2
$c_r$ [N/A]	Rolling friction coefficient of the wheels	0.5

Further, the matched and unmatched uncertainties  $\Phi(t, x)$  and  $\Delta\Psi(t, x)$  satisfy the

conditions

$$\|\Phi(t, x)\| \leq \underbrace{0.25 \sin x_4}_{\zeta_1(t, x)} + \underbrace{0.4 \|y\|}_{\zeta_2(t, y)} \quad (6.54)$$

$$\|\Delta\Psi(t, x)\| \leq \underbrace{0.005 \sin^2 x_4}_{\xi_1(t, x)} + \underbrace{0.001 \sin^2 y_3 \|y_1\|}_{\xi_2(t, y)} \quad (6.55)$$

From Assumption 6.2, although there are several methods mentioned in [119] for determining the matrix  $K$ , such as output feedback pole placement method, etc. It is still not intuitive to choose gains to stabilise the TWIP system. Therefore, Figure 6.2 illustrates an admissible stable region in the shaded open set for selecting appropriate design parameters  $K_1$  and  $K_2$ .

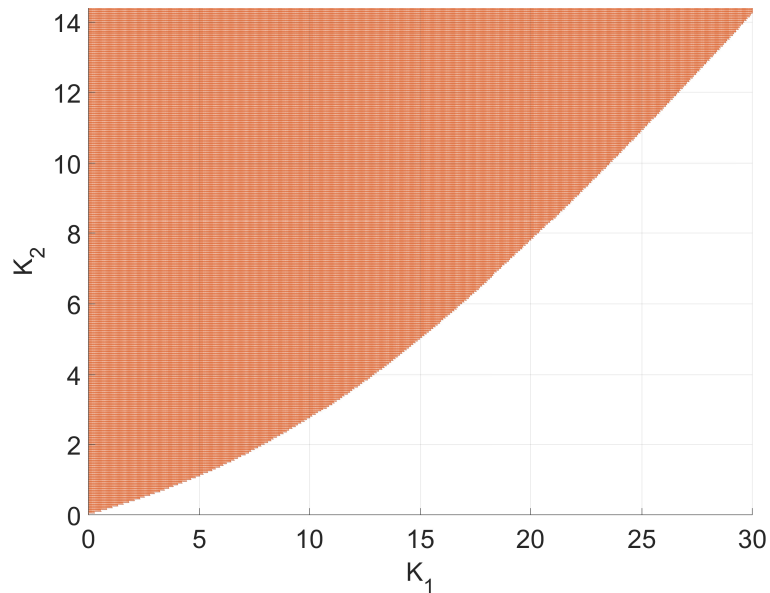


Figure 6.2: The admissible region of gains  $K_1$  and  $K_2$  to satisfy Assumption 6.2

**Remark 6.10.** In Figure 6.2, it is worth mentioning that increasing  $K_1$  and decreasing  $K_2$  simultaneously will generate system oscillations. The larger  $K_1$  and the lower  $K_2$  are chosen, the higher chance system will lead to instability. On the contrary, reducing  $K_1$  and boosting  $K_2$  together result in extended convergence time. Hence, to achieve decent control performance, the values of  $K_1$  and  $K_2$  should be selected as close as possible within the shaded area whilst satisfying the sufficient condition (6.41).

Therefore, choosing  $K_1 = 9.9$ ,  $K_2 = 7.6$  and applying the algorithm in [116], the

coordinate transformation matrix  $T$  in (6.12) can be defined as

$$T = \begin{bmatrix} 0 & 0 & -1 & -0.75252 \\ 1 & 0 & 0 & 0 \\ 0 & 1 & 0 & 0 \\ 9.9 & 7.6 & 0 & 1 \end{bmatrix} \quad (6.56)$$

Then the corresponding matrices of  $e_z$  systems in (6.34)-(6.36) can be described by

$$\begin{aligned} \begin{bmatrix} \hat{A}_{11} & \hat{A}_{12} \\ \hat{A}_{21} & \hat{A}_{22} \end{bmatrix} &= \left[ \begin{array}{ccc|c} -16.507 & 122.98 & 63.863 & -12.422 \\ -1 & 7.45 & 5.7192 & -0.75252 \\ 0 & -9.9 & -7.6 & 1 \\ \hline -72.495 & 1129.8 & 1057.6 & -114.04 \end{array} \right] \\ \begin{bmatrix} \tilde{E}_1 \\ K\bar{C}_2\tilde{E}_1 + \tilde{E}_2 \end{bmatrix} &= \begin{bmatrix} 33.014 \\ 0 \\ 0 \\ \hline 125.19 \end{bmatrix}, \quad \begin{bmatrix} 0 \\ \hat{B}_2 \end{bmatrix} = \begin{bmatrix} 0 \\ 0 \\ 0 \\ \hline -335.42 \end{bmatrix} \\ \begin{bmatrix} 0 & \hat{C}_2 \end{bmatrix} = \begin{bmatrix} 0 & \hat{C}_{21} & \hat{C}_{22} \end{bmatrix} &= \left[ \begin{array}{cc|c} 0 & 1 & 0 & 0 \\ 0 & 0 & 1 & 0 \\ 0 & -9.9 & -7.6 & 1 \end{array} \right] \end{aligned} \quad (6.57)$$

Since  $\hat{A}_{11}$  in (6.57) is stable, for  $Q_{z_1} = I_3$ , the solution of Lyapunov function (6.40) is calculated as

$$P_{z_1} = \begin{bmatrix} 0.0378 & -0.1237 & -0.0689 \\ -0.1237 & 6.4488 & 3.3671 \\ -0.0689 & 3.3671 & 2.0205 \end{bmatrix} \quad (6.58)$$

By direct computation,  $\|\tilde{E}_1\| = 33.014$ ,  $\xi_1(\cdot) \leq 0.005$  and  $\xi_2(\cdot) \leq 0.001\|y_1\|$ . When the system is restricted to the sliding surface,  $\|e_{z_1}\| = 33.744$ ,  $\|P_{z_1}e_{z_1}\| = 117.75$  and  $\|y_1\| = 16.324$ , it is straightforward to verify that the condition in Theorem 6.1 is satisfied. Hence, the sliding motion associated with the sliding surface is uniformly ultimately bounded. Then, choosing  $\mathcal{L}_{\zeta_1} = 0.5$ ,  $\mathcal{L}_{\xi_1} = 0.01$ ,  $\delta = 7.7626$  and  $\rho =$

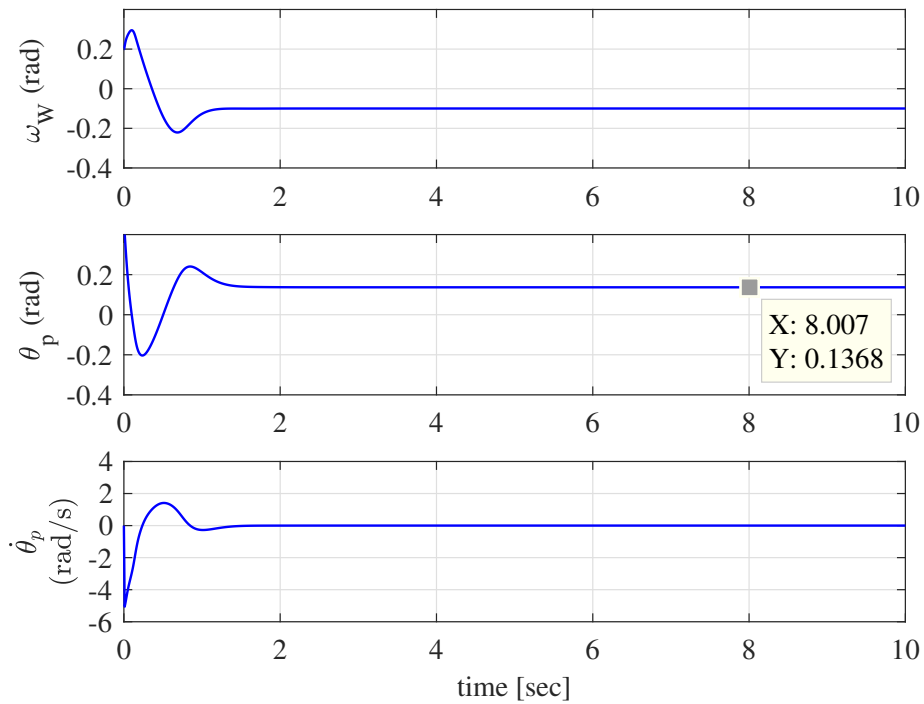


Figure 6.3: Time responses of the system outputs  $y(t)$  under matched and unmatched uncertainties of the TWIP system driven on an inclined surface  $\alpha = 5^\circ$

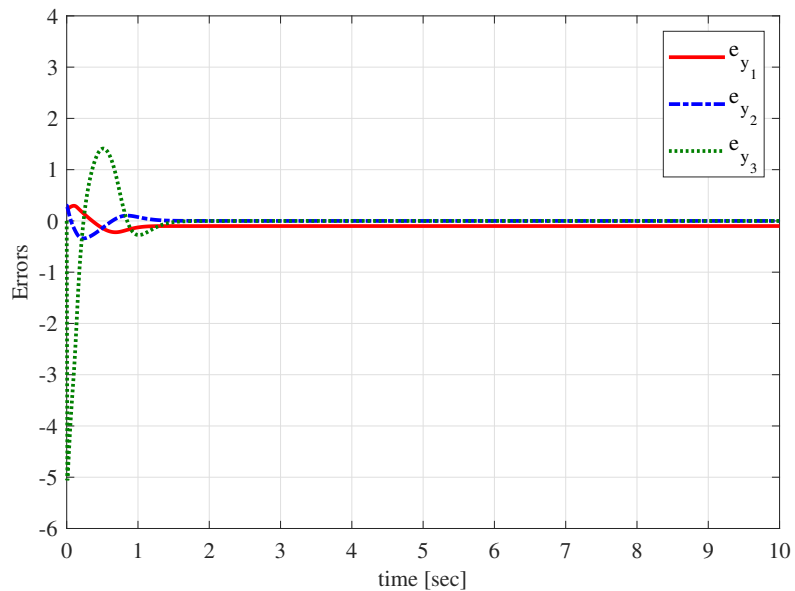


Figure 6.4: Time responses of the error outputs  $e_y(t)$  under matched and unmatched uncertainties of the TWIP system driven on an inclined surface  $\alpha = 5^\circ$

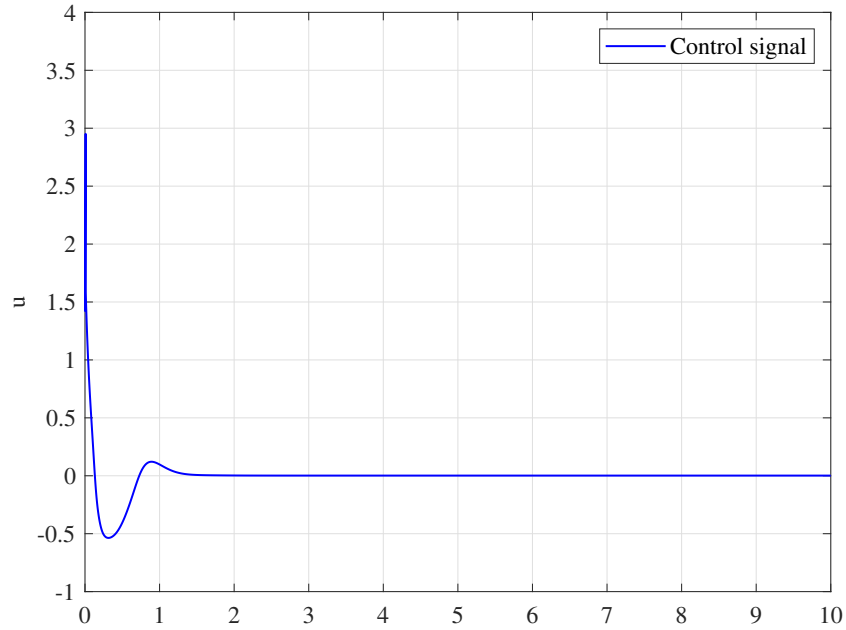


Figure 6.5: Time responses of the control signal of the TWIP system driven on an inclined surface  $\alpha = 5^\circ$

10. From Theorem 6.2 and reachability analysis in Section 6.2.2, the following output feedback SMC is designed to ensure that the system can be driven to the sliding surface in finite time.

$$u = 0.00298 \left[ 206.83y_2 - 124.43y_3 + \frac{\sigma(e_y)}{\|\sigma(e_y)\|} \left( 83.855 \sin y_2 + 134.17 \|y\| + 0.62595 \sin^2 y_3 + 0.1252 \sin^2 y_2 \|y_1\| + 2972.7 \right) \right] \quad (6.59)$$

Figures 6.3, 6.4 and 6.5 show the time responses of the simulated output states, error outputs, and control signal in the presence of matched uncertainty  $\tau_M = 0.6x_2 + 0.3 \operatorname{sgn}(y_1)$  and unmatched uncertainty  $\tau_W = 0.1x_2 + 0.2 \operatorname{sgn}(y_2)$ , similar friction representations can be referred in [152, 153]. The results demonstrate the effectiveness of the proposed control law in (6.59).

## 6.4. CONCLUSION

In this chapter, a static output feedback SMC has been proposed for regulating a TWIP system using the output variables. Matched and unmatched uncertainties are considered in the system design and the reduced-order sliding mode dynamics are utilised to underpin the stability analysis. By taking advantage of the nonlinear bounds on the uncertainties in both the sliding motion analysis and the control design, the system is less conservative and the robustness is enhanced. The simulation results demonstrate the performance of the proposed control method on a TWIP system.

## CHAPTER. 7

---

# CONCLUSIONS AND FUTURE WORK

---

## 7.1. SUMMARY AND CONCLUSIONS

This thesis has presented control designs for TWMRs using sliding mode techniques, mainly focusing on the trajectory tracking SMC on a TWMR system and setpoint regulation SMC on a TWIP system based on full-state feedback and static output feedback approaches. Before diving into the main contents, some background knowledge of mathematics and control theories has been reviewed in Chapters 2 and 3.

This thesis has drawn the following conclusions.

- A nonlinear SMC law has been proposed to track the predefined trajectories on a TWMR with caster wheels. By employing a new structure of the sliding function, the original nonlinear tracking error system can be transformed to a reduced-order sliding mode dynamic to facilitate stability analysis of tracking error dynamics, which reduces conservatism. Moreover, the tracking results for the ideal trajectories, such as line, circle and lemniscate curve, have demonstrated the more effectiveness and better tracking performance of the proposed SMC scheme than a PID

approach in the presence of matched and unmatched uncertainties.

- A SMC law has been designed to regulate a TWIP system using full-state variables. The system was modelled based on the Lagrangian dynamics considering unknown matched and unmatched uncertainties bounded by known nonlinear functions. Then the model was linearised and further transformed into a regular form to facilitate the stability analysis and design. Finally, both simulation and experiment results have been presented to demonstrate the feasibility and effectiveness of the developed method.
- A static output feedback SMC has been presented for regulating a TWIP system when only the partial state variables are accessible. Matched and unmatched uncertainties have been considered in the control design and the reduced-order sliding mode dynamics are utilised to underpin the stability analysis. By taking advantage of the nonlinear bounds on the uncertainties in both the sliding motion analysis and the control design, the results are less conservative and the robustness is enhanced. The simulation results have demonstrated the effectiveness of the proposed SMC scheme.

## 7.2. IDEAS FOR FUTURE RESEARCH

There are some possible ideas for future research.

For the trajectory tracking control of the TWMR system, although the tracking performance is achieved in both simulation and experiment, the thesis only considers the kinematic layer of the system, which is not ideal for the situations where uncertainties and disturbances are encountered. Therefore, one of the further researches is to study both the dynamic and kinematic layers of the TWMR system with the consideration of unknown matched and unmatched uncertainties. A few other possible approaches can be combined with SMC design to further enhance robustness and achieve better performance to deal with uncertainties and disturbances specifically when the considered system involves parametric uncertainties, for example, adaptive, neural network with intelligence,

etc. However, from the existing literature, many researchers focus on the robust control designs, adaptive SMC and neural network SMC, only on the dynamic layer of the TWMR system, which only guarantee the robustness and performance of the linear and angular velocities of TWMR tracking control, not the posture of the robot. Therefore, a possible solution is to apply one SMC law with an adaptive or neural network method for robustly tracking the posture of the TWMR system on the kinematic layer whilst controlling the robot velocities on the dynamic layer using another adaptive or neural network SMC under the presence of uncertainties and disturbances. Moreover, the other possible improvement of the proposed trajectory tracking control is to design a nonlinear SMC law with a novel nonlinear sliding surface to globally stabilise the system so that the forward and backward tracking can be performed simultaneously without modifying the switching function in advance, as mentioned in Remark 4.5 of Chapter 4.

In the case of control designs of the TWIP system, the approximate linearisation approach for original nonlinear TWIP dynamics is applied, which makes the designed controller may not work well or even result in unstable closed-loop system in implementation. Hence, a novel nonlinear SMC design becomes crucial for TWIP systems considering partial linearisation or full nonlinear. Furthermore, the control robustness of the TWIP system can be further enhanced by introducing the disturbance observer-based SMC approach to estimate the unmatched uncertainties caused by the drift of the robot. Lastly, in Chapter 6, the proposed static output feedback SMC law may not be applicable by using a different output matrix  $C$ , which means that the selected output information of the TWIP system can be restricted case by case. Therefore, the reduced-order state observers can be a solution at the cost of increased system dimensions to tackle this issue.

Finally, since this thesis presents the trajectory tracking control on a TWMR with caster wheels and stabilisation of a TWIP system, the research of trajectory tracking SMC on a TWIP system, which is the combination of the works as mentioned earlier, is also an exciting and challenging area. As the TWIP systems are only considered longitudinal modelling in this thesis, it might be an interesting but challenging research topic to combine longitudinal and lateral models together to obtain better description for the TWIP system and further to improve the control performance from all aspects.

# Appendices

## APPENDIX. A

---

# DYNAMIC MODELLING OF A TWO-WHEELED INVERTED PENDULUM

---

In Figure A.1, the positions and velocities of the body and wheel are described by

$$\left\{ \begin{array}{l} x_B = L\sin\theta_p + R\Psi_l\cos\alpha + R\Psi_r\cos\alpha \\ y_B = L\cos\theta_p + R\Psi_l\sin\alpha + R\Psi_r\sin\alpha \\ x_W = R\Psi_l\cos\alpha + R\Psi_r\cos\alpha \\ y_W = R\Psi_l\sin\alpha + R\Psi_r\sin\alpha \\ \Psi_W = \frac{\Psi_l + \Psi_r}{2} \end{array} \right. \quad (\text{A.1})$$

where  $(x_B, y_B)$  and  $(x_W, y_W)$  represents the coordinates of the TWIP body and wheel, respectively.  $\theta_p$  is the attitude pitch angle of the TWIP body,  $L$  is the length between the wheel axis and the centre of gravity (CoG) of the body,  $R$  is the radius of the wheels,  $\Psi_l$ ,  $\Psi_r$  and  $\Psi_W$  denote the angular displacements of the left, right and the TWIP wheels respectively,  $\alpha$  is the inclination angle of a ramp.

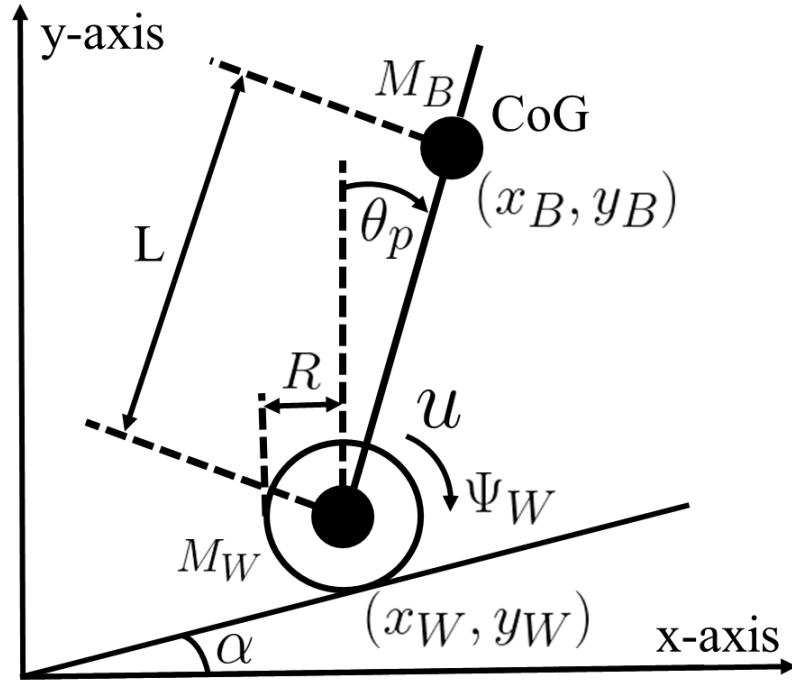


Figure A.1: Modelling of a two-wheeled inverted pendulum

Then, (A.1) can be rewritten as follows

$$\begin{cases} x_B = L \sin \theta_p + R \cos \alpha (\Psi_l + \Psi_r) = L \sin \theta_p + 2R \cos \alpha \Psi_W \\ y_B = L \cos \theta_p + R \sin \alpha (\Psi_l + \Psi_r) = L \cos \theta_p + 2R \sin \alpha \Psi_W \\ x_W = R \cos \alpha (\Psi_l + \Psi_r) = 2R \cos \alpha \Psi_W \\ y_W = R \sin \alpha (\Psi_l + \Psi_r) = 2R \sin \alpha \Psi_W \end{cases} \quad (\text{A.2})$$

The derivatives of (A.2) can be described by

$$\begin{cases} \dot{x}_B = L \dot{\theta}_p \cos \theta_p + 2R \cos \alpha \dot{\Psi}_W \\ \dot{y}_B = -L \dot{\theta}_p \sin \theta_p + 2R \sin \alpha \dot{\Psi}_W \\ \dot{x}_W = 2R \cos \alpha \dot{\Psi}_W \\ \dot{y}_W = 2R \sin \alpha \dot{\Psi}_W \end{cases} \quad (\text{A.3})$$

The Lagrangian  $L$  for the TWIP system can be defined as

$$L = V_B + V_W - U_B - U_W \quad (\text{A.4})$$

where  $V_B$ ,  $V_W$ ,  $U_B$ , and  $U_W$  represent the kinetic and potential energies of the body and wheel, respectively.

Further, the kinetic energies of the TWIP body  $V_B$  and the wheels  $V_W$  are described by

$$\begin{aligned}
V_B &= \frac{1}{2}M_B(\dot{x}_B^2 + \dot{y}_B^2) + \frac{1}{2}J_{\theta_p}\dot{\theta}_p^2 \\
&= \frac{1}{2}M_B \left[ \left( L\dot{\theta}_p \cos\theta_p + 2R\cos\alpha\dot{\Psi}_W \right)^2 + \left( -L\dot{\theta}_p \sin\theta_p + 2R\sin\alpha\dot{\Psi}_W \right)^2 \right] + \frac{1}{2}J_{\theta_p}\dot{\theta}_p^2 \\
&= \frac{1}{2}M_B \left( L^2\dot{\theta}_p^2 \cos^2\theta_p + 4LR\dot{\theta}_p\dot{\Psi}_W \cos\theta_p \cos\alpha + 4R^2 \cos^2\alpha \dot{\Psi}_W^2 + L^2\dot{\theta}_p^2 \sin^2\theta_p \right. \\
&\quad \left. - 4LR\dot{\theta}_p\dot{\Psi}_W \sin\theta_p \sin\alpha + 4R^2 \sin^2\alpha \dot{\Psi}_W^2 \right) + \frac{1}{2}J_{\theta_p}\dot{\theta}_p^2 \\
&= \frac{1}{2}M_B \left( L^2\dot{\theta}_p^2 + 4LR\dot{\theta}_p\dot{\Psi}_W (\cos\theta_p \cos\alpha - \sin\theta_p \sin\alpha) + 4R^2 \dot{\Psi}_W^2 \right) + \frac{1}{2}J_{\theta_p}\dot{\theta}_p^2 \\
&= \frac{1}{2}M_B \left( L^2\dot{\theta}_p^2 + 4LR\dot{\theta}_p\dot{\Psi}_W \cos(\theta_p + \alpha) + 4R^2 \dot{\Psi}_W^2 \right) + \frac{1}{2}J_{\theta_p}\dot{\theta}_p^2 \\
V_W &= \frac{1}{2}M_W(\dot{x}_W^2 + \dot{y}_W^2) + \frac{1}{2}J_W\dot{\Psi}_W^2 \\
&= \frac{1}{2}M_W \left[ \left( 2R\cos\alpha\dot{\Psi}_W \right)^2 + \left( 2R\sin\alpha\dot{\Psi}_W \right)^2 \right] + \frac{1}{2}J_W\dot{\Psi}_W^2 \\
&= \frac{1}{2}M_W \left[ 4R^2 \cos^2\alpha \dot{\Psi}_W^2 + 4R^2 \sin^2\alpha \dot{\Psi}_W^2 \right] + \frac{1}{2}J_W\dot{\Psi}_W^2 \\
&= \frac{1}{2}M_W 4R^2 \dot{\Psi}_W^2 + \frac{1}{2}J_W\dot{\Psi}_W^2 \\
&= 2M_W R^2 \dot{\Psi}_W^2 + \frac{1}{2}J_W\dot{\Psi}_W^2
\end{aligned} \tag{A.5}$$

where  $M_B$  and  $M_W$  are the masses of the TWIP body and wheel, respectively.  $J_{\theta_p}$  and  $J_W$  represents the moment of inertias of the body w.r.t y-axis and the wheels, accordingly.

Next, the potential energies of the TWIP body  $U_B$  and the wheels  $U_W$  can be given as

$$\begin{aligned}
U_B &= M_B g (L \cos\theta_p + R\Psi_l \sin\alpha + R\Psi_r \sin\alpha) \\
&= M_B g (L \cos\theta_p + 2R \sin\alpha \Psi_W) \\
U_W &= M_W g R \Psi_l \sin\alpha + M_W g R \Psi_r \sin\alpha \\
&= 2M_W g R \sin\alpha \Psi_W
\end{aligned} \tag{A.6}$$

From (A.4), (A.5) and (A.6), the Lagrangian  $L$  for the TWIP system can be ex-

panded by

$$\begin{aligned}
L &= \frac{1}{2}M_B \left( L^2 \dot{\theta}_p^2 + 4LR \dot{\theta}_p \dot{\Psi}_W \cos(\theta_p + \alpha) + 4R^2 \dot{\Psi}_W^2 \right) + \frac{1}{2}J_{\theta_p} \dot{\theta}_p^2 + 2M_W R^2 \dot{\Psi}_W^2 + \frac{1}{2}J_W \dot{\Psi}_W^2 \\
&\quad - M_B g (L \cos \theta_p + 2R \sin \alpha \Psi_W) - 2M_W g R \sin \alpha \Psi_W \\
&= \frac{1}{2}M_B L^2 \dot{\theta}_p^2 + 2M_B L R \dot{\theta}_p \dot{\Psi}_W \cos(\theta_p + \alpha) + 2M_B R^2 \dot{\Psi}_W^2 + \frac{1}{2}J_{\theta_p} \dot{\theta}_p^2 + 2M_W R^2 \dot{\Psi}_W^2 \\
&\quad + \frac{1}{2}J_W \dot{\Psi}_W^2 - M_B g L \cos \theta_p - 2M_B g R \sin \alpha \Psi_W - 2M_W g R \sin \alpha \Psi_W
\end{aligned} \tag{A.7}$$

Further, the Lagrangian dynamic modelling of the TWIP system can be described by

$$\begin{aligned}
\frac{d}{dt} \left( \frac{\partial L}{\partial \dot{\theta}_p} \right) - \frac{\partial L}{\partial \theta_p} &= -u - \tau_B \\
\frac{d}{dt} \left( \frac{\partial L}{\partial \dot{\Psi}_W} \right) - \frac{\partial L}{\partial \Psi_W} &= u + \tau_B - \tau_W
\end{aligned} \tag{A.8}$$

where  $\tau_B, \tau_W$  represent the friction torque forces related to the TWIP body and the ground, respectively.  $u$  denotes the total torque (control input) applied to the wheels of the TWIP.

Substituting the Lagrangian motion equation (A.7) into (A.8) and taking the derivatives, it follows that

$$\begin{aligned}
\frac{d}{dt} \left( \frac{\partial L}{\partial \dot{\theta}_p} \right) - \frac{\partial L}{\partial \theta_p} &= \left( M_B L^2 \ddot{\theta}_p + 2M_B L R \cos(\theta_p + \alpha) \ddot{\Psi}_W + J_{\theta_p} \ddot{\theta}_p \right) - M_B g L \sin \theta_p \\
\frac{d}{dt} \left( \frac{\partial L}{\partial \dot{\Psi}_W} \right) - \frac{\partial L}{\partial \Psi_W} &= \left( 4(M_B + M_W) R^2 + J_W \right) \ddot{\Psi}_W + 2M_B L R \cos(\theta_p + \alpha) \ddot{\theta}_p \\
&\quad - 2M_B L R \sin(\theta_p + \alpha) \dot{\theta}_p^2 + 2gR(M_B + M_W) \sin \alpha
\end{aligned} \tag{A.9}$$

Therefore, the final Lagrangian dynamic model of the TWIP system can be described by

$$\begin{aligned}
c_1 \ddot{\theta}_p + c_2 \cos(\theta_p + \alpha) \ddot{\Psi}_W - c_3 \sin \theta_p &= -u - \tau_B \\
c_4 \ddot{\Psi}_W + c_2 \cos(\theta_p + \alpha) \ddot{\theta}_p - c_2 \sin(\theta_p + \alpha) \dot{\theta}_p^2 + c_5 \sin \alpha &= u + \tau_B - \tau_W
\end{aligned} \tag{A.10}$$

where  $c_i$  for  $i = 1, 2, 3, 4, 5$  are constants and defined as

$$\begin{aligned}c_1 &= M_B L^2 + J_{\theta_p} \\c_2 &= 2M_B L R \\c_3 &= M_B g L \\c_4 &= 4(M_B + M_W) R^2 + J_W \\c_5 &= 2gR(M_B + M_W)\end{aligned}\tag{A.11}$$

# APPENDIX. B

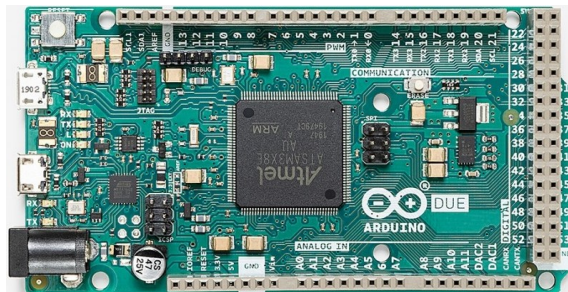
---

## HARDWARE DESCRIPTIONS FOR TWO-WHEELED MOBILE ROBOTS

---

### B.1. CHOICE OF MICROCONTROLLER BOARDS

It is well-known that robotic microcontroller boards are the core processing units for sensors data acquisition, control laws execution and data communication between robots and PC terminals. When selecting the microcontroller boards, researchers often consider



(a)



(b)

Figure B.1: Microcontroller boards. (a) Arduino Due. (b) STM32F407

the specifications in terms of the processors' performance, power consumptions, prices, sizes of the boards, etc. Among all the different types of embedded chips for microcontroller boards, such as ARM, DSP and FPGA, ARM boards own relatively robust tasks management functionality, which can be used to run interfaces and control applications more conveniently. Therefore, in this thesis, two different ARM microcontroller boards have been chosen to demonstrate the TWMR controls. The former is the Arduino Due in Figure B.1(a) for trajectory tracking control of a TWMR system and the latter is the STM32F407 in Figure B.1(b) for regulation controls on a TWIP system. Both of these two boards have the advantages of low power consumption, small sizes, low prices with twice the processing capacity of STM32F407 (168 MHz operating frequency) compared to Arduino Due (84 MHz).

It is worth mentioning that the reason for employing Arduino Due for the earlier research related to the trajectory tracking control is to utilise the Arduino user-friendly open-source software libraries and its IDE for easy implementation and demonstration. However, the drawbacks of using Arduino related software are the slow compilation time and low code efficiency due to the heavy dependency of the built-in libraries. Therefore, the utilisation of STM32F407, for the TWIP system with the software architecture designed in Section 5.4, is an upgrade version of the Arduino Due board for better control performance.

## B.2. OPTION OF ACTUATORS AND MOTOR DRIVERS

The selected gear motor is a powerful 12V brushed DC motor with a 30:1 metal gearbox, which is illustrated in Figure B.2(b). The detailed specifications are listed in Table B.1. It is worth mentioning that the values of the friction constant  $B_M$  and the moment of inertia  $J_M$  of this motor are retrieved based on the parameter identification processes described in Section C.2.2. Moreover, the motor drive, depicted in Figure B.2(c), is a fully integrated H-bridge high current motor driver for bidirectional speed control of the DC brushed motor along with a hall effect current sensing module for motor current measurement.

Table B.1: Specifications of DC Brushed Motor

DC Brushed Motor	
No-load speed @ 12V	350 RPM
No-load current @ 12V	0.3 A
Stall current @ 12V	5 A
Stall torque @ 12V	0.7768 N.m
Resistance ( $R_M$ )	3.4 $\Omega$
Inductance ( $L_M$ )	1.78x10 <sup>-3</sup> H
Torque constant ( $K_t$ )	0.1653 N.m/A
Back EMF ( $K_e$ )	0.2996 V.s/rad
Friction constant ( $B_M$ )	0.000585 N.m.sec/rad
Moment of inertia ( $J_M$ )	0.001032 N.m.sec <sup>2</sup> /rad
Gear ratio	30:1

### B.3. SELECTION OF SENSORS

This section describes two primary sensors employed in the TWMR and TWIP systems: the IMU and the quadrature encoder attached at the back of the motor.

- The MPU9250, illustrated in Figure B.2(a), is a popular lightweight and cost-effective nine-axis micro-electromechanical system (MEMS) motion tracking device, which consists of a three-axis of gyroscope, three-axis of accelerometer and three-axis magnetometer. It is worth mentioning that only the gyroscope and accelerometer are utilised in the trajectory tracking and regulation controls of the TWMR and TWIP systems. It is widely known that the gyroscope measures the angular velocity, and the accelerometer is used to sense the total acceleration eliminating gravity or the non-gravitational force per unit mass. The specifications of the gyroscope and accelerometer are listed in Table B.2, which are allowed to measure up to  $\pm 2000$  degrees per second and  $\pm 16$  non-gravitational force per unit mass according to the full-scale range. Moreover, the sensitivity scale factor is a number



Table B.2: Specifications of gyroscope and accelerometer

Inertial Measurement Unit (MPU9250)		
	Gyroscope	Accelerometer
Full-Scale Range	$\pm 250$ [ $^{\circ}/s$ ]	$\pm 2$ [ $g$ ]
	$\pm 500$ [ $^{\circ}/s$ ]	$\pm 4$ [ $g$ ]
	$\pm 1000$ [ $^{\circ}/s$ ]	$\pm 8$ [ $g$ ]
	$\pm 2000$ [ $^{\circ}/s$ ]	$\pm 16$ [ $g$ ]
Sensitivity Scale Factor	131 [ $LSB/(^{\circ}/s)$ ]	16384 [ $LSB/g$ ]
	65.5 [ $LSB/(^{\circ}/s)$ ]	8192 [ $LSB/g$ ]
	32.8 [ $LSB/(^{\circ}/s)$ ]	4096 [ $LSB/g$ ]
	16.4 [ $LSB/(^{\circ}/s)$ ]	2048 [ $LSB/g$ ]



Figure B.3: Outputs of encoder channel A and B when the motor runs at 12V

B.2(b), is a two-channel (A and B) Hall effect encoder, which is used to sense the rotation of a magnetic disk of the motor shaft. The quadrature encoder provides a resolution of 64 counts per revolution (CPR) of the motor shaft when counting both rising and falling edges of both channels. To compute the CPR of the gearbox output, multiply the gear ratio by 64. Based on the abovementioned DC brushed

motor with gear ratio 30:1, the gearbox output of the motor is  $64 * 30 = 1920$  CPR. Moreover, the A and B outputs are square waves approximately  $90^\circ$  out of phase. The frequency of the transitions represents the speed of the motor, and the order of the transitions indicates the motor direction. Figure B.3 shows the channels A and B (yellow and cyan) of encoder outputs when the motor runs at 12 volts. It is worth noting that the encoder is not only to measure the angular displacement of the motor but also an important device to output data for calculating the position coordinate of the TWMR system in trajectory tracking control.

## **APPENDIX. C**

---

# **SOFTWARE DESCRIPTIONS FOR TWO-WHEELED MOBILE ROBOTS**

---

The appendix will describe the software related to the trajectory tracking and regulation controls of TWMR and TWIP systems.

### **C.1. MATLAB SIMULATION**

#### **C.1.1. GRAPHICAL USER INTERFACE FOR TRAJECTORY TRACKING CONTROL OF A TWO-WHEELED MOBILE ROBOT**

Figure C.1 shows an intuitive approach to testify the trajectory tracking control on a TWMR system by using a self-developed Matlab GUI, which is able to configure the initial postures of the desired and actual robots, the design parameters of the SMC law, and the trajectory types, such as line, circle. Once all the information are configured properly, the corresponding tracking motion can be seen on the right axes with the initial desired

and actual robots plotted in red and green colours, respectively. The time responses of the tracking errors, sliding surfaces, and control signals can be displayed by clicking the 'Detail Results' button, which is illustrated in Figure C.2.

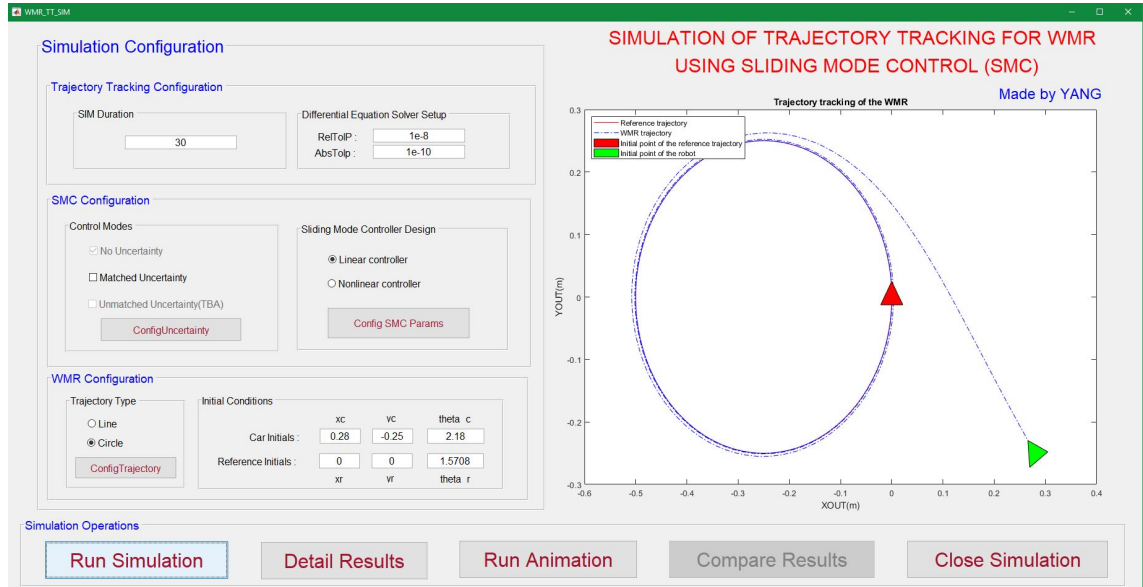


Figure C.1: Graphical user interface for the trajectory tracking control of a TWMR system under Matlab simulation



Figure C.2: Details information of the trajectory tracking control on a TWMR system under Matlab simulation

## C.2. PRACTICAL EXPERIMENTATION

### C.2.1. ORIENTATION FILTER FUSION USING MAHONY ALGORITHM FOR INERTIAL MEASUREMENT UNIT

With the utilisation of IMU described in Section B.3 and before the gyroscope and accelerometer are to be used in the implementation of feedback control laws, it is necessary to perform the calibration processes due to the manufactured misalignment errors, etc. A typical IMU calibration process usually estimates scale-factors, orthogonality or misalignment errors and offsets of both triads with a so-called sensor error model (SEM) [154] [155]. Based on the SEM and referenced calibration method, the calibration results of accelerometer and gyroscope are illustrated in Figures C.3 and C.4, respectively. In Figure C.3, the black dotted graphs represent the uncalibrated accelerometer data of x, y, z axes, and the blue dash-dotted plots correspond to the calibrated ones. Similar to Figures C.3, the red lines in Figure C.4 depict the calibrated gyroscope data whereas the blue dotted graphs indicate the uncalibrated counterparts.

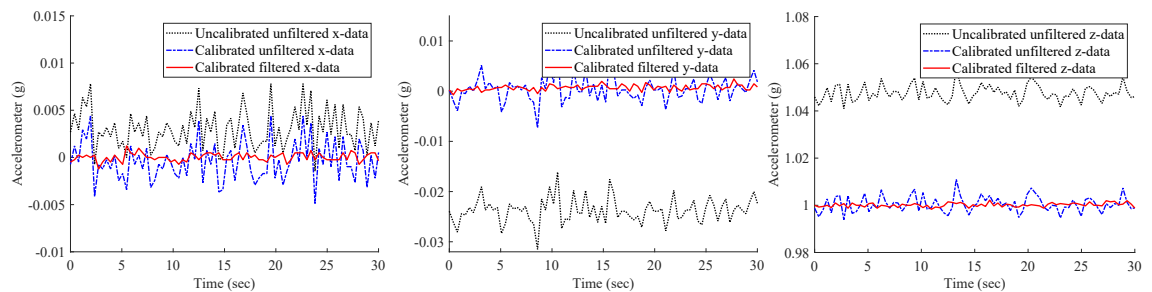


Figure C.3: Results of calibration and filtration of three-axis accelerometer data

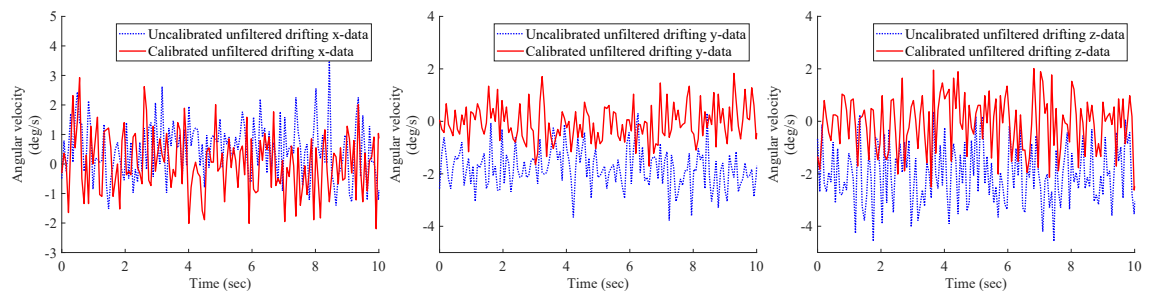


Figure C.4: Calibration results of three-axis gyroscope data

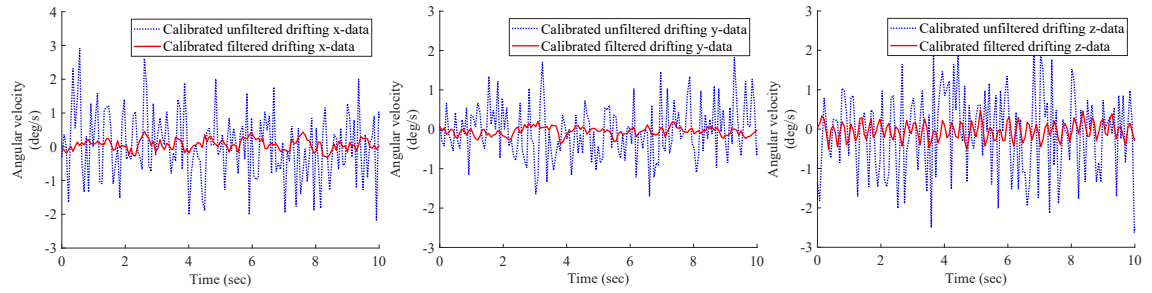


Figure C.5: Filtration results of three-axis gyroscope data

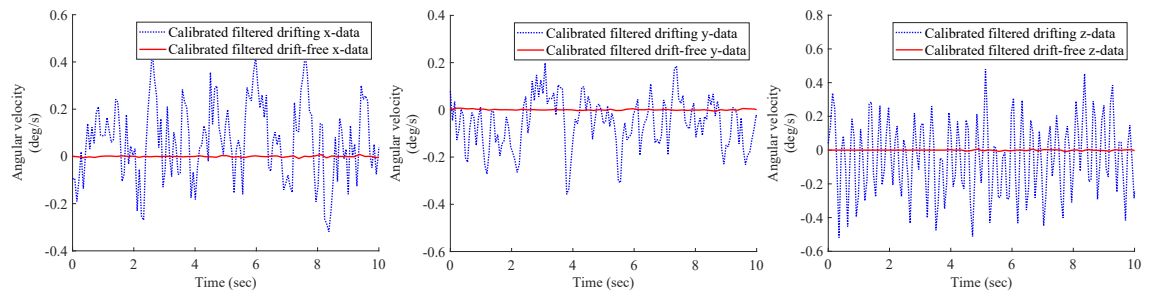


Figure C.6: Drift-free results of three-axis gyroscope data

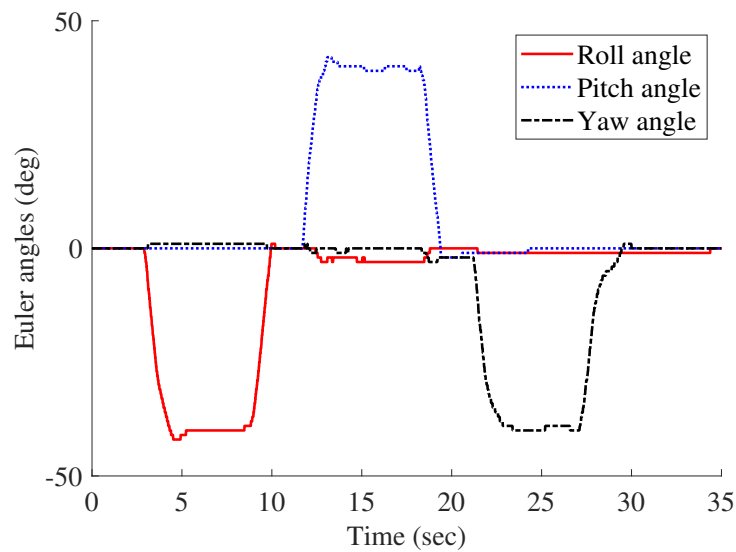


Figure C.7: Roll, pitch, and yaw Euler angles computed by Mahony algorithm

Further, it can be noticed from Figures C.3 and C.4 that there exist a large amount of measurement Gaussian white noises in the gyroscope and accelerometer, which could result in wear and tear of the actuators. Therefore, it is vital to carry out some filtration processes for the IMU sensor. In [156] and the references therein, there are several filtration methods, such as first-order low pass filter, second-order biquadratic filter, bandpass

filter, notch filter, etc. In this thesis, the second-order biquadratic filter is employed to filter the measurement noises of the gyroscope and accelerometer, and the corresponding results are depicted in Figures C.3 and C.5. The filtered accelerometer and gyroscope data of the three-axis are illustrated in red lines in both diagrams. It is obvious to see that the magnitudes of both white Gaussian noises are reduced significantly.

Lastly, a Mahony data fusion algorithm [147] is applied to resolve the drift over time issues caused by the gyroscope using an internal PI controller and transform the output quaternion data to the roll, pitch and yaw Euler angles for the implementation of trajectory tracking and setpoint regulation controls. Figure C.6 shows the results of calibrated filtered drift-free three-axis gyroscope data in red lines, and the Euler angles are illustrated in Figure C.7 with a series of rolling to the left, followed by pitching backwards then a yawing to the left manoeuvres.

### **C.2.2. PARAMETER IDENTIFICATION OF DC BRUSHED MOTORS**

Some of the factories provide all the specification information for their motors, which eliminate numerous inconvenience for practical implementation of the motor control. Unfortunately, the motors employed in this thesis, illustrated in Figure B.2 (b), do not have the full parameters data with unavailable information of the friction constant and the moment of inertia. Although some of the existing literature neglect the friction constant of the motor by configuring it to zero [116], the motor parameters are required to be measured relatively accurate to achieve better control performance. This section studies the parameter identification in practical processes for obtaining the friction constant and moment of inertia of the wheels provided in Tables 5.1, 6.1, and B.1, respectively.

The DC motor can be modelled as follows.

$$T_M(t) = K_T i_M(t) \quad (\text{C.1})$$

$$T_L(t) = B_M \omega_M(t) + T_W(t) \quad (\text{C.2})$$

$$T_{\text{Total}}(t) = T_M(t) - T_L(t) \quad (\text{C.3})$$

$$\dot{\omega}_M(t) = \frac{1}{J_M} T_M(t) - \frac{1}{J_M} T_L(t) = \frac{K_T}{J_M} i_M(t) - \frac{B_M}{J_M} \omega_M(t) - \frac{1}{J_M} T_W(t) \quad (\text{C.4})$$

$$\dot{i}_M(t) = -\frac{R_M}{L_M} i_M(t) - \frac{K_E}{L_M} \omega_M(t) + \frac{1}{L_M} V_S(t) \quad (\text{C.5})$$

where  $T_M(t)$  is the motor torque,  $T_L(t)$  is the load torque,  $T_{\text{Total}}$  is the total torque.  $\omega_M(t)$  and  $i_M(t)$  represent the motor's angular velocity and current value, respectively.  $T_W(t)$  and  $V_S(t)$  denote the wheel torque and voltage of the motor.  $K_T$  is the torque constant,  $K_E$  is the electromotive force (e.m.f) constant,  $R_M$  is the motor resistance,  $L_M$  is the internal inductance of the motor,  $B_M$  and  $J_M$  denote the friction constant and moment of inertia of the motor.

Define the state vector  $x(t) = [x_1(t), x_2(t), x_3(t)]^T = [\theta_M(t), \omega_M(t), i_M(t)]^T$ ,  $\theta_M(t)$  is the angular position of the motor. The motor system can be described in state-space representation by

$$\dot{x}(t) = Ax(t) + Bu(t) \quad (\text{C.6})$$

where  $x(t) = [x_1, x_2, x_3]^T = [\theta_M, \omega_M, i_M]^T$  denotes the state vector.  $u(t) = [u_1(t), u_2(t)]^T = [T_W(t), V_S(t)]^T$  is the control input. The corresponding matrices  $A$  and  $B$  are defined by

$$A = \begin{bmatrix} 0 & 1 & 0 \\ 0 & -\frac{B_M}{J_M} & \frac{K_T}{J_M} \\ 0 & -\frac{K_E}{L_M} & -\frac{R_M}{L_M} \end{bmatrix}, \quad B = \begin{bmatrix} 0 & 0 \\ -\frac{1}{J_M} & 0 \\ 0 & \frac{1}{L_M} \end{bmatrix} \quad (\text{C.7})$$

It should be mentioned that the parameters of  $K_T$ ,  $K_E$  can be calculated from the stall and no-load current and torque values provided in Table B.1 using the following equations.

$$K_T = \frac{T_{\text{Stall}}}{I_{\text{Stall}} - I_{\text{No-load}}} \quad (\text{C.8})$$

$$K_E = \frac{V_{\text{Max}} - I_{\text{No-load}} \times R_M}{\omega_{\text{No-load}}} \quad (\text{C.9})$$

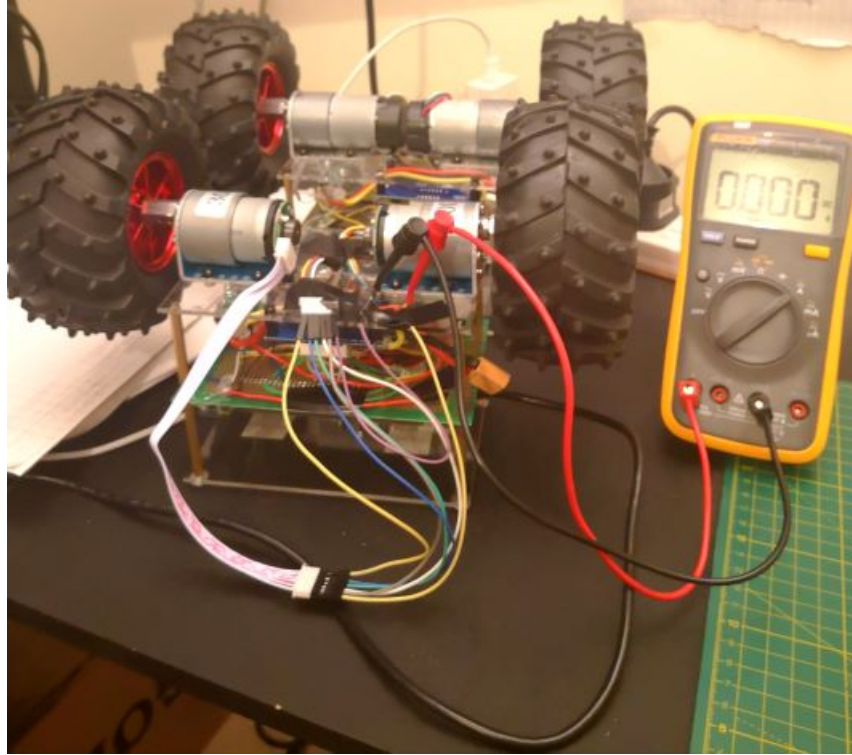


Figure C.8: The motor testing rig for obtaining the friction constant  $B_M$  and the moment of inertia  $J_M$

where  $T_{\text{Stall}}$  is the stall torque,  $I_{\text{Stall}}$  and  $I_{\text{No-load}}$  are the stall and no-load current values.  $V_{\text{Max}}$  is the maximum voltage allowed to be applied on the motor, which is 12 V in this case.  $\omega_{\text{No-load}}$  is the no-load velocity. Moreover, the motor resistance and inductance can be directly measured from two terminals of the motor.

Further, the processes of obtaining the friction constant  $B_M$  and the moment of inertia  $J_M$  can be described as follows.

#### **Friction constant $B_M$**

From (C.4), it is straightforward to see that the friction constant can be determined when the angular acceleration of the motor  $\dot{\omega}(t)$  is set to zero, i.e. when the motor spins at constant velocities. Since the current value can be measured in real-time using multimeter as illustrated in Figure C.8 and the angular velocity can be computed based on the angular position data and the central difference method at time  $t_{-1}$ ,  $t_0$ , and  $t_1$  by

$$\omega_M(t) = \dot{\theta}_M \approx \frac{\theta_M(t_1) - \theta_M(t_{-1})}{2\Delta t} + \mathcal{O}(\Delta t^2) \quad (\text{C.10})$$

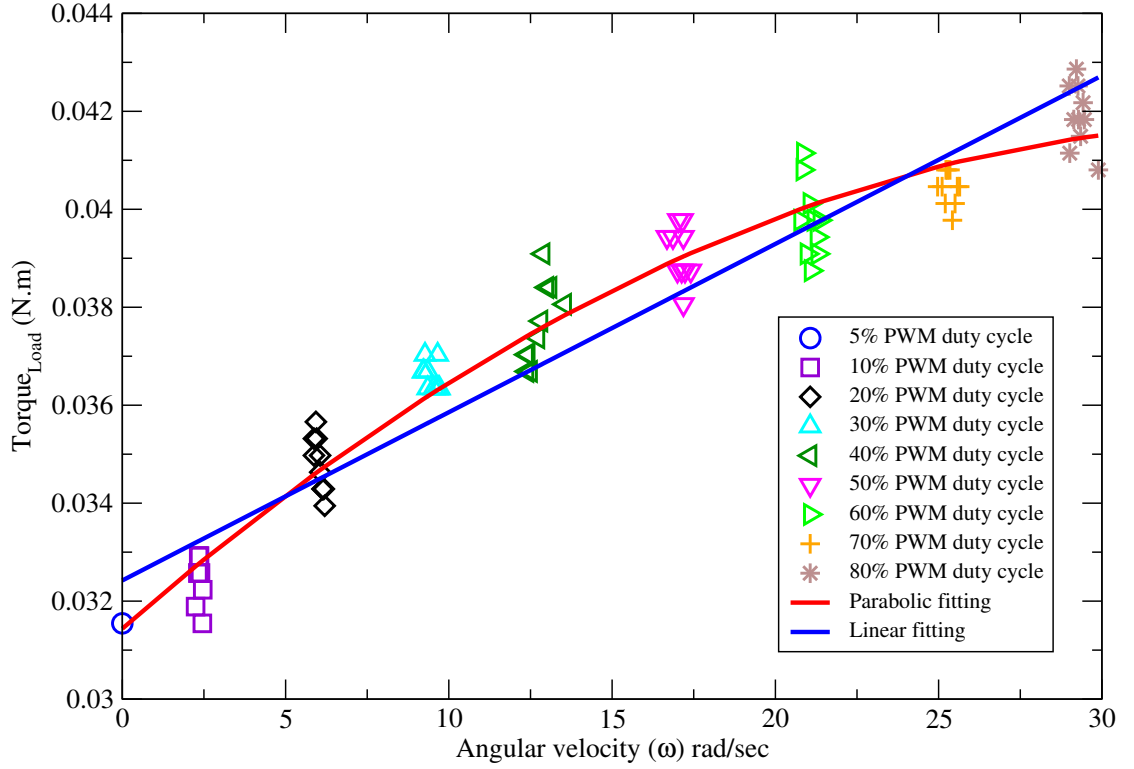


Figure C.9: The results of obtaining the friction constant  $B_M$  of the motor using linear and parabolic fitting methods

where  $\Delta t$  is the time interval between two sampled data. Since the central difference method is an approximation approach, it should be noted that the angular velocity may not be calculated accurately. Therefore, the results of the friction constant and the moment of inertia can be subject to computational bias.

The experiment is conducted under nine different configurations of the PWM duty cycles, from 5% to 80%. Moreover, the testing process collects ten measurements of current and velocity data for each PWM duty cycle. Figure C.9 shows the results of two different fitting methods for retrieving the friction constant  $B_M$  based on the load torque equation of (C.2). The linear and parabolic fitting equations can be described by

$$T_{L_{\text{linear}}} = B_M\omega(t) + T_W(t) = B_M\omega(t) + T_i(t) = 0.000325\omega(t) + 0.0328 \quad (\text{C.11})$$

$$\begin{aligned} T_{L_{\text{parabola}}} &= B_M\omega(t) + T_W(t) = B_M\omega(t) + T_i(t) + C_M\omega^2(t) \\ &= 0.000585\omega(t) + 0.03144 - 0.000008295\omega^2(t) \end{aligned} \quad (\text{C.12})$$

where  $T_i(t)$  is the intrinsic torque to counteract the motor resistance to barely spin the

wheel.

It can be seen from Figure C.9 that the parabolic fitting results are more accurate than the linear one. Hence, the friction constant is chosen to be  $B_M = 0.000585 \text{ N.m.sec/rad}$ .

### Moment of Inertia $J_M$

The moment of inertial of the motor can be computed from (C.1)-(C.3) and (C.12) as follows.

$$J_M = \frac{T_{\text{Total}}}{d\omega(t)/dt} = \frac{K_T i_M(t) - T_i(t) - B_M \omega(t) - C_M \omega^2(t)}{d\omega(t)/dt} \quad (\text{C.13})$$

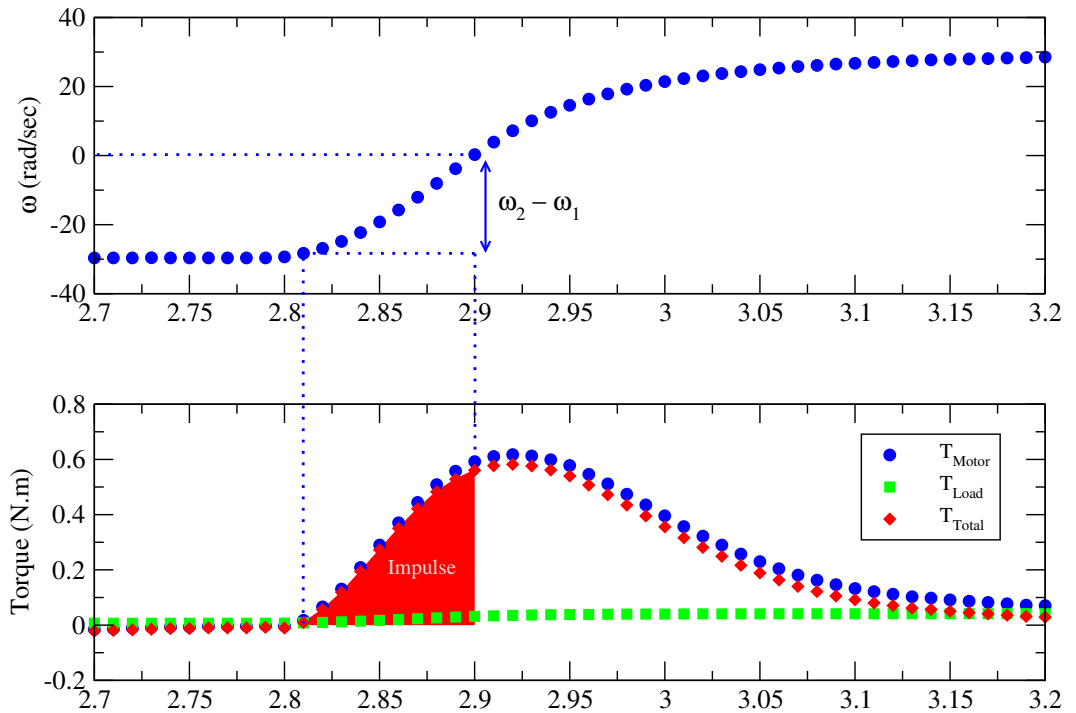


Figure C.10: The results of the total torque  $T_{\text{Total}}$  and the velocity difference  $(\omega_2 - \omega_1)$  during the acceleration stage

By re-arranging (C.13) and taking the integration from both sides, it follows that

$$\begin{aligned} J_M d\omega(t) &= T_{\text{Total}} dt \\ \implies \int_{\omega_1}^{\omega_2} J_M d\omega(t) &= \int_{t_1}^{t_2} T_{\text{Total}} dt \\ \implies J_M (\omega_2 - \omega_1) &= \int_{t_1}^{t_2} T_{\text{Total}} dt \\ \implies J_M &= \frac{\int_{t_1}^{t_2} T_{\text{Total}} dt}{(\omega_2 - \omega_1)} \end{aligned} \quad (\text{C.14})$$

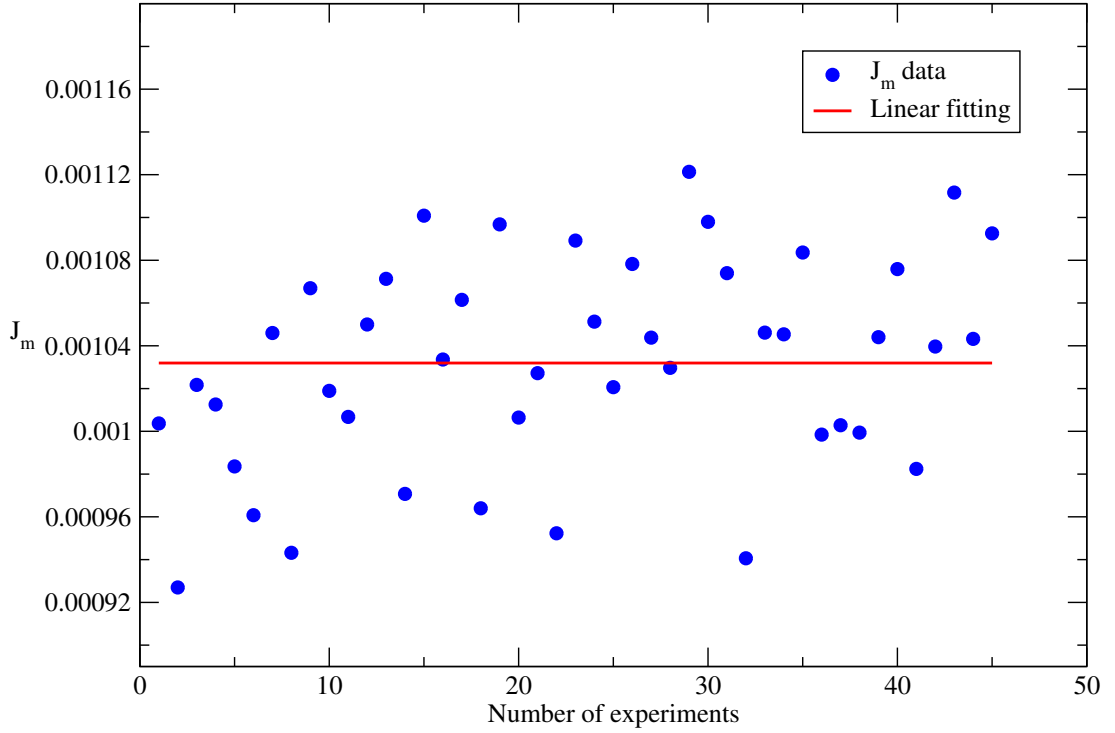


Figure C.11: The results of the moment of inertia  $J_M$  under 45 repetitive experiment

The angular velocities of  $\omega_1$  and  $\omega_2$  in (C.14) can be computed based on (C.10).

Figure C.10 illustrate the total torque  $T_{\text{Total}}$  in red region and the velocity difference ( $\omega_2 - \omega_1$ ) between the time 2.81 second to 2.9 second during the motor acceleration stage under a single experimentation. The corresponding moment of inertia can be computed based on (C.14).

The final value of  $J_M$  is obtained by fitting with 45 experiment data depicted in Figure C.11 as follows.

$$J_M = 1.032 \times 10^{-3} \pm 4.86 \times 10^{-5} \text{ N.m.sec}^2 / \text{rad} \quad (\text{C.15})$$

## APPENDIX. D

---

### LIST OF PUBLICATION

---

#### JOURNAL PAPERS

- [1] Y. K. Yang and X. G. Yan and K. Sirlantzis and G. Howells, “Regular Form Based Sliding Mode Control Design on a Two-wheeled Inverted Pendulum,” *International Journal of Modelling, Identification and Control*, 2021. (Accepted)
- [2] Y. K. Yang and X. G. Yan and K. Sirlantzis and G. Howells, “Trajectory Tracking Sliding Mode Control for a Two-Wheeled Mobile Robot,” *International Journal of Advanced Robotic Systems*, 2021. (Under first round review)
- [3] Y. K. Yang and X. G. Yan and K. Sirlantzis and G. Howells, “Static Output Feedback Sliding Mode Control on a Two-wheeled Inverted Pendulum System,” *Complexity*, 2021. (Submitted)

#### CONFERENCE PAPERS

- [1] Y. K. Yang and X. G. Yan and K. Sirlantzis and G. Howells, “Application of Sliding Mode Trajectory Tracking Control Design for Two-Wheeled Mobile Robots,” in

*2019 NASA/ESA Conference on Adaptive Hardware and Systems (AHS)*, 2019.

- [2] Y. K. Yang and X. G. Yan and K. Sirlantzis and G. Howells, “Static Output Feedback Control of a Two-wheeled Inverted Pendulum Using Sliding Mode Technique,” in *International Conference on Robotics and Control Systems*, 2021. (Accepted)

---

## BIBLIOGRAPHY

---

- [1] D. G. Luenberger, *Introduction to Dynamic Systems: Theory, Models, and Applications*. John Wiley & Sons, 1979.
- [2] V. Utkin, “Variable structure systems with sliding modes,” *IEEE Transactions on Automatic Control*, vol. 22, no. 2, pp. 212–222, 1977.
- [3] S. G. Tzafestas, *Introduction to Mobile Robot Control*. Elsevier, 2014.
- [4] M. Aicardi, G. Casalino, A. Bicchi, and A. Balestrino, “Closed loop steering of unicycle like vehicles via lyapunov techniques,” *IEEE Robotics & Automation Magazine*, vol. 2, no. 1, pp. 27–35, 1995.
- [5] S. A. P. Ramaswamy and S. N. Balakrishnan, “Formation control of car-like mobile robots: A lyapunov function based approach,” *American Control Conference*, 2008.
- [6] Y. N. Wang, Z. Q. Miao, H. Zhong, and Q. Pan, “Simultaneous stabilization and tracking of nonholonomic mobile robots: A lyapunov-based approach,” *IEEE Transactions on Control Systems Technology*, vol. 23, no. 4, pp. 1440–1450, 2015.
- [7] A. Astolfi, “On the stabilization of nonholonomic systems,” *Proceedings of 1994 33rd IEEE Conference on Decision and Control*, 1994.

- 
- [8] G. Oriolo, A. Luca, and M. Vendittelli, "Wmr control via dynamic feedback linearization: design, implementation, and experimental validation.," *IEEE Transactions on Control Systems Technology*, vol. 10, no. 6, pp. 835–852, 2002.
- [9] K. Pathak, J. Franch, and S. K. Agrawal, "Velocity and position control of a wheeled inverted pendulum by partial feedback linearization," *IEEE Transactions on Robotics*, vol. 21, no. 3, pp. 505–513, 2005.
- [10] J. G. Elliot and R. F. Gans, "Closed-loop control of an underactuated sheet registration device using feedback linearization and gain scheduling," *IEEE Transactions on Control Systems Technology*, vol. 16, no. 4, pp. 589–599, 2008.
- [11] D. Chwa, "Tracking control of differential-drive wheeled mobile robots using a backstepping-like feedback linearization," *IEEE Transactions on Systems, Man, and Cybernetics - Part A: Systems and Humans*, vol. 40, no. 6, pp. 1285–1295, 2010.
- [12] F. Rubio, F. Valero, and C. Llopis-Albert, "A review of mobile robots: Concepts, methods, theoretical framework, and applications," *International Journal of Advanced Robotic Systems*, vol. 16, no. 2, pp. 1–22, 2019.
- [13] C. Zhang, H. K. Lam, J. Qiu, P. Qi, and Q. Chen, "Fuzzy-model-based output feedback steering control in autonomous driving subject to actuator constraints," *IEEE Transactions on Fuzzy Systems*, vol. 29, no. 3, pp. 457–470, 2021.
- [14] R. H. Abiyev, N. Akkaya, and I. Günsel, "Control of omnidirectional robot using z-number-based fuzzy system," *IEEE Transactions on Systems, Man, and Cybernetics: Systems*, vol. 49, no. 1, pp. 238–252, 2019.
- [15] J. Huang, M. H. Ri, D. R. Wu, and S. H. Ri, "Interval type-2 fuzzy logic modeling and control of a mobile two-wheeled inverted pendulum," *IEEE Transactions on Fuzzy Systems*, vol. 26, no. 4, pp. 2030–2038, 2018.
- [16] C. F. Juang, M. G. Lai, and W. T. Zeng, "Evolutionary fuzzy control and navigation for two wheeled robots cooperatively carrying an object in unknown environments," *IEEE Transactions on Cybernetics*, vol. 45, no. 9, pp. 1731–1743, 2015.

- [17] Z. Chen, Y. Liu, W. He, H. Qiao, and H. Ji, "Adaptive-neural-network-based trajectory tracking control for a nonholonomic wheeled mobile robot with velocity constraints," *IEEE Transactions on Industrial Electronics*, vol. 68, no. 6, pp. 5057–5067, 2021.
- [18] S. Li, L. Ding, H. Gao, Y. J. Liu, N. Li, and Z. Deng, "Reinforcement learning neural network-based adaptive control for state and input time-delayed wheeled mobile robots," *IEEE Transactions on Systems, Man, and Cybernetics: Systems*, vol. 50, no. 11, pp. 4171–4182, 2020.
- [19] H. Taghavifar, "Neural network autoregressive with exogenous input assisted multi-constraint nonlinear predictive control of autonomous vehicles," *IEEE Transactions on Vehicular Technology*, vol. 68, no. 7, pp. 6293–6304, 2019.
- [20] C. G. Yang, Z. J. Li, R. X. Cui, and B. G. Xu, "Neural network-based motion control of an underactuated wheeled inverted pendulum model," *IEEE Transactions on Neural Networks and Learning Systems*, vol. 25, no. 11, pp. 2004–2016, 2014.
- [21] S. O. Haykin, *Neural Networks: A Comprehensive Foundation*. Pearson Education, 1998.
- [22] A. Swief, A. El-Zawawi, and M. El-Habrouk, "A survey of model predictive control development in automotive industries," *International Conference on Applied Automation and Industrial Diagnostics (ICAAID)*, 2019.
- [23] J. Hung, W. Gao, and J. Hung, "Variable structure control: a survey," *IEEE Transactions on Industrial Electronics*, vol. 40, no. 1, pp. 2–22, 1993.
- [24] U. Itkis, *Control systems of variable structure*. Halsted Press, 1976.
- [25] V. Utkin, J. Guldner, and J. X. Shi, *Sliding mode control in electro-mechanical systems*. CRC Press, 2009.
- [26] X. H. Yu, B. Wang, and X. J. Li, "Computer-controlled variable structure systems: The state-of-the-art," *IEEE Transactions on Industrial Informatics*, vol. 8, no. 2, pp. 197–205, 2012.

- 
- [27] A. Šabanovic, “Variable structure systems with sliding modes in motion control—a survey,” *IEEE Transactions on Industrial Informatics*, vol. 7, no. 2, pp. 212–223, 2011.
- [28] G. Bartolini, A. Ferrara, L. Giacomini, and A. Usai, “Properties of a combined adaptive/second-order sliding mode control algorithm for some classes of uncertain nonlinear systems,” *IEEE Transactions on Automatic Control*, vol. 45, no. 7, pp. 1334–1341, 2000.
- [29] Y. Chang, “Adaptive sliding mode control of multi-input nonlinear systems with perturbations to achieve asymptotical stability,” *IEEE Transactions on Automatic Control*, vol. 54, no. 12, pp. 2863–2869, 2009.
- [30] V. I. Utkin and A. S. Poznyak, “Adaptive sliding mode control with application to super-twist algorithm: equivalent control method,” *Automatica*, vol. 49, no. 1, pp. 39–47, 2013.
- [31] J. Davila, “Exact tracking using backstepping control design and high-order sliding modes,” *IEEE Transactions on Automatic Control*, vol. 58, no. 8, pp. 2077–2081, 2013.
- [32] L. Y. Sun, S. Tong, and Y. Liu, “Adaptive backstepping sliding mode  $h_\infty$  control of static var compensator,” *IEEE Transactions on Control Systems Technology*, vol. 19, no. 5, pp. 1178–1185, 2011.
- [33] S. Tong and H. X. Li, “Fuzzy adaptive sliding-mode control for mimo nonlinear systems,” *IEEE Transactions on Fuzzy Systems*, vol. 11, no. 3, pp. 354–360, 2003.
- [34] R. J. Wai, “Fuzzy sliding-mode control using adaptive tuning technique,” *IEEE Transactions on Industrial Electronics*, vol. 54, no. 1, pp. 586–594, 2007.
- [35] J. Huang, S. Ri, T. Fukuda, and Y. Wang, “A disturbance observer based sliding mode control for a class of underactuated robotic system with mismatched uncertainties,” *IEEE Transactions on Automatic Control*, vol. 64, no. 6, pp. 2480–2487, 2019.

- [36] W. A. Apaza-Perez, J. A. Moreno, and L. Fridman, "Global sliding mode observers for some uncertain mechanical systems," *IEEE Transactions on Automatic Control*, vol. 65, no. 3, pp. 1348–1355, 2020.
- [37] J. Huang, M. S. Zhang, S. H. Ri, C. H. Xiong, Z. J. Li, and Y. Kang, "High-order disturbance-observer-based sliding mode control for mobile wheeled inverted pendulum systems," *IEEE Transactions on Industrial Electronics*, vol. 67, no. 3, pp. 2030–2041, 2020.
- [38] X. G. Yan, C. Edwards, and S. K. Spurgeon, "Decentralised robust sliding mode control for a class of nonlinear interconnected systems by static output feedback," *Automatica*, vol. 40, no. 4, pp. 613–620, 2004.
- [39] X. G. Yan, C. Edwards, S. K. Spurgeon, and J. Bleijs, "Decentralised sliding mode control for multimachine power systems using only output information," *IEE Proc. Part D Control Theory Appl*, vol. 151, no. 5, pp. 627–631, 2004.
- [40] X. G. Yan, S. K. Spurgeon, and C. Edwards, "On discontinuous static output feedback control for linear systems with nonlinear disturbances," *Systems & Control Letters*, vol. 58, no. 5, pp. 314–319, 2009.
- [41] X. G. Yan, S. K. Spurgeon, and C. Edwards, "Memoryless static output feedback sliding mode control for nonlinear systems with delayed disturbances," *IEEE Transactions on Automatic Control*, vol. 59, no. 7, pp. 1906–1912, 2014.
- [42] R. W. Brockett, "Asymptotic stability and feedback stabilization," *Differential Geometric Control Theory*, pp. 181–191, 1983.
- [43] G. Walsh, D. Tilbury, S. Sastry, R. Murray, and J. P. Laumond, "Stabilization of trajectories for systems with nonholonomic constraints," *IEEE Transactions on Automatic Control*, vol. 39, no. 1, pp. 216–222, 1994.
- [44] O. J. Sordalen and O. Egeland, "Exponential stabilization of nonholonomic chained systems," *IEEE Transactions on Automatic Control*, vol. 40, no. 1, pp. 35–49, 1995.

- 
- [45] C. Samson, “Control of chained systems application to path following and time-varying point-stabilization of mobile robots,” *IEEE Transactions on Automatic Control*, vol. 40, no. 1, pp. 64–77, 1995.
- [46] J.-M. Godhavn and O. Egeland, “A lyapunov approach to exponential stabilization of nonholonomic systems in power form,” *IEEE Transactions on Automatic Control*, vol. 42, no. 7, pp. 1028–1032, 1997.
- [47] Z. P. Jiang and H. Nijmeijer, “A recursive technique for tracking control of nonholonomic systems in chained form,” *IEEE Transactions on Automatic Control*, vol. 44, no. 2, pp. 265–279, 1999.
- [48] Z. P. Wang, G. B. Li, X. Z. Chen, H. Zhang, and Q. J. Chen, “Simultaneous stabilization and tracking of nonholonomic wms with input constraints: Controller design and experimental validation,” *IEEE Transactions on Industrial Electronics*, vol. 66, no. 7, pp. 5343–5352, 2019.
- [49] M. A. Maghenem, A. Loría, and E. Panteley, “Cascades-based leader–follower formation tracking and stabilization of multiple nonholonomic vehicles,” *IEEE Transactions on Automatic Control*, vol. 65, no. 8, pp. 3639–3646, 2020.
- [50] A. Astolfi, “Discontinuous control of nonholonomic systems,” *Systems & Control Letters*, vol. 27, no. 1, pp. 37–45, 1996.
- [51] W. Lin, R. Pongvuthithum, and C. J. Qian, “Control of high-order nonholonomic systems in power chained form using discontinuous feedback,” *IEEE Transactions on Automatic Control*, vol. 47, no. 1, pp. 108–115, 2002.
- [52] B. M. Kim and P. Tsiotras, “Controllers for unicycle-type wheeled robots: Theoretical results and experimental validation,” *IEEE Transactions on Robotics and Automation*, vol. 18, no. 3, pp. 294–307, 2002.
- [53] F. Fontes and L. Magni, “Min-max model predictive control of nonlinear systems using discontinuous feedbacks,” *IEEE Transactions on Automatic Control*, vol. 48, no. 10, pp. 1750–1755, 2003.

- [54] J. Ghommam, F. Mnif, A. Benali, and N. Derbel, "Asymptotic backstepping stabilization of an underactuated surface vessel," *IEEE Transactions on Control Systems Technology*, vol. 14, no. 6, pp. 1150–1157, 2006.
- [55] D. V. Dimarogonas and K. J. Kyriakopoulos, "On the rendezvous problem for multiple nonholonomic agents," *IEEE Transactions on Automatic Control*, vol. 52, no. 5, pp. 916–922, 2007.
- [56] I. Kolmanovsky and N. H. McClamroch, "Developments in nonholonomic control problems," *IEEE Control Systems Magazine*, vol. 15, no. 6, pp. 20–36, 1995.
- [57] P. Morin and C. Samson, *Motion control of wheeled mobile robots*. Springer-Verlag, 2008.
- [58] B. Thuilot, B. d'AAndrea Novel, and A. Micaelli, "Modeling and feedback control of mobile robots equipped with several steering wheels," *IEEE Transactions on Robotics and Automation*, vol. 12, no. 3, pp. 375–390, 1996.
- [59] C. Samson and K. Ait-Abderrahim, "Mobile robot control. part 1 : Feedback control of nonholonomic wheeled cart in cartesian space," in *INRIA report*, 1990.
- [60] Y. Kanayama, Y. Kimura, F. Miyazaki, and T. Noguchi, "A stable tracking control method for an autonomous mobile robot," *IEEE International Conference on Robotics and Automation*, 1990.
- [61] D.-H. Kim and J.-H. Oh, "Tracking control of a two-wheeled mobile robot using input–output linearization," *Control Engineering Practice*, vol. 7, no. 3, pp. 369–373, 1999.
- [62] R. Fierro and F. L. Lewis, "Control of a nonholonomic mobile robot: backstepping kinematics into dynamics," *34th IEEE Conference on Decision and Control*, vol. 4, 1995.
- [63] R. Fierro and F. L. Lewis, "Control of a nonholonomic mobile robot using neural networks," *IEEE Transactions on Neural Networks*, vol. 9, no. 4, pp. 589–600, 1998.

- [64] M. Asif, M. J. Khan, and N. Cai, "Adaptive sliding mode dynamic controller with integrator in the loop for nonholonomic wheeled mobile robot trajectory tracking," *International Journal of Control*, vol. 87, no. 5, pp. 964–975, 2014.
- [65] T. Fukao, H. Nakagawa, and N. Adachi, "Adaptive tracking control of a nonholonomic mobile robot," *IEEE Transactions on Robotics and Automation*, vol. 16, no. 5, pp. 609–615, 2000.
- [66] C. Y. Chen, T. H. S. Li, Y. C. Yeh, and C. C. Chang, "Design and implementation of an adaptive sliding-mode dynamic controller for wheeled mobile robots," *Mechatronics*, vol. 19, no. 2, pp. 156–166, 2009.
- [67] X. G. Yan, S. K. Spurgeon, and C. Edwards, *Variable Structure Control of Complex Systems*. Springer, Berlin, Germany, 2017.
- [68] J. Yang and J. Kim, "Sliding mode control for trajectory tracking of nonholonomic wheeled mobile robots.," *IEEE Transactions on Robotics and Automation*, vol. 15, no. 3, pp. 578–587, 1999.
- [69] M. Belhocine, M. Hamerlain, and F. Meraoubi, "Variable structure control for a wheeled mobile robot.," *Advanced Robotics*, vol. 17, no. 9, pp. 909–924, 2003.
- [70] B. S. Park, S. J. Yoo, J. B. Park, and Y. H. Choi, "Adaptive neural sliding mode control of nonholonomic wheeled mobile robots with model uncertainty," *International Journal of Control, Automation and Systems*, vol. 17, no. 1, pp. 207–214, 2009.
- [71] A. Azzabi and K. Nouri, "Design of a robust tracking controller for a nonholonomic mobile robot based on sliding mode with adaptive gain," *International Journal of Advanced Robotic Systems*, vol. 18, no. 1, pp. 1–18, 2021.
- [72] Y. Koubaa, M. Boukattaya, and T. Damak, "Adaptive sliding mode control for trajectory tracking of nonholonomic mobile robot with uncertain kinematics and dynamics," *Applied Artificial Intelligence*, vol. 32, no. 9-10, pp. 924–938, 2018.

- [73] S. Tokat, I. Eksin, and M. Guzelkaya, "Sliding mode control of high order systems using a constant nonlinear sliding surface on a transformed coordinate axis," *Journal of Vibration and Control*, vol. 14, no. 6, pp. 909–927, 2008.
- [74] S. B. Choi, D. W. Park, and S. Jayasuriya, "A time-varying sliding surface for fast and robust tracking control of second-order uncertain systems," *Automatica*, vol. 30, no. 5, pp. 899–904, 1994.
- [75] M. Ertugrul, O. Kaynak, and F. Kerestecioglu, "Gain adaptation in sliding mode control of robotic manipulators," *International Journal of Systems Science*, vol. 31, no. 9, pp. 1099–1106, 2000.
- [76] S. J. Huang, K. S. Huang, and K. C. Chiou, "Development and application of a novel radial basis function sliding mode controller," *Mechatronics*, vol. 13, no. 4, pp. 313–329, 2003.
- [77] Q. P. Ha, D. C. Rye, and H. F. Durrant-Whyteu, "Fuzzy moving sliding mode control with application to robotic manipulators," *Automatica*, vol. 35, no. 4, pp. 607–616, 1999.
- [78] V. K. Chu and M. Tomizuka, "Sliding mode control with nonlinear sliding surfaces," *IFAC Proceedings Volumes*, vol. 29, no. 1, pp. 2877–2882, 1996.
- [79] S. Kim and S. J. Kwon, "Nonlinear optimal control design for underactuated two-wheeled inverted pendulum mobile platform," *IEEE/ASME Transactions on Mechatronics*, vol. 22, no. 6, pp. 2803–2808, 2017.
- [80] M. Yue, C. An, and Z. J. Li, "Constrained adaptive robust trajectory tracking for wip vehicles using model predictive control and extended state observer," *IEEE Transactions on Systems, Man, and Cybernetics: Systems*, vol. 48, no. 5, pp. 733–742, 2018.
- [81] P. V. Lam and Y. Fujimoto, "A robotic cane for balance maintenance assistance," *IEEE Transactions on Industrial Informatics*, vol. 15, no. 7, pp. 3998–4009, 2019.

- [82] W. Sun, S. F. Su, J. W. Xia, and Y. Q. Wu, "Adaptive tracking control of wheeled inverted pendulums with periodic disturbances," *IEEE Transactions on Cybernetics*, vol. 50, no. 5, pp. 1867–1876, 2020.
- [83] J. Tian, J. Ding, Y. P. Tai, and Z. S. Ma, "Control of different-axis two-wheeled self-balancing vehicles," *IEEE Access*, vol. 8, 2020.
- [84] Y. Q. Liu, H. Jing, X. Liu, and Y. L. Lv, "An improved hybrid error control path tracking intelligent algorithm for omnidirectional agv on ros," *International Journal of Computer Applications in Technology*, vol. 64, no. 2, pp. 115–125, 2020.
- [85] E. S. Elyoussef, N. A. Martins, D. W. Bertol, E. R. D. Pieri, and U. F. Moreno, "Simulation results and practical implementation of a pd-super-twisting second order sliding mode tracking control for a differential wheeled mobile robot," *International Journal of Computer Applications in Technology*, vol. 63, no. 3, pp. 213–227, 2020.
- [86] C.-H. Chiu, Y.-T. Hung, and Y.-F. Peng, "Design of a decoupling fuzzy control scheme for omnidirectional inverted pendulum real-world control," *IEEE Access*, vol. 9, pp. 26083–26092, 2021.
- [87] M. Yue, X. Wei, and Z. J. Li, "Zero-dynamics-based adaptive sliding mode control for a wheeled inverted pendulum with parametric friction and uncertain dynamics compensation," *Transactions of the Institute of Measurement and Control*, vol. 37, no. 1, pp. 91–99, 2015.
- [88] J. Huang, F. Ding, T. Fukuda, and T. Matsuno, "Modeling and velocity control for a novel narrow vehicle based on mobile wheeled inverted pendulum," *IEEE Transactions on Control Systems Technology*, vol. 21, no. 5, pp. 1607–1617, 2013.
- [89] C. C. Tsai, H. C. Huang, and S. C. Lin, "Adaptive neural network control of a self-balancing two-wheeled scooter," *IEEE Transactions on Industrial Electronics*, vol. 57, no. 4, pp. 1420–1428, 2010.

- [90] Y. Kim, S. H. Kim, and Y. K. Kwak, "Dynamic analysis of a nonholonomic two-wheeled inverted pendulum robot," *Journal of Intelligent and Robotic Systems*, vol. 44, no. 1, pp. 25–46, 2005.
- [91] M. Baloh and M. Parent, "Modeling and model verification of an intelligent self-balancing two-wheeled vehicle for an autonomous urban transportation system," *Proc. of the Conf. on Computational Intelligence, Robotics, and Autonomous Systems*, 2003.
- [92] A. Salerno and J. Angeles, "A new family of two wheeled mobile robot: modeling and controllability," *IEEE Transactions on Robotics*, vol. 23, no. 1, pp. 169–173, 2007.
- [93] S. Kim and S. Kwon, "Dynamic modeling of a two-wheeled inverted pendulum balancing mobile robot," *International Journal of Control, Automation and Systems*, vol. 13, no. 4, pp. 926–933, 2015.
- [94] F. Grasser, A. D'Arrigo, S. Colombi, and A. C. Rufer, "Joe: a mobile, inverted pendulum," *IEEE Transactions on Industrial Electronics*, vol. 49, no. 1, pp. 107–114, 2002.
- [95] S. Miao and Q. Cao, "Modeling of self-tilt-up motion for a two-wheeled inverted pendulum," *Industrial Robot: An International Journal*, vol. 38, no. 1, pp. 76–85, 2011.
- [96] C.-H. Huang, W.-J. Wang, and C.-H. Chiu, "Design and implementation of fuzzy control on a two-wheel inverted pendulum," *IEEE Transactions on Industrial Electronics*, vol. 58, no. 7, pp. 2988–3001, 2011.
- [97] Z. Li and J. Luo, "Adaptive robust dynamic balance and motion controls of mobile wheeled inverted pendulums," *IEEE Transactions on Control Systems Technology*, vol. 17, no. 1, pp. 233–241, 2009.
- [98] J. Huang, Z. H. Guan, T. Matsuno, T. Fukuda, and K. Sekiyama, "Sliding mode velocity control of mobile-wheeled inverted-pendulum systems," *IEEE Transactions on Robotics*, vol. 26, no. 4, pp. 750–758, 2010.

- [99] M. C. Tsai and J. S. Hu, "Pilot control of an autobalancing two wheeled cart," *Advanced Robotics*, vol. 21, no. 7, pp. 817–827, 2007.
- [100] M. Muhammad, S. Buyamin, M. N. Ahmad, S. W. Nawawi, and A. A. Bature, "Multiple operating points model-based control of a two-wheeled inverted pendulum mobile robot," *International Journal of Mechanical & Mechatronics Engineering*, vol. 13, no. 5, pp. 1–9, 2013.
- [101] M. R. Romlay, A. M. Ibrahim, S. F. Toha, and M. Rashid, "Two-wheel balancing robot; review on control methods and experiments," *International Journal of Recent Technology and Engineering (IJRTE)*, vol. 7, no. 6, pp. 106–112, 2019.
- [102] T. Takei, R. Imamura, and S. Yuta, "Baggage transportation and navigation by a wheeled inverted pendulum mobile robot," *IEEE Transactions on Industrial Electronics*, vol. 56, no. 10, pp. 3985–3994, 2009.
- [103] S. C. Lin and C. C. Tsai, "Development of a self-balancing human transportation vehicle for the teaching of feedback control," *IEEE Transactions on Education*, vol. 52, no. 1, pp. 157–168, 2009.
- [104] J.-S. Hu and M.-C. Tsai, "Design of robust stabilization and fault diagnosis for an auto-balancing two-wheeled cart," *IEEE Transactions on Education*, vol. 22, no. 2-3, pp. 319–338, 2008.
- [105] C. F. Huang and T. J. Yeh, "Anti slip balancing control for wheeled inverted pendulum vehicles," *IEEE Transactions on Control Systems Technology*, vol. 28, no. 3, pp. 1042–1049, 2020.
- [106] Z. J. Li and J. Luo, "Adaptive robust dynamic balance and motion controls of mobile wheeled inverted pendulums," *IEEE Transactions on Control Systems Technology*, vol. 17, no. 1, pp. 233–241, 2009.
- [107] S.-C. Lin, C.-C. Tsai, and H.-C. Huang, "Adaptive robust self-balancing and steering of a two-wheeled human transportation vehicle," *Journal of Intelligent & Robotic Systems*, vol. 62, pp. 103–123, 2011.

- [108] S. Jung and S. S. Kim, "Control experiment of a wheel-driven mobile inverted pendulum using neural network," *IEEE Transactions on Control Systems Technology*, vol. 16, no. 2, pp. 297–303, 2008.
- [109] J. X. Xu, Z. Q. Guo, and T. H. Lee, "Design and implementation of integral sliding-mode control on an underactuated two-wheeled mobile robot," *IEEE Transactions on Industrial Electronics*, vol. 61, no. 7, pp. 3671–3681, 2014.
- [110] V. Utkin and J. Shi, "Integral sliding mode in systems operating under uncertainty conditions," *Proceedings of 35th IEEE Conference on Decision and Control*, 2002.
- [111] M. Chen, "Robust tracking control for self-balancing mobile robots using disturbance observer," *IEEE/CAA Journal of Automatica Sinica*, vol. 4, no. 3, pp. 458–465, 2017.
- [112] C. Silvestre and A. Pascoal, "Control of the infante auv using gain scheduled static output feedback," *Control Engineering Practice*, vol. 12, no. 12, pp. 1501–1509, 2004.
- [113] A.-T. Nguyen, P. Chevrel, and F. Claveau, "Lpv static output feedback for constrained direct tilt control of narrow tilting vehicles," *IEEE Transactions on Control Systems Technology*, vol. 28, no. 2, pp. 661–670, 2020.
- [114] J. Gadewadikar, F. L. Lewis, K. Subbarao, K. M. Peng, and B. M. Chen, "H-infinity static output-feedback control for rotorcraft," *Journal of Intelligent & Robotic Systems*, vol. 54, no. 4, pp. 629–646, 2009.
- [115] E. K. Boukas, "Static output feedback control for stochastic hybrid systems: Lmi approach," *Automatica*, vol. 42, no. 1, pp. 183–188, 2006.
- [116] C. Edwards and S. K. Spurgeon, *Sliding Mode Control: Theory and Applications*. London, U.K: Taylor & Francis, 1998.
- [117] A. Pande and R. Munie, "Fast output sampling feedback with two delayed inputs for mimo system," *International Conference On Advances in Communication and Computing Technology (ICACCT)*, 2018.

- 
- [118] T. Saha, N. Murmu, S. Chakraborty, and M. Maitra, “Stabilization of cart inverted pendulum system by 2-rate controllers based on pso technique,” *IEEE Applied Signal Processing Conference (ASPCON)*, 2020.
- [119] V. L. Syrmos, C. T. Abdallah, P. Dorato, and K. Grigoriadis, “Static output feedback - a survey,” *Automatica*, vol. 33, no. 2, pp. 125–137, 1997.
- [120] H. J. Marquez, *Nonlinear control systems: analysis and design*. Wiley-Interscience Hoboken, 2002.
- [121] H. K. Khalil, *Nonlinear systems*. Prentice Hall, 2002.
- [122] F. W. Warner, *Foundations of Differentiable Manifolds and Lie Groups*. Springer Science & Business Media, 1983.
- [123] E. Davison, “On pole assignment in linear systems with incomplete state feedback,” *IEEE Transactions on Automatic Control*, vol. 15, no. 3, pp. 348–351, 1970.
- [124] E. Davison and R. Chatterjee, “A note on pole assignment in linear systems with incomplete state feedback,” *IEEE Transactions on Automatic Control*, vol. 16, no. 1, pp. 98–99, 1971.
- [125] E. Davison and S. Chow, “An algorithm for the assignment of closed-loop poles using output feedback in large linear multivariable systems,” *IEEE Transactions on Automatic Control*, vol. 18, no. 1, pp. 74–75, 1973.
- [126] E. Davison and S. Wang, “On pole assignment in linear multivariable systems using output feedback,” *IEEE Transactions on Automatic Control*, vol. 20, no. 4, pp. 516–518, 1975.
- [127] H. Kimura, “Pole assignment by gain output feedback,” *IEEE Transactions on Automatic Control*, vol. 20, no. 4, pp. 509–516, 1975.
- [128] H. Kimura, “A further result on the problem of pole assignment by output feedback,” *IEEE Transactions on Automatic Control*, vol. 22, no. 3, pp. 458–463, 1977.
- [129] V. Blondel and J. Tsitsiklis, “Np-hardness of some linear control design problems,” *Proceedings of 1995 34th IEEE Conference on Decision and Control*, 1995.

- [130] M. Y. Fu and Z.-Q. Luo, "Computational complexity of a problem arising in fixed order output feedback design," *Systems & Control Letters*, vol. 30, no. 5, pp. 209–215, 1997.
- [131] M. Y. Fu, "Pole placement via static output feedback is np-hard," *IEEE Transactions on Automatic Control*, vol. 49, no. 5, pp. 855–857, 2004.
- [132] V. I. Utkin, *Sliding Modes in Control and Optimization*. Springer-Verlag, Berlin, 1992.
- [133] A. F. Filippov, "Differential equations with discontinuous right hand-sides," *American Mathematical Society Translations*, vol. 42, pp. 199–231, 1964.
- [134] A. F. Filippov, *Differential Equations with Discontinuous Righthand Sides*. Springer-Science & Business Media, Berlin, 1988.
- [135] P. Kachroo and M. Tomizuka, "Chattering reduction and error convergence in the sliding-mode control of a class of nonlinear systems," *IEEE Transactions on Automatic Control*, vol. 41, no. 7, pp. 1063–1068, 1996.
- [136] S. C. Chung and C.-L. Lin, "A general class of sliding surface for sliding mode control," *IEEE Transactions on Automatic Control*, vol. 43, no. 1, pp. 115–119, 1998.
- [137] P. Kachroo, "Existence of solutions to a class of nonlinear convergent chattering-free sliding mode control systems," *IEEE Transactions on Automatic Control*, vol. 44, no. 8, pp. 1620–1624, 1999.
- [138] W.-C. Su, S. Drakunov, and U. Ozguner, "An  $o(t/\sup 2/)$  boundary layer in sliding mode for sampled-data systems," *IEEE Transactions on Automatic Control*, vol. 45, no. 3, pp. 482–485, 2000.
- [139] M.-S. Chen, Y.-R. Hwang, and M. Tomizuka, "A state-dependent boundary layer design for sliding mode control," *IEEE Transactions on Automatic Control*, vol. 47, no. 10, pp. 1677–1681, 2002.

- [140] S. K. SPURGEON, “Choice of discontinuous control component for robust sliding mode performance,” *International Journal of Control*, vol. 53, no. 1, pp. 163–179, 1991.
- [141] J. I. Neimark and N. A. Fufaev, *Dynamics of Nonholonomic Systems*. American Mathematical Society, 1972.
- [142] T. P. Nascimento, C. E. T. Dorea, and L. M. G. Goncalves, “Nonholonomic mobile robots’ trajectory tracking model predictive control: a survey,” *Robotica*, vol. 36, no. 5, pp. 676–696, 2018.
- [143] O. Sordalen and O. Egeland, “Exponential stabilization of nonholonomic chained systems,” *IEEE Transactions on Automatic Control*, vol. 40, no. 1, pp. 35–49, 1995.
- [144] J.-P. Laumond, “Feasible trajectories for mobile robots with kinematic and environment constraints,” *International Conference of Intelligent Autonomous Systems, Amsterdam, The Netherlands*, pp. 346–354, 1986.
- [145] G. Campion, B. D. Novel, and G. Bastin, “Controllability and state feedback stabilizability of non holonomic mechanical systems,” *Advanced Robot Control*, vol. 162, pp. 106–124, 1991.
- [146] A. M. Bloch, *Nonholonomic Mechanics and Control*. Springer, 2003.
- [147] R. Mahony, T. Hamel, and J. M. Pflimlin, “Nonlinear complementary filters on the special orthogonal group,” *IEEE Transactions on Automatic Control*, vol. 53, pp. 1203–1217, 2008.
- [148] C. Sanchez, H.-G. V.M., R. Ortigoza, and et al., “Intuitive planning, generation, and tracking of trajectory for wmr with mobile computing device and embedded system.,” *IEEE Access*, vol. 8, pp. 160627–160642, 2020.
- [149] X. G. Yan, C. Edwards, and S. K. Spurgeon, “Output feedback sliding mode control for non-minimum phase systems with non-linear disturbances,” *International Journal of Control*, vol. 77, no. 15, pp. 1353–1361, 2007.

- 
- [150] G. W. Ogar and J. J. D’Azzo, “A unified procedure for deriving the differential equations of electrical and mechanical systems,” *IRE Transactions on Education*, vol. E-5, no. 1, pp. 18–26, 1962.
- [151] Y. F. Yin, J. X. Liu, J. A. Sanchez, L. G. Wu, S. Vazquez, J. I. Leon, and L. G. Franquelo, “Observer-based adaptive sliding mode control of npc converters: An rbf neural network approach,” *IEEE Transactions on Power Electronics*, vol. 34, no. 4, pp. 3831–3841, 2019.
- [152] B. A. H elouvry, P. Dupont, and C. C. D. Wit, “A survey of models, analysis tools and compensation methods for the control of machines with friction,” *Automatica*, vol. 30, no. 7, pp. 1083–1138, 1994.
- [153] Z. J. Li and C. G. Yang, “Neural-adaptive output feedback control of a class of transportation vehicles based on wheeled inverted pendulum models,” *IEEE Transactions on Control Systems Technology*, vol. 20, no. 6, pp. 1583–1591, 2012.
- [154] J. Rohac, M. Sipos, and J. Simanek, “Calibration of low-cost triaxial inertial sensors,” *IEEE Instrumentation & Measurement Magazine*, vol. 18, no. 6, pp. 32–38, 2015.
- [155] D. Jurman, M. Jankovec, R. Kamnik, and M. Topi c, “Calibration and data fusion solution for the miniature attitude and heading reference system,” *Sensors and Actuators A: Physical*, vol. 138, no. 2, pp. 411–420, 2007.
- [156] P. A. Regalia, S. K. Mitra, and P. P. Vaidyanathan, “The digital all-pass filter: a versatile signal processing building block,” *Proceedings of the IEEE*, vol. 76, no. 1, pp. 19–37, 1988.